Probing Control

Analysis and Design with Application to Fed-Batch Bioreactors

Velut, Stéphane

2005

Document Version:
Publisher's PDF, also known as Version of record

Probing Control

Analysis and Design with Application to Fed-Batch Bioreactors

Probing Control
Analysis and Design with Application to Fed-Batch Bioreactors

Stéphane Velut

Department of Automatic Control
Lund Institute of Technology
Lund, June 2005

A ma famille

Department of Automatic Control
Lund Institute of Technology
Box 118
SE-221 00 LUND
Sweden

ISSN 0280–5316
ISRN LUTFD2/TFRT--1072--SE

Printed in Sweden by Media-Tryck.
Lund 2005

Abstract

In most control problems the objective is to control the output at a desired value in spite of disturbances. In some cases, the best setpoint is not known *a priori* and it should be found online to optimize the process performance. This thesis examines a probing strategy that can be applied for this class of problems. The focus is on the application of the technique to the control of feed supply in fed-batch fermentations of the bacterium *Escherichia coli*.

The thesis is divided into three parts. In the first part, the convergence properties of the probing algorithm are examined. The analysis is limited to processes modeled by a linear time-invariant dynamic in series with a static nonlinearity. Stability and performance analysis taking into account the process dynamic are performed. Tuning guidelines that help the user for the design are also derived.

The second part presents a novel cultivation technique based on the probing approach. The fermentation technique combines the advantages of probing control and temperature-limited fed-batch technique. The feeding strategy is well adapted for prolonged operation at the maximum oxygen transfer capacity of the reactor. The efficiency of the method is demonstrated by simulations and experimental results. The strategy leads to a high biomass and it limits the degradation of the recombinant protein activity in the late production phase.

In the third part, the probing feeding strategy is evaluated in industrial-scale bioreactors. Based on experimental results the influence of scale and complex medium is discussed. It is shown that the flexibility and robustness of the technique makes it a useful tool for process development.

Acknowledgements

This thesis could not have been completed without the help and support from many people. It is therefore a great pleasure to have the opportunity to express my gratitude.

First of all, I would like to thank all my colleagues and friends at the department, who have provided with an outstanding environment of enthusiasm, creativity and friendship. The department of Automatic Control at Lund Institute of Technology is a wonderful place to make a PhD and it is a honor to be part of it.

I would like to express my sincere gratitude to my supervisor Per Hagander. He together with Mats Åkesson introduced me to the exciting field of control of biotechnology processes. Per has always been enthusiastic and encouraging. I have benefited a lot from his criticism and from his generous sharing of time, also under time-pressure in the late stage of writing.

I would like to thank all my co-workers and co-authors, with whom it has been a pleasure and honor to work. I sincerely enjoyed the long-lasting collaboration with my colleague and friend Lena de Maré who is co-author of many publications in the thesis. I am most grateful to Jan-Peter Axelsson who, with great engagement, generously shared his experience and time. I have also been fortunate to benefite from his industrial contact network. Many thanks to Jan Haglund and Per Sandgren for the implementation and support for the experiments at Pfizer, Strängnäs. I have truly appreciated my stimulating and enriching visit at Pfizer Kalamazoo, special thanks to Kevin Short and his team for their hospitality. I also wish to thank Andreas Castan at Biovitrum for the great discussions and for all the fun we had in Chicago. Most of the experimental work presented in Chapter 4 of the thesis has been performed at the Department of Biotechnology in Lund and this collaboration is gratefully acknowledged. Special thanks to Santosh Ramchuran, Eva Nordberg-Karlsson, Pernilla Turner and Olle Holst. It has also been a great pleasure to work with

Erika Ledung, Bo Norrman and Magnus Holmgren at the Biotechnology Center in Strängnäs.

Many thanks to Andrey Ghulchack for his excellent courses and his pedagogical skills to explain mathematics.

I also want to thank my former roommate Anton Cervin for his great company and his introduction to the subtilities of "särskrivning" in the swedish language. He together with Anders Robertsson and Bo Bernardsson are gratefully acknowledged for their numerous valuable comments on the manuscript. Many thanks to Leif Andersson and Anders Blomdell for their excellent computer support. I would also like to mention the always helpful and positive secretaries at the fifth floor who contribute a lot to the nice atmosphere at the department.

Thanks to all my friends for having shared many joyful moments during my PhD studies. You are too many to be named but I really hope to share with you similar moments also in the future.

Last but not least, I would like to thank my family in France who supported me and encouraged me during all the years in spite of the distance. Most of all I would like to thank my dear Jenny for her patience, support and love.

Stéphane

Financial support

I gratefully acknowledge the financial support for this work, received from The Nonlinear and Adaptive Control network (NACO2, Contract number HPRN-CT-1999-00046), The Swedish Agency for Innovation Systems (VINNOVA, P10432-2) and Pfizer.

Contents

1

Introduction

1.1 Motivation

Today, many pharmaceuticals are produced using genetically modified microorganisms. Since the first gene cloning in the beginning of the 1970s, it is possible to modify a microorganism to produce a desired substance, often a protein. The recombinant organism is then grown in a bioreactor to large numbers to obtain considerable quantities of the target protein. The environment inside the bioreactor should allow optimal growth and product synthesis. To achieve reproducible results feedback is commonly used to control parameters like temperature, pH and dissolved oxygen.

In fed-batch processes, the main carbon source is added during the cultivation to meet the actual cell demand. The feeding strategy has been reported to have a large impact on the process performance. The bacterium *Escherichia coli* is a common host organism that can be quickly grown to high cell densities. A drawback, however, is the formation of the by-product acetate, inhibiting both cell growth and product formation [Luli and Strohl, 1990; Bauer *et al.*, 1990; Bech Jensen and Carlsen, 1990]. Acetate can be formed in two situations: under anaerobic conditions and by overflow metabolism, that is, when the carbon source, often glucose, is in excess. The major problem is that neither acetate or glucose can be measured online to the required accuracy. Most of the feeding strategies that avoid acetate formation are based on specific process knowledge or require non-standard sensors.

A feeding strategy based on standard dissoved oxygen measurement has shown good results in laboratory scale reactors [Åkesson, 1999]. The key idea is to detect the saturation of the respiratory capacity of the cells, and thereby the onset of acetate formation, by superimposing short pulses in the feed rate. A feedback algorithm updates the feed rate based on the

pulse response in the dissolved oxygen signal. High cell density can be achieved in short times while minimizing acetate formation.

The probing control strategy is an efficient technique that exploits the full capacity of a bioreactor while operating in a safe region. The control strategy is applicable in other contexts for online optimization of processes with unknown but limited capacity. Rigorous analysis of the closed-loop system would be valuable for a better understanding of the probing technique. The analysis should account for the process dynamics and lead to simple tuning guidelines.

The feeding strategy tends to maximize the feed rate with respect to the constraints from the cells and the reactor. The sole manipulation of the feed rate can however lead to undesirable effects like product degradation or release of toxins into the medium [Rozkov, 2001; Han, 2002]. For a better product synthesis the strategy could be further improved, especially in the late part of the cultivation when operating at the maximum oxygen transfer rate.

The good results obtained with the probing strategy in laboratory-scale reactors are promising for a successful transfer of the technique to industrial applications. In a large scale fermenter, problems related to mixing are however susceptible to perturb the probing technique. To improve a process productivity, complex media, *i.e.* containing a not well-defined mixture of various nutrients, can be used. The metabolic shifts occuring in connection with the depletion of preferred substrates can lead to quick variations in the glucose or oxygen demand. The effects of scale-up and medium composition need to be investigated for the application of the probing approach to industrial reactors.

1.2 Outline and contributions of the thesis

The goal of the thesis is threefold:

- To analyse the stability and the performance of the probing strategy accounting for the process dynamics.
- To improve the probing feeding strategy in the late fed-batch phase when operating close to the maximum oxygen transfer capacity of the reactor.
- To evaluate the performance and limitations of the feeding strategy in large scale systems and systems with complex media.

Below, the contents and main contributions of the thesis are summarized. References to related publications are also given.

Chapter 2: Background

This chapter provides the context for the main contributions presented in the following chapters. A brief introduction to fermentation techniques is given, followed by a description of a probing feeding strategy.

Chapter 3: Analysis and tuning of the probing strategy

This chapter presents an analysis of the probing control strategy accounting for the process dynamics. The process to be controlled is modeled by a linear, time-invariant system in series with a static nonlinearity. A discrete-time representation of the closed-loop system is derived to facilitate the analysis. When the nonlinearity is modeled by a piecewise affine function, as in the bioreactor example, stability and performance of the probing scheme can be investigated by solving a set of linear matrix inequalities. The analysis methods are applied to some simple examples where it is desirable to control the process to a saturation. Based on those results, tuning guidelines for the probing controller are derived. It is also shown how the closed-loop system representation can be used to prove absolute stability in the case of a static concave nonlinearity.

Publications

Velut S. and P. Hagander (2005): "Control of fed-batch bioreactors." Under review for publication in *NACO2 book chapter*.

Velut S. and P. Hagander (2004): "A Probing Control Strategy: Stability and Performance." In *Proceedings of the 43rd IEEE Conference on Decision and Control*. Paradise Island, Bahamas.

Velut S. and P. Hagander (2003): "Analysis of a probing control strategy." In *Proceedings of the American Control Conference*. Denver, Colorado.

Chapter 4: Substrate and temperature limited fed-batch techniques

In this chapter, a novel cultivation technique for fed-batch fermentations with high oxygen demand is proposed. The strategy combines the advantages of probing control and the temperature limited fed-batch technique. When the maximum oxygen transfer capacity of the reactor is reached, the oxygen demand from the cells is lowered by decreasing the temperature of the culture. Dissolved oxygen control is achieved by simultaneous manipulation of temperature and agitation speed, in a mid-ranging configuration. Analysis and tuning guidelines of the feeding strategy are presented. The efficiency of the method is illustrated by simulations and experimental results from fed-batch cultivations of two different *E. coli* strains. The technique leads to a high productivity and minimizes the late product degradation that often occurs with the substrate limited fed-batch technique.

Publications

Velut S., L. de Maré and P. Hagander (2005): "Application of probing control to the temperature-limited fed-batch technique." Manuscript in preparation.

de Maré L., S. Velut, E. Ledung, C. Cimander, B. Norrman, E. Norberg Karlsson, O. Holst and P. Hagander (2005): "A cultivation technique for *E. coli* fed-batch cultivations operating close to the maximum oxygen transfer capacity of the reactor." Accepted for publication in *Biotechnology letters*.

Velut S., L. de Maré and P. Hagander (2004): "A modified probing feeding strategy: control aspects." In *Proceedings of Reglermöte*. Gothenburg, Sweden.

de Maré L., S. Velut, S. Briechle, C. Wennerberg, C. Cimander, G. Silfversparre, O. Holst and P. Hagander (2004): "Temperature limited fed-batch cultivation with a probing feeding strategy for *Escherichia coli*." In *Proceedings of the Computer Applications in Biotechnology 9th International Symposium*. Nancy, France.

Chapter 5: Large scale and complex medium

This chapter examines the impact of the reactor scale and the medium on the performance of the probing strategy. Performance and limitations of the technique are highlighted using experimental results. When compared to other feeding strategies, good results can be obtained after the first attempts. Additional efforts should however be devoted to the design of the dissolved oxygen controller. It is also shown that the application of the probing strategy can imply a considerable gain of time in process development.

Publications

Velut S., A. Castan, K.A. Short, J.-P. Axelsson, P. Hagander, B.A. Zditosky and C.W. Rysenga (2005): "Probing control for large-scale reactors and complex medium." *Manuscript in preparation*.

Velut S. and L. de Maré, J.-P. Axelsson and P. Hagander (2002): "Evaluation of a probing feeding strategy in large scale cultivations." *Technical report ISRN LUTFD2/TFRT--7601--SE*. Department of Automatic Control, Lund Institute of Technology, Sweden.

Chapter 6: Concluding remarks

The contents of the thesis are summarized and suggestions for future work are given.

Other Publications

Work that is not presented in the thesis but is related to it include

de Maré L., S. Velut, P. Hagander and M. Åkesson (2001): "Feedback control of flow rate from a peristaltic pump using balance measurements." In *Proceedings of the European Control Conference*. Porto, Portugal.

Ramchuran S., E. Nordberg Karlsson, S. Velut, L. de Maré, P. Hagander and O. Holst (2002): "Production of heterologous thermostable glycoside hydrolases and the presence of host-cell proteases in substrate limited fed-batch cultures of *Escherichia coli* BL21(DE3)." In *Applied Microbiology and Biotechnology*.

Norberg Karlsson E., S. Ramchuran, P. Turner, L. de Maré, C. Cimander, S. Velut, Å. Ekman, C. Wennerberg, P. Hagander and O. Holst (2005): "Production of two glycoside hydrolases of thermophilic origin in *E. coli* and analysis of released endotoxins using substrate limited and temperature limited fed-batch cultivation strategies." Submitted to *Journal of Biotechnology*.

Haugwitz S., M. Karlsson, S. Velut and P. Hagander (2005): "Anti-windup in mid-ranging control." Submitted to *44th IEEE Conference on Decision and Control and European Control Conference ECC 2005*.

2

Background

This thesis deals with control strategies for fermentation processes where the bacterium *Escherichia coli* produces recombinant proteins. The purpose of this chapter is to provide background for the following chapters. A brief introduction to fermentation techniques is given, followed by a description of a probing feeding strategy. More information on bioprocess technology in general can be found in the texts [Enfors and Häggström, 1994; Pirt, 1985; Doran, 1998].

2.1 Production of recombinant proteins

Recombinant DNA technology

In recent decades, genetic engineering has been revolutionized by a technique known as recombinant DNA technology. The technique appeared in the 1970s and consists in excising segments of DNA from one species of organism and inserting them into the DNA of another species. The cells with the new genetic material become ”factories” for the production of the protein coded by the inserted DNA. By cultivating the recombinant cells to large numbers, the recombinant protein can be produced in high quantities. The first medical use of a recombinant DNA protein goes back to 1982. A recombinant *E. coli* was cultivated to produce the hormone insulin that was previously available in limited quantities from hogs. Recombinant DNA concerns now a number of industries including medicine, vegetal and animal food production or pollution control.

Cultivation of microorganisms

The biochemical reactions take place in a vessel called bioreactor, containing water, nutrients and cells. There are various types of reactors, each one meeting needs specific to the process of interest. A common reactor is

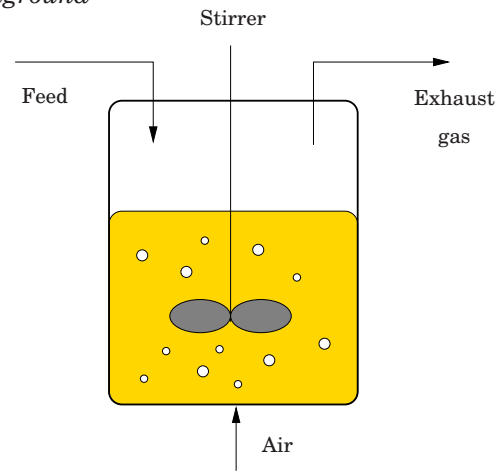

Figure 2.1 Schematic view of a stirred and aerated reactor with incoming feed.

the stirred and aerated reactor shown in Figure 2.1. In this tank, air is sparged at the bottom and mixing is achieved mechanically by impellers.

The reactor broth should contain all the nutrients necessary for cell growth and product synthesis. There are two kinds of media: defined and complex. A defined medium consists of various components, each of them being chemically well-characterized. The development of such a medium is a long process that can be facilitated by considering the cell and product composition. The carbon source is often a sugar such as glucose. A complex medium contains nutrients that are not completely well-defined, such as yeast extract or molasses, that can vary in composition or quality. The benefits of using complex media may be enhanced productivity or lower cost but it can also give less reproducible fermentation results.

To provide environmental conditions suitable for growth and production, reactors are equipped with instruments for monitoring and control of essential parameters. Feedback control is commonly used to regulate parameters such as pH, temperature, agitation speed or feed-flow rate. Another important factor affecting reactor performance is the mode of operation. There are three different modes: batch, fed-batch and continuous. A batch process operates as a closed system: nutrients are added at the beginning of the fermentation and products are removed only at the end. Nothing but air enters the reactor during the cultivation. In a fed-batch reactor, feed is added at a limiting rate in order to supplement the contents of the reactor. Except for the exhaust gas, nothing leaves the reactor before the end of the cultivation. A continuous reactor operates in

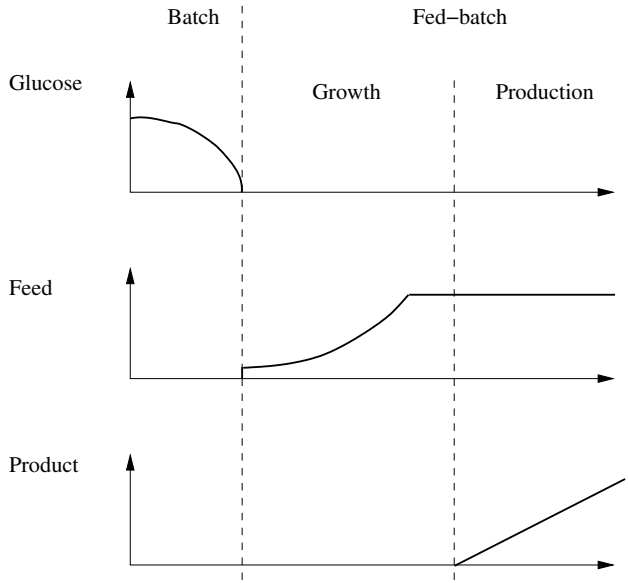

Figure 2.2 A reactor operating in fed-batch mode begins with a batch phase. After depletion of the initial glucose, feed is added at a limiting rate to avoid inhibitory concentrations. The fed-batch phase is often divided into a growth phase and a production phase.

a stationary state where the inlet flow is in balance with the outlet flow. The fed-batch mode is commonly used for high cell density cultures. A typical profile for a fed-batch cultivation is shown in Figure 2.2. The fermentation begins with a batch phase. After depletion of the initial glucose amount, additional glucose is fed to the reactor, at a limiting rate. The cell density grows exponentially and the feed rate is adjusted to meet the growing glucose demand. The oxygen transfer capacity of the reactor may become limiting and the feed rate cannot be increased any more. When the cell density is sufficiently high, the expression phase is started, often by addition of a chemical agent. The starting time of the protein synthesis is often referred as ”induction”.

Process development

In recombinant DNA biotechnology, many steps are required to convert the idea of a product into a commercial reality. A broad range of disciplines are involved in this long process. The first steps in the process development is concerned with cloning. Major concerns of this stage are

the stability of the recombinant organism and the level of expression of the target product, often a protein. Determination of the growth and production characteristics represents the second phase of the process. Small-scale cultures in shake flasks are first carried out in order to determine the optimal environmental conditions. After that, the scale-up process commences by cultivating the cells in a small-scale reactor (from one to two liters). Various measurements are perfomed and further cultivation conditions are optimized. The expression capability of the organism is assessed for evaluation of the economical feasibility of the process. Then, the system is again scaled-up to a pilot-scale reactor with volume of several hundred liters. Many scale-related factors such as mixing or the control configuration may have an impact on the productivity of the process. Economical issues are once again considered before the technology transfer to an industrial-scale bioreactor.

The fermentation is followed by a recovery step with the objective to isolate and purify the desired product from the culture broth. This step, also called downstream processing, can account for a substantial part of the total production cost. It is thus important to optimize the fermentation process for an efficient and inexpensive isolation procedure. Finally, before the release of the product onto the market, clinical trials as well as thorough controls by regulatory authorities are carried out.

2.2 Fed-batch cultivation of *Escherichia coli*

A common host for recombinant protein production is the bacterium *Escherichia coli*. It is well characterized and it can be quickly grown to high cell densities. The fed-batch technique is an efficient way for maximizing both cell mass and foreign protein concentration.

A drawback when using *E. coli* is the formation of acetic acid that has been reported to reduce both growth [Luli and Strohl, 1990] and product formation [Bauer *et al.*, 1990; Bech Jensen and Carlsen, 1990]. Acetate can be formed in two situations:

- Under anaerobic conditions, that is when the dissolved oxygen concentration is low
- Under fully aerobic conditions by overflow metabolism, that is when the carbon source, often glucose, is in excess.

Acetate is metabolized when glucose is no longer in excess, see [Prieto *et al.*, 2004].

Various methods have been developed to avoid acetate accumulation, see for instance [Lee, 1996; Yee and Blanch, 1992]. The feeding profile has

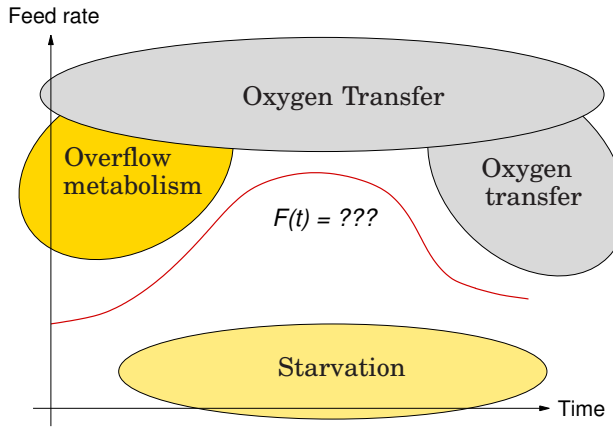

Figure 2.3 Illustration of the typical constraints on the feed rate $F(t)$ in a *E. coli* fed-batch cultivation.

a great impact on the fermentation results, see [Zabriskie *et al.*, 1987]. Figure 2.3 illustrates the typical constraints on the feed rate in a fed-batch cultivation. At an early stage, when the cell density is low, the feed rate is mainly limited by the overflow metabolism. As the cells grow, the feed rate can be gradually increased, eventualy to the point where the oxygen transfer capacity of the reactor is limiting. In that case, the feed rate is kept approximately constant to maintain aerobic conditions. In connection with induction, changes in the process may lead to overfeeding [Qiu *et al.*, 1998] and result in acetate accumulation. When the fermentation is run for a long time at the maximum oxygen transfer capacity of the reactor, the low feed rate relative to the cell density can lead to starvation.

Control problem

The feeding strategy should maximize the feed flow rate while avoiding anaerobic conditions and overflow metabolism. Aerobic conditions can be guaranteed by controlling the dissolved oxygen concentration in the bioreactor to a sufficiently high level. Agitation speed can for instance be used for that purpose. The main difficulty consists in finding the optimal feed rate. High feed rates result in short cultivation times, thereby high productivity, but may lead to overfeeding. The critical glucose concentration, above which the respiratory capacity of the cells saturates and acetate is produced, is unknown and may vary during a cultivation. Furthermore, accurate online measurement of such low glucose concentrations is not

available. The time-varying and uncertain nature of the process makes the control task even more difficult. For good robustness properties, the strategy should be simple and be based on standard measurements.

Model

We consider a bioreactor running in fed-batch mode. Air is sparged into the reactor and the dissolved oxygen concentration is controlled by manipulation of the agitation speed. The model described below is a simple model that does not take the acetate concentration into account. The full model inspired by [Xu *et al.*, 1999], and used in some simulations can be found in [Åkesson *et al.*, 2001c].

Mass balances. The mass balance equations for the media volume V, the cell concentration X, the glucose concentration G, and the dissolved oxygen concentration C_o are

$$\begin{aligned} \frac{dV}{dt} &= F \\ \frac{d(VX)}{dt} &= \mu(G)VX \\ \frac{d(VG)}{dt} &= FG_{in} - q_g(G)VX \\ \frac{d(VC_o)}{dt} &= K_La(N)V(C_o^* - C_o) - q_o(G)VX \end{aligned} \tag{2.1}$$

where F, G_{in}, K_La and C_o^* are the feed flow rate, the glucose concentration in the feed, the volumetric oxygen transfer coefficient and the oxygen concentration in equilibrium with the oxygen in gas bubbles, respectively. Further, μ, q_o and q_g denote the specific rates for growth, oxygen uptake, and glucose uptake.

Metabolic relations. The glucose uptake rate is supposed to follow a Monod type law,

$$q_g(G) = q_g^{max}\frac{G}{k_s + G} \tag{2.2}$$

The specific oxygen uptake rate is modeled by

$$q_o = \min(Y_{og}q_g, q_o^{max}) = \begin{cases} Y_{og}q_g & q_g < q_g^{crit} \\ q_o^{max} & q_g > q_g^{crit} \end{cases} \tag{2.3}$$

The critical specific glucose uptake rate $q_g^{crit} = \dfrac{q_o^{max}}{Y_{og}}$ defines the limit for overfeeding. Above q_g^{crit} the respiratory capacity of the cells saturates and the byproduct acetate is produced.

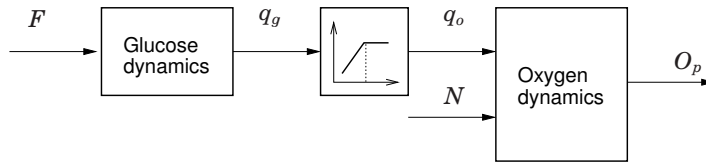

Figure 2.4 Simplified model of the fed-batch reactor. The inputs are the feed flow rate F and the agitation speed N. The measured output is the dissolved oxygen tension O_p. The specific rates for glucose and oxygen consumption, respectively denoted by q_g and q_o, are not measurable.

Most sensors measure the dissolved oxygen tension O instead of the dissolved oxygen concentration C_o. They are related by Henry's law

$$O = HC_o \tag{2.4}$$

The dynamics in the oxygen probe can also be taken into account and it is modeled by a first order system with time constant T_p:

$$T_p \frac{dO_p}{dt} + O_p = O \tag{2.5}$$

Linearization. During short periods of time, the volume V and the biomass X are approximately constant. The variations in the dissolved oxygen tension and in the glucose concentration are described by

$$\begin{aligned} T_g \frac{d\Delta G}{dt} + \Delta G &= K_g \Delta F \\ T_o \frac{d\Delta O}{dt} + \Delta O &= K_N \Delta N + K_o q_o(\Delta G) \end{aligned} \tag{2.6}$$

where

$$\begin{aligned} T_g &= \left(X \frac{\partial q_g}{\partial G} \right)^{-1} \qquad K_g = \left(\frac{VX}{G_i} \frac{\partial q_g}{\partial G} \right)^{-1} \qquad K_o = -HX(K_L a)^{-1} \\ T_o &= (K_L a)^{-1} \qquad K_N = \frac{\partial K_L a}{\partial N}(O^* - O)(K_L a)^{-1} \end{aligned} \tag{2.7}$$

In Figure 2.4 a block-diagram of the linearized model is shown.

Process variations. At the beginning of the fermentation, the cell density is low and the time constant T_g is large. The input dynamics is consequently dominant. At the end of the cultivation, the oxygen probe at the output represents the dominating dynamic.

The increasing biomass has an effect on the gains K_o and K_g, which can be written as

$$K_o = K_o^0 X \tag{2.8}$$
$$K_g = K_g^0 X^{-1} \tag{2.9}$$

Neglecting the glucose dynamics we get

$$\begin{aligned} K_o q_o(\Delta G) &= K_o \min(Y_{og} K_g \Delta F, q_o^{max}) \\ &= K_o^0 X \min(Y_{og} K_g^0 X^{-1} \Delta F, q_o^{max}) \\ &= K_o^0 \min(Y_{og} K_g^0 \Delta F, X q_o^{max}) \end{aligned} \tag{2.10}$$

which implies that the effect of an increasing biomass can be viewed as an increase in q_o^{max}.

2.3 A probing feeding strategy

Principles

The probing feeding strategy described in [Åkesson and Hagander, 2000] can be used to avoid acetate accumulation. The idea of the probing approach is to detect the saturation of the respiration, and thereby the onset of acetate formation. This is done by superimposing short pulses in the feed, see Figure 2.5. The size of the pulse response, which depends on the local gain of the nonlinearity, is used to adjust the control signal, namely the glucose feed rate:

- When the response in the dissolved oxygen is large enough, the feed rate is increased proportionally to the size of the pulse response.
- When there is no visible response in the dissolved oxygen, the feed rate is decreased with a fixed proportion.

The dissolved oxygen is controlled between the pulses using the stirrer speed. During a feed pulse the stirrer speed is frozen to make it easier to quantify the response in the dissolved oxygen signal.

When the maximum oxygen transfer capacity of the reactor is reached, *i.e.* the maximum stirrer speed, the probing feeding strategy decreases the feed rate to keep the reactor working under aerobic conditions. The decrease is made at a constant rate:

$$\frac{dF}{dt} = -\gamma F$$

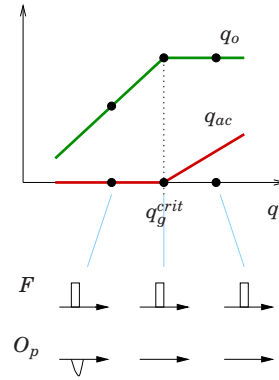

Figure 2.5 The superimposed pulses in the glucose feed rate F affect the glucose uptake rate q_g. When glucose is limiting, variations in the oxygen uptake q_o can be clearly seen in the dissolved oxygen measurement O_p. In this way acetate formation can be detected.

Experiment

The control algorithm has been implemented on real plants where good performance could be achieved, see for instance [Åkesson *et al.*, 2001a], [de Maré *et al.*, 2003]. The controller is able to adapt to process changes such as variations in the maximum oxygen uptake rate, that typically occur when the foreign protein starts to be produced. Figure 2.6 shows a part of an experiment using the probing strategy. The feed started after depletion of the initial batch glucose, detected by a peak in the dissolved oxygen signal. The feed is thereafter increased by the feedback algorithm to meet the glucose demand of the growing biomass. At two occasions, the feed is decreased because of the absence of a clear pulse response. This is a good illustration of the sensitivity of the cells to glucose feeding and it demonstrates the ability of the strategy to adapt to the time-varying demand in glucose. Good dissolved oxygen control is required for the strategy to work well. A PID controller, gain-scheduled with respect to the stirrer speed was implemented to get good performance throughout the cultivation [Åkesson and Hagander, 1999]. A good control of the feed flow entering the reactor is also a necessity. Exact dosing and fast setpoint following are essential conditions in order to perform short and small pulses in the feed. When flow measurements are not available, it is possible to use balance data for observer-based control of the feed rate, see [de Maré *et al.*, 2001].

The efficiency of the probing feeding strategy has been demonstrated by many experimental results. The reproducibility of the technique makes it an ideal optimization tool when investigating the influence of a specific

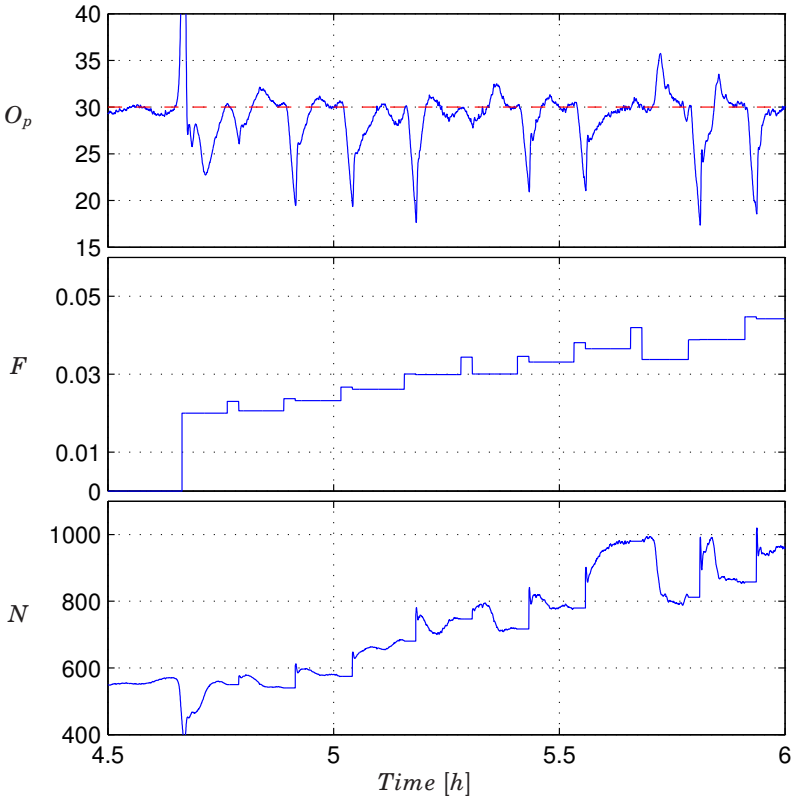

Figure 2.6 Detail of a fed-batch experiment using the probing strategy. From top to bottom: dissolved oxygen tension (O_p, [%]), feed flow rate (F, $[lh^{-1}]$) and stirrer speed (N, [rpm]). A cycle consists of a probing phase with length T_p and a control phase with length T_c. During the control phase, dissolved oxygen is brought back to the setpoint value 30%.

cultivation parameter. The feed strategy was used for instance to investigate how cell-mass concentration at the time of induction influences the protein production, see [Ramchuran *et al.*, 2002].

3

Analysis and Tuning of the Probing Strategy

3.1 Introduction

In the background chapter, a substrate feeding technique for *Escherichia coli* fed-batch fermentation was presented. The control strategy is simple and requires a minimum of process information. It has been implemented on various platforms with successful results [Åkesson, 1999].

The probing technique is a powerful tool to fully exploit the capacity of a process while operating in a safety region. The control strategy was used in various contexts for online optimization of processes with limited capacity. A pulse technique for feed rate control in an activated sludge process was early proposed in [Yongaçoglu *et al.*, 1982]. In [Liu *et al.*, 2004], the probing technique was applied to an anaerobic digestion process for wastewater treatment. By driving the plant to its maximum capacity, performance could be optimized online. Ethanol production by fermentation of materials containing toxic compounds is another application where the probing strategy has given results, see [Taherzadeh *et al.*, 2000]. The probing pulses can also be performed for identification purposes as in [Lin *et al.*, 2001].

In spite of its simplicity, the control strategy results in a complex closed-loop system that is nonlinear and time-varying, with continuous as well as discrete states. Rigorous analysis of the closed-loop system is valuable for a better understanding and tuning of the probing controller. In [Åkesson *et al.*, 2001c], stability conditions for the closed-loop system are derived. The process dynamics is however not taken into account and the analysis is only local.

The objective of the chapter is to study the properties of the probing

controller in order to help the user for the design. Simple process models, inspired by Section 2.2 will be considered. The convergence properties of the technique and its ability to track a time-varying saturation will be examined. The analysis should lead to a better insight into the probing technique. The achievable performance and the influence of the process dynamic are examples of issues to be adressed.

Related work

The idea of introducing deliberate perturbations to get information on a process for control purposes is related to the area of extremum and dual control. In extremum control, the optimal setpoint is not known and is often given by the extremum of a static input-output map. The classical approach to this problem consists in adding a known time-varying signal to the process input and correlating the output with the perturbation signal to get information about the nonlinearity gradient. The controller continuously adjusts the control signal towards the optimum. An introduction to extremum control can be found in [Åström and Wittenmark, 1995] and a good overview is provided in [Sternby, 1980]. Many successful applications of extremum control have been reported in the literature, see for instance [Dumont and Åström, 1988], [Gäfvert *et al.*, 2004], [Wang *et al.*, 2000], [Popovic *et al.*, 2003].

Extremum control was a popular research topic of the control community in the 1960s. Few analyses of the self-optimizing scheme using the perturbation method are available in the literature. In [Krstic and Wang, 1997], the authors present stability analysis of an extremum seeking scheme for a general nonlinear dynamical system. Stability of the scheme is proven under restrictive conditions: small adaptation gain and fast plant dynamic. In [Krstic, 2000], a tighter analysis where the process is modelled by a Wiener-Hammerstein system is given. No stability region is provided. Recently, [Guay and Zhang, 2003] proposed an observer-based extremum-seeking scheme together with stability analysis using Lyapunov theory. The same approach was applied for the control of a continuous tank bioreactor, see [Marcos *et al.*, 2004]. [Teel and Popovic, 2001] propose an extremum-seeking method using discrete-time nonlinear programming algorithms. Assuming stability for the static plant and regarding the plant dynamic as a deviation from the static case, convergence properties of the scheme can be proven.

3.2 Closed-loop system representation

The interconnection of a process described by (2.6) with the probing controller is rather complex, but analysis is feasible when some dynamics are

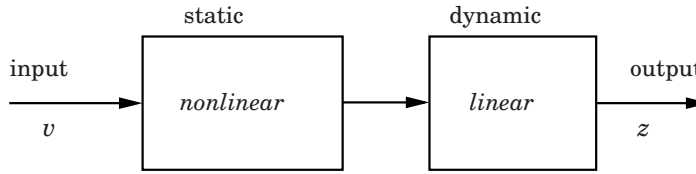

Figure 3.1 Hammerstein model with input v and output z.

neglected. The periodic nature of the total controller, with one regulation phase followed by a probing phase, suggests a sampled-data description.

Process model

For now, we assume that the process is a Hammerstein model: a static nonlinearity followed by a dynamical linear process, see Figure 3.1. The case of input dynamics will be studied later. A state-space representation of the process can be written as

$$\begin{aligned} \dot{x} &= Ax + Bf(v) \quad x \in R^n \\ z &= Cx \end{aligned} \tag{3.1}$$

The control objective is to find and track the optimal setpoint v defined by the nonlinear function f. The nonlinearity f could for instance present an extremum that one wants to locate. It will be assumed that A has all its eigenvalues in the open left half-plane. No extra process input for output control will be considered unless stated differently.

Probing controller

The probing controller gets information about the nonlinearity from pulses that are periodically superimposed to the control signal. The input signal v to the process is the sum of the piecewise constant signal u_k and the perturbation signal $u_p(t)$:

$$v(t) = u_k + u_p(t) \qquad t \in [kT,\ kT + T] \tag{3.2}$$

Here, $u_p(t)$ is a pulse train with period T and amplitude u_p^0:

$$u_p(t) = \begin{cases} 0 & t \in [kT,\ kT + T_c) \\ u_p^0 & t \in [kT + T_c, (k+1)T) \end{cases} \tag{3.3}$$

T_c is the duration of the waiting phase, while T_p is the length of the probing pulse. We have the equality

$$T = T_c + T_p \tag{3.4}$$

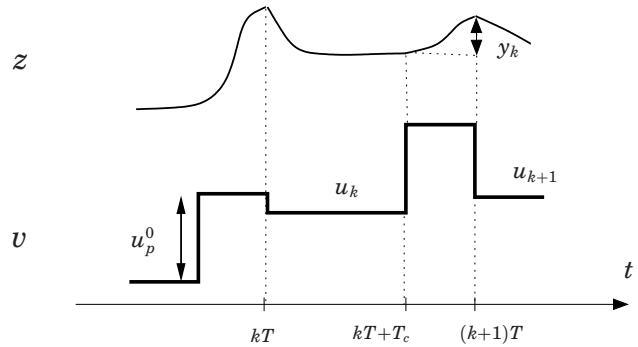

Figure 3.2 Illustration of the probing controller. A pulse in the input signal v leads to a response in the output z. The size y_k of the pulse response is used to compute the change $u_{k+1} - u_k$.

The piecewise constant control signal u_k is adjusted at the end of every pulse, depending on the size y_k of the pulse response, see Figure 3.2 for a graphical illustration. The control variable u_k is the output of a linear discrete-time system with sampling interval T:

$$\begin{aligned} \xi_{k+1} &= A_p \xi_k + B_p y_k \\ u_k &= C_p \xi_k + D_p y_k \end{aligned} \tag{3.5}$$

Response to a pulse

We will now derive a discrete-time representation of the response y_k to the pulse number k, defined by

$$y_k = z(kT + T) - z(kT + T_c) \tag{3.6}$$
$$= Cx(kT + T) - Cx(kT + T_c) \tag{3.7}$$

Integration over a probing cycle. A probing cycle starts with a waiting phase, that can possibly be used to control the output z to a desired value. The process input v is kept constant at u_k during a time interval with length T_c:

$$\dot{x} = Ax + Bf(u_k) \qquad t \in [kT, kT + T_c) \tag{3.8}$$

After integration between kT and $kT + T_c$, we get

$$x(kT + T_c) = A_{d1} x(kT) + (A_{d1} - I) d f(u_k) \tag{3.9}$$

where A_{d1} and d are given by $A_{d1} = e^{AT_c}$ and $d = A^{-1}B$. During the probing phase with length T_p, a pulse of size u_p^0 is performed in the input v:

$$\dot{x} = Ax + Bf(u_k + u_p^0) \qquad t \in [kT + T_c, kT + T) \tag{3.10}$$

After integration between $kT + T_c$ and $kT + T$, we get

$$x(kT + T) = A_{d2}x(kT + T_c) + (A_{d2} - I)df(u_k + u_p^0) \tag{3.11}$$

where A_{d2} is given by $A_{d2} = e^{AT_p}$. From Equations (3.9) and (3.11) it is possible to express y_k as the output of a discrete-time system with sample interval T:

$$\begin{aligned} x_{k+1} &= A_{tot}x_k + B_{tot}\begin{bmatrix} f(u_k) \\ f(u_k + u_p^0) \end{bmatrix} \\ y_k &= C_{tot}x_k + D_{tot}\begin{bmatrix} f(u_k) \\ f(u_k + u_p^0) \end{bmatrix} \qquad x_k = x(kT) \end{aligned} \tag{3.12}$$

where the linear part $G_{tot} = (A_{tot}, B_{tot}, C_{tot}, D_{tot})$ is defined by

$$\begin{aligned} A_{tot} &= A_{d2}A_{d1} & B_{tot} &= [\,A_{d2}(A_{d1} - I)d \quad (A_{d2} - I)d\,] \\ C_{tot} &= C(A_{d2} - I)A_{d1} & D_{tot} &= C(A_{d2} - I)\,[\,(A_{d1} - I)d \quad d\,] \end{aligned} \tag{3.13}$$

G_{tot} can also be represented by the transfer function

$$G_{tot}(z) = C(A_{d2} - I)(zI - A_{d1}A_{d2})^{-1}\,[\,z(A_{d1} - I)d \quad (zI - A_{d1})d\,] \tag{3.14}$$

This discrete-time representation will be very useful for the analysis. Similar representations can be obtained when output control takes place between the pulses, or in the case of an output nonlinearity, see Appendix A.1.

Input transformation. To facilitate the analysis in the coming sections, we express y_k as

$$y_k = G_1(z)f(u_k) + G_2(z)(f(u_k + u_p^0) - f(u_k)) \tag{3.15}$$

where

$$G_2(z) = G_{tot}(z)\begin{bmatrix} 0 \\ 1 \end{bmatrix} \tag{3.16}$$

$$G_1(z) = G_{tot}(z)\begin{bmatrix} 1 \\ 1 \end{bmatrix} \tag{3.17}$$

and using (3.14)

$$\begin{bmatrix} G_1(z) \\ G_2(z) \end{bmatrix}^T = C(A_{d2} - I)(zI - A_{d1}A_{d2})^{-1}\,[\,(zA_{d1} - A_{d1})d \quad (zI - A_{d1})d\,] \tag{3.18}$$

Closed-loop system

Equations (3.5) and (3.12) describe the closed-loop system obtained by interconnecting the plant (3.1) with the probing controller. The augmented state is $X_k = [\,x_k \quad \xi_k\,]^T$ and a state space representation is given by

$$\begin{aligned} X_{k+1} &= A_{closed}X_k + B_{closed}\begin{bmatrix} f(u_k) \\ f(u_k+u_p^0)-f(u_k)\end{bmatrix} \\ u_k &= C_{closed}X_k \end{aligned} \tag{3.19}$$

where

$$A_{closed} = \begin{bmatrix} A_{tot} & 0 \\ B_pC_{tot} & A_p\end{bmatrix} \qquad B_{closed} = \begin{bmatrix} B_{tot}T^{-1} \\ B_pD_{tot}T^{-1}\end{bmatrix}$$
$$C_{closed} = [\,D_pC_{tot} \quad C_p\,] \qquad T^{-1} = \begin{bmatrix} 1 & 0 \\ 1 & 1\end{bmatrix}$$

3.3 Equilibrium point and static gain analysis

A static analysis of the discrete-time representation can be made to characterize the equilibrium points of the closed-loop system.

Static gain

The static gains of the transfer functions G_1 and G_2 can be easily computed from (3.18)

$$G_1(1) = 0 \tag{3.20}$$
$$G_2(1) = C(A_{d2}-I)(I-A_{d1}A_{d2})^{-1}(I-A_{d1})d \triangleq \beta \tag{3.21}$$

Note that $I-A_{d1}A_{d2}$ is invertible as it was assumed that the process (3.1) does not have any pole at the origin. Using (3.15) the stationary probing pulse response $y_\infty(u)$ becomes

$$y_\infty(u) = \beta(f(u+u_p^0)-f(u)) \tag{3.22}$$

Equilibrium point

Convergence to an extremum. Assume now that f is a strictly concave function presenting a maximum at $u = u^*$. If the control law (3.5) contains an integrator and $\beta \neq 0$, then the closed-loop system has a unique equilibrium (x_∞, u_∞) and $u_\infty \in [u^*-u_p^0, u^*+u_p^0]$.

Remark 1: The existence of an equilibrium follows from the strict monotonicity of $y_\infty(u)$ in (3.22), which also vanishes for a unique u.
Remark 2: The condition $\beta \neq 0$ means that $G_2(z)$ has no zero at $z = 1$, that would cancel out with the integrator pole from the control law.
Remark 3: Concavity of f is sufficient but not necessary for the uniqueness of the equilibrium point.

Convergence to a saturation. The nonlinear functions f of interest in our application are saturation-type functions, without any extremum point. The aim is then to drive the system close to the saturation. Driving a process to an extremum or a saturation are actually similar problems. Using an integrating feedback law with setpoint y_r as the desired pulse response:

$$u_{k+1} = u_k + K(y_k - y_r) \tag{3.23}$$

the equilibrium point would be (x_∞, u_∞) such that

$$\beta(f(u_\infty + u_p^0) - f(u_\infty)) = y_r \tag{3.24}$$

or equivalently when $\beta \neq 0$

$$g(u_\infty + u_p^0) - g(u_\infty) = 0 \qquad g(u) = f(u) - \frac{y_r}{\beta u_p^0} u \tag{3.25}$$

When f is a saturation-like function and $y_r > 0$ is appropriately chosen, g presents an extremum point close to the saturation level. The reference value y_r can be viewed as introducing a possibility to drive the system to a point of the static input-output map f with a specific slope:

$$\frac{df}{du}(u_\infty) \approx \frac{y_r}{\beta u_p^0} \tag{3.26}$$

The static analysis indicates that the probing strategy can drive a process to the best operating point. Do we have convergence to the optimal point when the dynamics from the process and the controller are taken into account? Is the probing strategy able to track a time-varying nonlinearity?

3.4 Tools for piecewise affine analysis

The nonlinearity f of interest in the bioreactor example is modeled by a piecewise affine function. The closed-loop equations described by (3.19)

have consequently a piecewise affine structure. Stability analysis can be performed by searching for piecewise quadratic Lyapunov functions as in [Johansson, 1999]. When the probing controller (3.5) has integral action, modifications of the existing methods are necessary to investigate global asymptotic stability. As every Lyapunov function approach, it provides sufficient but not necessary conditions for stability. It will be shown in Section 3.5 that the approach is not conservative when applied to particular examples. This section does not give more insight into the probing technique, but it presents tools that will be helpful to investigate global stability and performance of the closed-loop system.

A discrete piecewise affine system can be represented as

$$X^+ = A_i X + a_i \qquad \text{for } X \in \mathbf{X}_i \tag{3.27}$$

where $\mathbf{X}_i \subseteq R^n$ is a partition of the state space into operating regimes. Every region $\mathbf{X}_i$ is associated with a linear dynamic defined by A_i and a_i. The regions will be assumed to be polyhedral, defined by a series of hyperplanes. Matrices E_i and vectors e_i are describing the region $\mathbf{X}_i$:

$$\mathbf{X}_i = \{X \in R^n,\ E_i X + e_i \succeq 0\} \tag{3.28}$$

The inequality is componentwise. For convenient treatment of affine terms in (3.27), the state vector X can be extended to

$$\bar{X} = \begin{bmatrix} X \\ 1 \end{bmatrix} \tag{3.29}$$

Equation (3.27) can thereby be rewritten as

$$\bar{X}^+ = \bar{A}_i \bar{X} \qquad \text{for } \bar{X} \in \mathbf{X}_i \tag{3.30}$$

with

$$\bar{A}_i = \begin{bmatrix} A_i & a_i \\ 0 & 1 \end{bmatrix} \tag{3.31}$$

We assume that there is only one equilibrium point, and that it is located in the region with index $i = i_0$. The origin is shifted such that $a_{i_0} = 0$, *i.e.* the equilibrium point is $X = 0$.

Stability analysis

The search for piecewise quadratic Lyapunov functions as in [Ferrari-Trecate *et al.*, 2001] and [Johansson, 1999] is a powerful tool for stability analysis. Denote by V the Lyapunov function candidate:

$$V(X) = \begin{cases} X^T P_i X & X \in \mathbf{X}_i \quad i = i_0 \\ \bar{X}^T \bar{P}_i \bar{X} & X \in \mathbf{X}_i \quad i \neq i_0 \end{cases} \tag{3.32}$$

For V to be a Lyapunov function, one should have for $i \neq i_0$:

$$\begin{aligned} V(X) &= \bar{X}^T \bar{P}_i \bar{X} > 0 && X \in \mathbf{X}_i \\ \Delta V(X) &= \bar{X}^T ({\bar{A}_i}^T \bar{P}_j \bar{A}_i - \bar{P}_i) \bar{X} < 0 && X \in \mathbf{X}_i, \quad X^+ \in \mathbf{X}_j \end{aligned} \tag{3.33}$$

and similarly for $i = i_0$. The search for the matrices $\bar{P}_i$ can be formulated as an optimization problem in terms of linear matrix inequalities (LMIs). The stability conditions (3.33) take the form of a LMI problem in $\bar{P}_i, U_i$ and W_{ij}:

$$\begin{aligned} &\bar{P}_i - {\bar{E}_i}^T U_i \bar{E}_i > 0 \\ &{\bar{A}_i}^T \bar{P}_j \bar{A}_i - \bar{P}_i + \bar{E}_{ij}^T W_{ij} \bar{E}_{ij} < 0 \end{aligned} \tag{3.34}$$

where the symmetric matrices U_i and W_{ij} have non-negative entries. The terms ${\bar{E}_i}^T U_i \bar{E}_i$ and $\bar{E}_{ij}^T W_{ij} \bar{E}_{ij}$ are used in the S-procedure [Boyd *et al.*, 1994] and they express the fact that the inequalities (3.33) are only required to hold for particular X, e.g. X in $\mathbf{X}_i$. More details can be found in [Johansson, 1999]. A solution to (3.34) implies the existence of $\gamma > 0$ such that

$$\Delta V(X) < -\gamma \|X\|^2, \quad \text{for all } X \tag{3.35}$$

When the state partition contains an unbounded region $\mathbf{X}_i$ with an integrator in A_i, it may not be possible to bound ΔV quadratically in all directions although it is strictly negative. Modifications of equations (3.34) for the regions with integrator are therefore necessary to prove asymptotic stability. Our approach is similar to that for linear systems in [Boyd *et al.*, 1994] and consists in deriving a reduced LMI set after removal of implicit equality constraints. Consider a region $\mathbf{X}$ of the state partition, where the dynamics contains an integrator. By a change of coordinates $Z = T^{-1}X$, the dynamics equation in $\mathbf{X}$ can be put in the form:

$$\bar{Z}^+ = \left[\begin{array}{cc|c} A_s & 0_{n-1\times 1} & T^{-1}a \\ 0_{1\times n-1} & 1 & \\ \hline 0_{1\times n-1} & 0 & 1 \end{array}\right] \bar{Z}, \qquad \bar{Z} = \left[\begin{array}{c} z_s \\ z_u \\ \hline 1 \end{array}\right]$$

where A_s has all its eigenvalues in the open unit disc. Defining $\bar{T} = \text{diag}\{T, 1\}$ and $\bar{Q} = \bar{T}^T P \bar{T}$, one can express $\Delta V(X)$ using the new coordinates $\bar{Z}$:

$$\Delta V(\bar{T}\bar{Z}) = \left[\begin{array}{c} z_s \\ z_u \\ \hline 1 \end{array}\right]^T \left[\begin{array}{cc|c} M_{ss} & M_{su} & M_s \\ M_{su}^T & 0 & m_u \\ \hline M_s^T & m_u & m \end{array}\right] \left[\begin{array}{c} z_s \\ z_u \\ \hline 1 \end{array}\right] \tag{3.36}$$

The absence of quadratic term in z_u is a consequence of the eigenvalue 1. If the region $\mathbf{X}$ is unbounded in the z_u direction, ΔV cannot be globally bounded as in (3.35). The unboundedness of $\mathbf{X}$ in z_u direction can be easily checked: the matrice E in (3.28), describing the region $\mathbf{X}$, should satisfy

$$ET \begin{bmatrix} 0 \\ 1 \end{bmatrix} \preceq 0 \text{ or } ET \begin{bmatrix} 0 \\ 1 \end{bmatrix} \succeq 0 \tag{3.37}$$

In that case, the region can be described without loss of generality by (see Appendix A.2 for more details)

$$\mathbf{X} = \{Z \mid \alpha_j z_u \leq [\, G_j \quad g_j \,] \begin{bmatrix} z_s \\ 1 \end{bmatrix}\} \tag{3.38}$$

where $\alpha_j \in \{0, 1\}$. Denote by I_1 the set $I_1 = \{j, \alpha_j \neq 0\}$ and $p = card\{I_1\}$. Define the constant matrices $H_j \in R^{n+1 \times n}$, $F_j \in R^{n \times p}$ and the vector $l \in R^{2n+2 \times 1}$ by

$$H_j = \begin{bmatrix} I & 0 \\ G_j & g_j \\ 0 & 1 \end{bmatrix} \qquad F_j = \begin{bmatrix} G_1 - G_j & g_1 - g_j \\ \vdots & \vdots \\ G_p - G_j & g_p - g_j \end{bmatrix} \tag{3.39}$$

$$l = [\, 0_{1 \times n-1} \quad 1 \quad 0 \quad 0_{1 \times n-1} \quad 0 \quad 1 \,]^T \tag{3.40}$$

The following result should be combined with (3.34) to investigate asymptotic stability of piecewise affine systems with integrators

THEOREM 3.1
Consider symmetric matrices Q, U and W_j such that $\bar{Q}_{su} = 0_{n-1 \times 1}$, and U, W_j with non-negative entries while $\bar{P} = \bar{T}^{-T} \bar{Q} \bar{T}^{-1}$ satisfies

$$\bar{P} - \bar{E}^T U \bar{E} > 0 \tag{3.41}$$

$$H_j^T \bar{T}^T (\bar{A}^T \bar{P} \bar{A} - \bar{P}) \bar{T} H_j + F_j^T W_j F_j < 0, \text{ for } j \in I_1 \tag{3.42}$$

$$l^T \begin{bmatrix} 0 & \bar{T}^T (\bar{A}^T \bar{P} \bar{A} - \bar{P}) \bar{T} \\ \bar{T}^T (\bar{A}^T \bar{P} \bar{A} - \bar{P}) \bar{T} & 0 \end{bmatrix} l > 0 \tag{3.43}$$

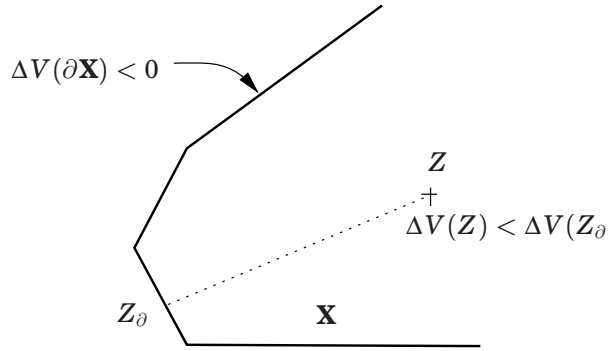

Figure 3.3 Negativity of ΔV in the region $\mathbf{X}$ is proven in two steps. ΔV is strictly negative on the boundary $\partial\mathbf{X}$, and for all $Z \in \mathbf{X}$ there exists $Z_\partial \in \partial\mathbf{X}$ such that $\Delta V(Z) < \Delta V(Z_\partial)$.

then $V(X) > 0$ and $\Delta V(X) < 0$ in $\mathbf{X}$.

Proof: See Appendix A.2. A graphical interpretation of the theorem is shown in Figure 3.3. □

Remark 1: The condition $\bar{Q}_{su} = 0$ is necessary for ΔV to be negative in the unbounded region and it is therefore not conservative.
Remark 2: Along the z_u direction, ΔV is linear and the inequality (3.43) imposes the correct sign of the slope to ΔV.
Remark 3: Since the search for Lyapunov functions is done in terms of $\bar{Q}$, *i.e.* in the new coordinate systems, it is easy to impose $\bar{Q}_{su} = 0$.

Performance analysis

The previous result provides a way to check global stability of piecewise affine systems with integrator, using standard LMI solvers. We will now present a way to assess performance in presence of disturbances or changes in the reference signal.

As in [Solyom and Rantzer, 2002], the servo-problem for a nonlinear system can be analysed in the framework shown in Figure 3.4. The distance between the system trajectory x and a reference trajectory x_r is used to measure the performance. To quantify the influence of a reference change on the error $x - x_r$, the L_2 gain between the time derivative $\dot{r}$ of the input and the error $x - x_r$ can be computed. The idea will be applied to piecewise affine systems in discrete-time. Consider the following piecewise affine system with input r

$$X(k+1) = A_i X(k) + B_i r(k) + a_i \tag{3.44}$$

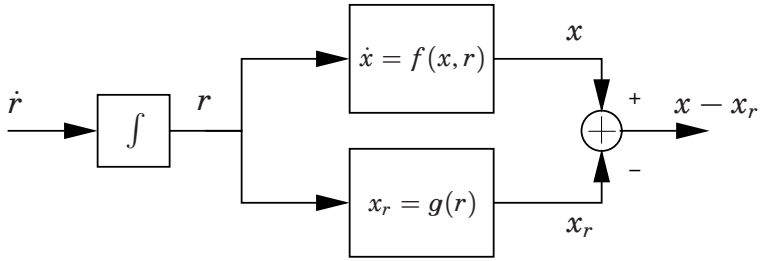

Figure 3.4 Configuration for performance assessement. The servo problem can be examined by looking at the effect of variations at the input r on the distance of x from a desired trajectory x_r.

The region partition may depend on the exogeneous signal $r(k)$. Assuming that for any constant $r \in \mathcal{R}$, the piecewise linear system has a unique equilibrium point located in $\mathbf{X}_{i_0}$, we can define X_r as

$$X_r(k) = (I - A_{i_0})^{-1} B_{i_0} r(k) \tag{3.45}$$

The performance is measured by a quadratic cost function, expressing the distance from X to the desired trajectory X_r:

$$J(X,r) = \sum_{k=0}^{\infty} (\bar{X}(k) - \bar{X}_r(k))^T \bar{Q}_i (\bar{X}(k) - \bar{X}_r(k)) \tag{3.46}$$

Define

$$\bar{A}_i = \begin{bmatrix} A_i & a_i & B_i + (A_i - I)(I - A_{i_0})^{-1} B_{i_0} \\ 0 & 1 & 0 \\ 0 & 0 & 1 \end{bmatrix}$$

$$\bar{B}_i = \begin{bmatrix} -(I - A_{i_0})^{-1} B_{i_0} \\ 0 \\ 1 \end{bmatrix}, \quad \bar{I} = \mathrm{diag}(I, 0, 0)$$

and the matrices $\bar{S}_i$ such that

$$\begin{bmatrix} X - X_r \\ 1 \\ r \end{bmatrix}^T \bar{S}_i \begin{bmatrix} X - X_r \\ 1 \\ r \end{bmatrix} > 0 \text{ for } X \in \mathbf{X}_i, r \in \mathcal{R}$$

After a stability check of (3.44) without exogeneous input, the following statement can be used to assess the performance.

THEOREM 3.2
If there exist $\gamma > 0$ and symmetric matrices $\bar{P}_i$ such that

$$\begin{bmatrix} \bar{A_i}^T \bar{P}_j \bar{A}_i - \bar{P}_i + \bar{Q}_i + \bar{S}_i & (\bar{B_i}^T \bar{P}_j \bar{A}_i)^T \\ \bar{B_i}^T \bar{P}_j \bar{A}_i & \bar{B_i}^T \bar{P}_j \bar{B}_i - \gamma^2 \end{bmatrix} < 0, \quad i, j \neq i_0$$

and similarly for $i = j = i_0$, then every trajectory defined by (3.44) with $X(0) = 0$ and $||r(k+1) - r(k)||_2 < \infty$ satisfies

$$J(X, r) \leq \gamma^2 \sum_{k=0}^{\infty} (r(k+1) - r(k))^2 \tag{3.47}$$

Proof: Similar to [Solyom and Rantzer, 2002]. See Appendix A.2 for a sketch of the proof. □

Remark 1: When the dynamic in some state space region contains an integrator, the corresponding LMI should be adapted as in Theorem 3.1 for a global analysis. Moreover, to get feasible LMIs the cost function J should not penalize quadratically the integrator state in the region with integrator.
Remark 2: The matrices $\bar{A}_i$ and $\bar{B}_i$ are describing the dynamics of $X - X_r$ with $r(k+1) - r(k)$ as input signal.

3.5 Saturation and output dynamic

In this section, we will examine the performance of the probing controller on an example inspired by the reactor model presented in Chapter 2. It is desirable to control the process to a saturation instead of an extremum. The process is assumed to be of the form (3.1). For symbolic computations, a first order process will be considered:

$$\dot{x} = -ax + bf(v) \tag{3.48}$$
$$y = cx \tag{3.49}$$

where $bc > 0$ and $a > 0$. It will also be used in the simulations as well as in the global analysis, together with the numerical values $a = 1,\ b = 1,\ c = 1$. The static nonlinearity f that models the saturation in the cell respiration system is taken to be a min function:

$$f(v) = \min(v, r_k) = \begin{cases} v, & v \leq r_k \\ r_k, & v > r_k \end{cases} \tag{3.50}$$

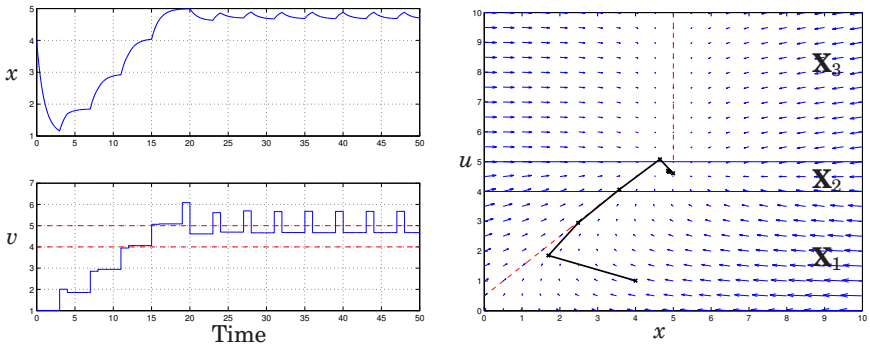

Figure 3.5 A trajectory of the closed-loop system using the numerical values T_c=3, T_p=1, K=2.5, y_r=0.2. Left: trajectory in the time domain. x is the process state and v the process input. Right: trajectory and phase plane of the corresponding discrete-time description. The solid lines are the cell borders and the dashed lines represent the eigendirections corresponding to the eigenvalue 1.

The saturation level r_k will be assumed to be constant during a probing period. An integrating feedback law with gain K and a desired pulse response $y_k = y_r$ will be used:

$$u_{k+1} = u_k + K(y_k - y_r) \tag{3.51}$$

The results from a simulation of the closed-loop system with $r_k = r = 5$ are shown in Figure 3.5 (left). The input v to the process starting below the saturation is gradually increased by the controller. At time $t \approx 15$, the saturation is passed and u is therefore decreased. At stationarity the pulse response is equal to the desired value $y_r = 0.2$ and the controller output u is slightly below the saturation $r = 5$. The closed-loop system described by (3.19) is here given by

$$\begin{aligned} X_{k+1} &= \begin{bmatrix} A_{tot} & 0 \\ KC_{tot} & 1 \end{bmatrix} X_k + \begin{bmatrix} B_{tot}T^{-1} \\ KD_{tot}T^{-1} \end{bmatrix} \begin{bmatrix} \min(u_k, r_k) \\ \min(u_k + u_p^0, r_k) - \min(u_k, r_k) \end{bmatrix} \\ &\quad + \begin{bmatrix} 0 \\ -Ky_r \end{bmatrix} \\ u_k &= [\,0 \quad 1\,]\, X_k \end{aligned} \tag{3.52}$$

This is actually a piecewise affine system with a state space partitioned into three regions:

$$\begin{aligned} \mathbf{X}_1 &= \{X_k,\ u_k - r_k < -u_p^0\} \\ \mathbf{X}_2 &= \{X_k,\ -u_p^0 < u_k - r_k < 0\} \\ \mathbf{X}_3 &= \{X_k,\ u_k - r_k > 0\} \end{aligned}$$

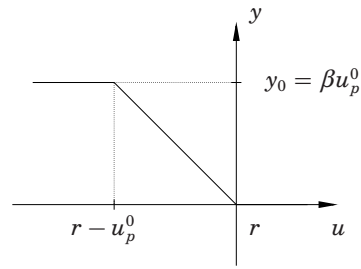

Figure 3.6 Stationary amplitude of the pulse response y as a function of the input u. Small responses indicate that u is close to the saturating point r.

The first and the third regions are associated to input signals v that are below, respectively above the saturation level. The middle region describes the case where v is below the saturation during the control phase and above during the probing pulse. The system equations can be written as

$$X_{k+1} = A_i X_k + B_i r_k + a_i, \quad \text{for} \quad X_k \in \mathbf{X}_i, \quad i \in I = \{1, 2, 3\} \tag{3.53}$$

where the matrices A_i, B_i and a_i are given in Appendix A.3. The dynamic in the extreme regions always contains an integrator. Figure 3.5 (right) shows the phase plane of the discrete-time description together with a trajectory $X_k = (x_k, u_k)$. According to the phase plane all trajectories seem to converge to a point close to the saturation level.

Equilibrium point

The stationary amplitude of the pulse response $y_\infty(u)$ corresponding to Equation (3.22) is plotted in Figure 3.6. It is assumed that r_k is a constant equal to r. When the desired pulse response y_r is in the interval

$$0 < y_r < \beta u_p^0 \tag{3.54}$$

there is a unique equilibrium point $X_\infty = (x_\infty, u_\infty)$ and it is such that

$$u_\infty = r - \frac{y_r}{\beta} \tag{3.55}$$

From (3.54) and (3.55), it is clear that the equilibrium point is always located in the middle region $\mathbf{X}_2$.

$$x_\infty = (I - A_{tot})^{-1} B_{tot} \begin{bmatrix} r - \frac{y_r}{\beta} \\ r \end{bmatrix} \tag{3.56}$$

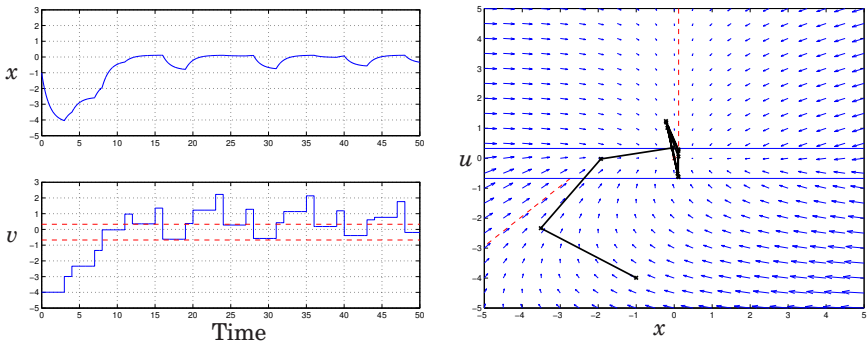

Figure 3.7 Oscillatory behaviors are observed when the probing gain is large. The long stays above the saturation may have dramatic consequences on the system performance. The numerical values used for the simulation are T_c=3, T_p=1, K=5, y_r=0.2.

Stability analysis

The saturating point r_k will be assumed to be constant for the stability analysis. A time-varying r_k will be considered later when assessing the performance of the probing technique. Figure 3.7 shows how the choice of the probing controller gain K influences the closed-loop performance. Large K values can lead to oscillatory behavior with long time intervals of operation above the saturation, which may be harmful for the process. First we will derive necessary conditions for stability, based on local analysis in every region. Those conditions will then be compared with the global stability test from Section 3.4.

Local analysis. The first order model (3.49) is used to derive symbolic constraints on the probing parameters. Local stability of the equilibrium point can be investigated by looking at the dynamic in $\mathbf{X}_2$. A necessary and sufficient condition for local stability takes the form (see Appendix A.3):

$$0 < K\beta < 2\frac{1+e^{-aT}}{1-e^{-aT}} \tag{3.57}$$

where β is given by

$$\beta = \frac{bc}{a}(1-e^{-aT_p})(1-e^{-aT_c})(1-e^{-aT})^{-1} \tag{3.58}$$

Condition (3.57) provides an upper bound for the probing controller gain K depending on the process characteristics. It is however not sufficient to guarantee convergence of the closed-loop system. When the frequency of

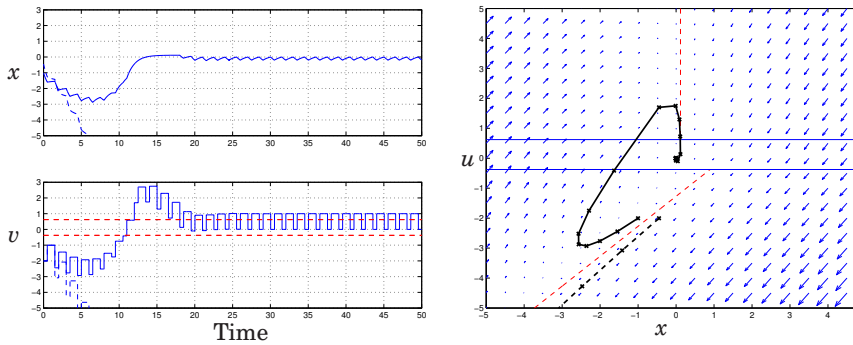

Figure 3.8 For short waiting times T_c, convergence of the probing scheme cannot be guaranteed for all initial conditions. Two simulations with slighlty different initial conditions have been carried out. The numerical values used are T_c=0.5, T_p=1, K=3, y_r=0.2.

the pulses is high, the interaction between the plant dynamic and the controller dynamic may lead to instability. Figure 3.8 illustrates a situation where the condition (3.57) is fulfilled, but the state diverges for some initial conditions. The discrete-time description of the interconnected system can help us to understand the situation. The presence of the integrator in the extreme regions may give rise to situations where the state vector tends to infinity along the critically stable eigendirections. The vector field should therefore be oriented towards the middle region on these directions, which can be expressed as (see Appendix A.3)

$$0 < \frac{y_r}{u_p^0} < \beta \tag{3.59}$$

and

$$e^{aT_c} > e^{-aT_p} + \frac{bc}{a} K(1 - e^{-aT_p}) \tag{3.60}$$

Equation (3.59), identical to (3.54) says that the setpoint y_r should not exceed the stationary pulse response βu_p^0. Equation (3.60) imposes a lower bound on the waiting time T_c depending on the gain K. Frequent probing combined with large gains leads to instability.

Global analysis. The stability conditions previously derived give us information on the parameter values that are not permissible when tuning the probing controller. They are however not sufficient to ensure convergence of the state towards their desired values. Since the equilibrium point is located close to a cell border, the validity of a local analysis is

rather limited. Furthermore, jump between regions cannot be predicted by local inspection of the vector field. For numerical computations we use the values from the simulation shown in Figure 3.5. We get the following closed-loop dynamic from (3.52)

$$X_+ = \begin{cases} \begin{bmatrix} 0.0183 & 0.9817 \\ -0.0787 & 1.0787 \end{bmatrix} X + \begin{bmatrix} 0.4255 \\ 1.0637 \end{bmatrix}, & \text{for } [0 \quad 1]\, X < -0.6731 \\ \begin{bmatrix} 0.0183 & 0.3496 \\ -0.0787 & -0.5016 \end{bmatrix} X, & \text{for } -0.6731 < [0 \quad 1]\, X < 0.3269 \\ \begin{bmatrix} 0.0183 & 0 \\ -0.0787 & 1 \end{bmatrix} X + \begin{bmatrix} 0.1143 \\ -0.4908 \end{bmatrix}, & \text{for } [0 \quad 1]\, X > 0.3269 \end{cases}$$

It can easily be checked that all local stability conditions are fulfilled. Global stability can be investigated using Theorem 3.1. The LMIs, implemented with the *IQCbeta Toolbox* [Jönsson *et al.*, 2004], turn out to be feasible. Convergence of u to a neighborhood of the saturation can therefore be guaranteed for all initial values of u and x. One set of matrices defining the piecewise quadratic Lyapunov function are

$$P_2 = \begin{bmatrix} 9.9304 & 1.8504 \\ 1.8504 & 23.5654 \end{bmatrix} \qquad \bar{P}_1 = \begin{bmatrix} 7.4053 & -8.7428 & -2.2145 \\ -8.7428 & 25.4308 & -3.0400 \\ -2.2145 & -3.0400 & 9.0127 \end{bmatrix}$$

$$\bar{P}_3 = \begin{bmatrix} 11.4103 & -1.5064 & 1.8395 \\ -1.5064 & 18.7955 & 5.1135 \\ 1.8395 & 5.1135 & 1.8720 \end{bmatrix}$$

Level curves of the Lyapunov function V as well as the variation ΔV along the system trajectories are shown in Figure 3.9. Note the linear decrease of ΔV along the eigendirections associated with the eigenvalue 1.

The global analysis is for this example not conservative as indicated by Figure 3.10 (left). In the figure, parameter pairs (K, T_c) for which global stability could be proven are marked by circles. The good agreement between local and global analysis indicates that local analysis is sufficient for first order dynamics. More complex behaviors are however to be expected when the plant dynamic is of higher order.

Influence of output control between the pulses. When output control takes place between the pulses as in Appendix A.1, the closed-loop dynamic is obviously affected. Consider the case of a static output feedback with $B_2 = 1$ and

$$w = \begin{cases} 3z & t \in [kT,\ kT + T_c) \\ w(kT + T_c) & t \in [kT + T_c, (k+1)T) \end{cases} \tag{3.61}$$

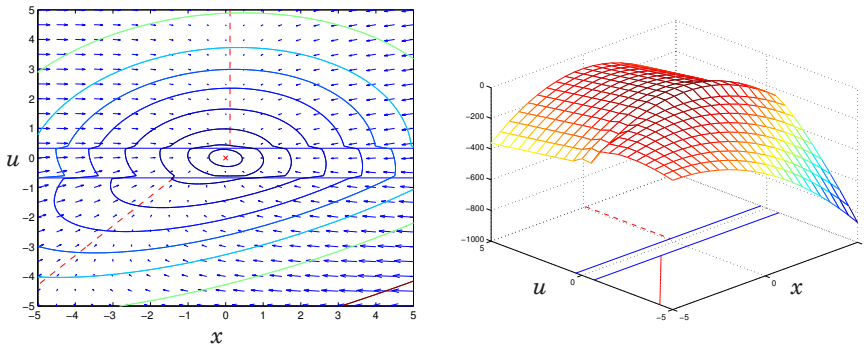

Figure 3.9 Phase plane with some level curves of the Lyapunov function (left) and $\Delta V(X)$ (right). $\Delta V(X)$ is linear along the eigendirections corresponding to the eigenvalue 1, marked in the figure by dashed lines.

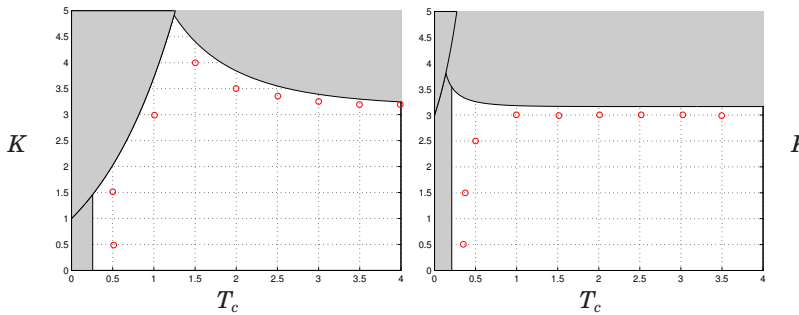

Figure 3.10 Stability region in the parameter space (K, T_c) with $T_p = 1$. The shaded area derived from local analysis corresponds to an unstable closed-loop system. The circles correspond to parameter pairs for which global stability could be proven. When output control takes place between the pulses (right) and the resulting dynamic is fast, shorter waiting times are allowed. The only remaining constraint is on the gain K.

This additional loop is used to speed up the process between the pulses: the open-loop continuous-time pole in $a = -1$ is moved to $a = -4$. The interaction between the process and the controller dynamics is weaker and the waiting time T_c could be shortened. Figure 3.10 (right) shows the impact of this fast output control. The benefit of output control is to allow shorter waiting periods between the pulses and thereby faster input updates and convergence. With output control, the constraint (3.60) can be relaxed.

Performance analysis

The analysis performed in the previous section helps the user to make admissible choices when designing the probing controller. Convergence of the scheme close to the optimal setpoint can thus be guaranteed for all initial conditions. However, no information about the convergence speed or the ability to track a time-varying setpoint was provided.

We will now consider a process with a time-varying saturation level r_k. The system can be cast into the framework from Section 3.4. From (3.55) and (3.56), the reference trajectory is given by

$$u_r(k) = r(k) - \frac{y_r}{\beta} \tag{3.62}$$

$$x_r(k) = (I - A_{tot})^{-1} B_{tot} \begin{bmatrix} r(k) - \frac{y_r}{\beta} \\ r(k) \end{bmatrix} \tag{3.63}$$

Because of the integrator in the control law and the min function properties, the dynamic of the error $X - X_r$ is independent of r_k and depends only on the rate of change $\Delta r(k) = r(k+1) - r(k)$. Denote by $\tilde{u}$ the error $\tilde{u}(k) = u(k) - u_r(k)$. Since

$$\min(u(k),\ r(k)) = \min(\tilde{u}(k),\ \frac{y_r}{\beta}) + r(k) - \frac{y_r}{\beta} \tag{3.64}$$

and defining $\tilde{f}$ by $\tilde{f}(u) = \min(u,\ \frac{y_r}{\beta})$, Equation (3.15) becomes

$$y_k = G_1(z)\tilde{f}(\tilde{u}_k) + G_2(z)(\tilde{f}(\tilde{u}_k + u_p^0) - \tilde{f}(\tilde{u}_k)) + G_1(z)(r(k) - \frac{y_r}{\beta}) \tag{3.65}$$

Since G_1 given by (3.18) can be rewritten as

$$G_1(z) = C_{tot}(zI - A_{tot})^{-1} d(z-1) \tag{3.66}$$

we get

$$G_1(z)(r(k) - \frac{y_r}{\beta}) = C_{tot}(zI - A_{tot})^{-1} d(r(k+1) - r(k)) \tag{3.67}$$

The integrating feedback law (3.51) becomes in the new coordinate

$$\tilde{u}(k+1) = \tilde{u}(k) + K(y_k - y_r) - (r(k+1) - r(k)) \tag{3.68}$$

From (3.65), (3.67) and (3.68) it is clear that the closed-loop dynamic is independent on $r(k)$ and linear in $\Delta r(k) = r(k+1) - r(k)$.

Linear increase. In a fed-batch cultivation, the feed rate should follow the glucose demand of an increasing biomass. As shown in (2.10), this requires that the probing controller is able to track a continuously increasing saturation point. When $\Delta r(k)$ is a constant equal to Δr_0, Theorem 3.1 can be applied to show that the probing controller is able to track the linearly increasing saturating point. We will instead derive necessary conditions involving y_r and K to track the increasing setpoint. When $\Delta r(k) = \Delta r_0 \neq 0$ the static map $y_\infty(\tilde{u}, \Delta r_0)$ of (3.65), (3.67) becomes

$$y_\infty(\tilde{u}, \Delta r_0) = \beta(\tilde{f}(\tilde{u} + u_p^0) - \tilde{f}(\tilde{u})) - \beta_r \Delta r_0 \tag{3.69}$$

with the constant β_r defined by

$$\beta_r = -C_{tot}(I - A_{tot})^{-1}d \tag{3.70}$$

Using (3.68) as feedback law, the necessary condition for having an equilibrium becomes

$$0 < y_r + \Delta r_0(\frac{1}{K} + \beta_r) < \beta u_p^0 \tag{3.71}$$

which simplifies to (3.54) when $\Delta r_0 = 0$. From (3.71) large K values are necessary to follow large variations Δr_0.

Arbitrary variations To illustrate the performance of the probing controller in presence of time-varying setpoints, a simulation with a particular trajectory r_k has been performed. The result is shown in Figure 3.11. The probing controller succeeds to track the time-varying saturation by using the pulse responses for feedback. Theorem 3.2 from last section can be used to quantify the performance and to give some help for the controller design. In all three regions we choose to quadratically penalize $\eta(k)$ given by

$$\eta(k) = \beta(\min(u(k) + u_p^0,\ r(k)) - \min(u(k),\ r(k)) - y_r \tag{3.72}$$

Note that this choice satisfies the condition of Remark 1 in Theorem 3.2. Using the numerical values $a = 1$, $T_c = 3$, $T_p = 1$ and $y_r = 0.31$, we get $\eta = \bar{C}_i(\bar{X} - \bar{X}_r)$ with

$$\begin{aligned}
\bar{C}_1 &= [\,0 \quad 0 \quad 0.29\,] \\
\bar{C}_2 &= [\,0 \quad 0.61 \quad 0\,] \\
\bar{C}_3 &= [\,0 \quad 0 \quad -0.31\,]
\end{aligned}$$

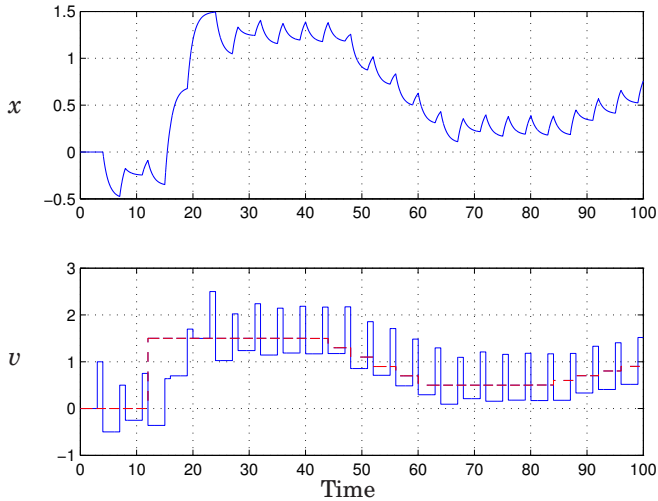

Figure 3.11 Simulation of the probing controller with a time-varying saturation. Top: process state x. Bottom: Process input v (solid) and time-varying saturation level r (dashed).

The closed-loop system was sampled to facilitate the analysis. Different waiting times T_c result in different sampling intervals for the closed-loop system description. A fair comparison between different controller settings should account for the continuous nature of the original signals. We choose therefore the following quadratic cost function for performance evaluation:

$$J(X) = \int_0^\infty \bar{X}(k)^T \bar{Q}_i \bar{X}(k) dt = T \sum_{k=0}^{\infty} \bar{X}(k)^T \bar{Q}_i \bar{X}(k) \tag{3.73}$$

where $\bar{Q}_i = \bar{C}_i^T \bar{C}_i$. We will restrict the input r to the set $\mathcal{R}$ of rate-limited signals:

$$r \in \mathcal{R} \;\Rightarrow\; |\Delta r(k)| = |r(k+1) - r(k)| < 5T \tag{3.74}$$

The set $\mathcal{R}$ corresponds to continuous-time signals with maximal time-derivative of 5. The restriction of the input signals Δr to the set $\mathcal{R}$ is implemented by using the S-procedure. Theorem 3.2 can be used to obtain an upper bound of the system gain γ from Δr to y:

$$J(X) < \gamma ||\Delta r||_2 \tag{3.75}$$

The LMIs from Theorem 3.2 turn out to be feasible. Minimizing γ subject to the constraints, one obtains $\gamma \approx 8.6$. A lower bound of 1.24 was obtained

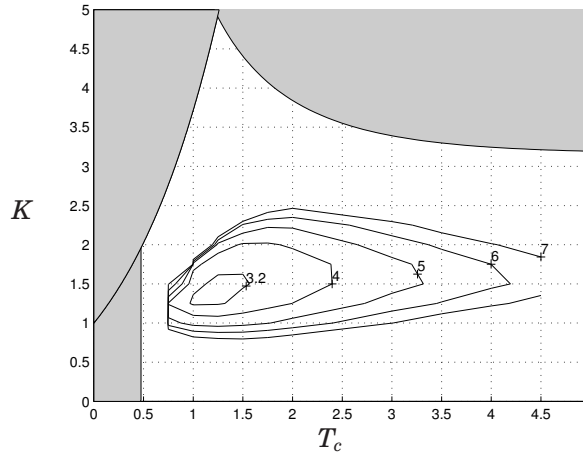

Figure 3.12 Performance in the plane (K, T_c) measured by level curves of γ in (3.75). The pulse duration was chosen to be $T_p = 1$. A waiting time $T_c \approx 1.3$ and a probing gain of $K \approx 1.4$ is suggested by the level curves.

by simulating the system with a particular signal r. A better estimate of the lower bound can be derived by searching for the worst-case reference change. The computations have been performed for various values of the gain K and the waiting time T_c. The result is plotted in Figure 3.12 together with the stability region from local analysis. The estimated gain appears to exhibit a minimum in a region of the parameter space (K, T_c). A waiting time $T_c \approx 1.3$ and a probing gain of $K \approx 1.4$ is suggested by the level curves. Long waiting times result in a slow tracking while short waiting times decrease the stability margin. A similar compromise is also valid for the probing gain K.

The analysis method provides valuable information for the design of the probing controller. It measures the ability to track a time-varying optimum without carrying out simulations with various disturbances r. When more information about the dynamic of the disturbance r is available, it can easily be integrated into the analysis to get more accurate results.

Tuning rules

Based on the analysis from the last section, it is possible to derive simple tuning rules. Similar patterns for the level curves of the system gain could actually be noticed when changing the process gain and time-constant. Based on those results, the following setting for the probing controller is

suggested:

$$\begin{aligned} K &= \frac{1}{\sigma(T_p)} \\ y_r &= \frac{\sigma(T_p)}{2} u_p^0 \\ 1 &< aT_c < 2 \end{aligned} \tag{3.76}$$

where $\sigma(t)$ denotes the unit step response of the linear dynamic. For large T_c the constant $\sigma(T_p)$ is approximately equal to β in (3.58). The constraint on the length T_c of the waiting phase can be relaxed with good output control.

The local stability conditions (3.57)-(3.60) and the tuning rules (3.76) do not impose any restriction on the pulse duration T_p. For a high probing frequency and thereby a fast convergence to the saturation, it is advantageous to have small T_p values. In practice, the measurement noise introduces limitations. For a low noise sensitivity, large gains K suggested by (3.76) when $T_p \to 0$ cannot be applied. The gain K corresponding to the maximal acceptable variance of u in presence of measurement noise would be easy to compute using the system matrix A_2 given in Appendix A.3. As it will be shown in the next section, the choice of T_p is further limited in the case of an output nonlinearity.

There is another factor that is not reflected by the tuning rules. According to (3.76), the gain K should be increased to compensate for a slow process. Inspection of the dynamic in the region $\mathbf{X}_2$ given in Appendix A.3 indicates a poorly damped closed-loop system when $a \to 0$. In the case of a slow process, a longer probing period T or other control laws than a single integrator would therefore be required.

3.6 Saturation and input dynamic

As it was mentioned in Chapter 2, the Hammerstein system with input nonlinearity is a good description of the fed-batch process in the later part of a cultivation where the oxygen dynamic including sensor dynamics is dominating over the glucose one. At the beginning of the fermentation, the situation is the opposite and the Wiener system (output nonlinearity) is a better description of the process. In spite of their similar static responses the two configurations are significantly different. Figure 3.13 illustrates the difference between the two configurations. Different behaviors can therefore be expected when applying the probing strategy to the two different systems. Figure 3.14 shows simulation results where the same setting for the probing controller was used for the Wiener and Hammerstein processes. A smooth convergence to the saturation can be seen

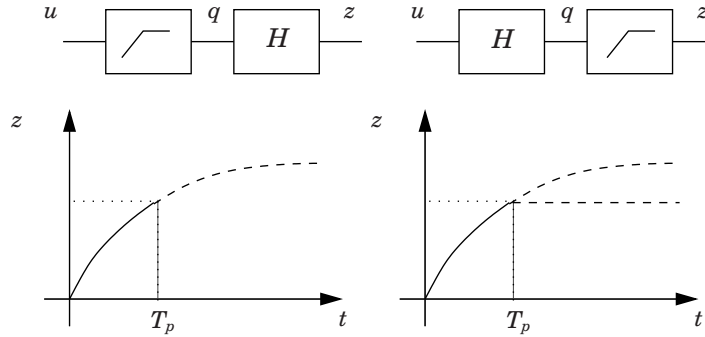

Figure 3.13 The effect of an unknown input nonlinearity (left) is to restrict the range of the input values to the linear dynamic. After a step change in u the output z will smoothly increase and it is possible to predict the future output from a finite time experiment. In the unknown output nonlinearity case (right), the output z cannot be predicted after a short time observation even if the dynamic H is fully known.

in the Hammerstein case while in the Wiener case sustained oscillations take place around the saturation level.

As shown in Appendix A.1, it is still possible in the Wiener case to describe the closed-loop system by means of a discrete-time nonlinear system. When f is a saturation function, the closed-loop system becomes a piecewise affine system with a state space divided into 4 regions. There are still two regions associated with dynamics containing an integrator and a region where the equilibrium point is located. The additional region describes the situation where the output q of the linear process is above the saturation at the beginning of a pulse and below the saturation at the end of the same pulse. Global stability analysis can be performed as in Section 3.4 but it will not be performed here. A good insight into the fundamental differences between the configurations can be obtained by considering the static map $y_\infty(u)$ derived from the representation in Appendix A.1:

$$y_\infty(u) = \min(-CA^{-1}Bu+(\beta+\beta_1)u_p^0, r)-\min(-CA^{-1}Bu+\beta_1 u_p^0, r) \quad (3.77)$$

where β_1 is given by

$$\beta_1 = CA_{d1}(I - A_{d2}A_{d1})^{-1}(A_{d2} - I)A^{-1}B$$

Interconnecting (3.77) with the controller (3.51), the local stability condition becomes

$$0 < -KCA^{-1}B < 2 \quad (3.78)$$

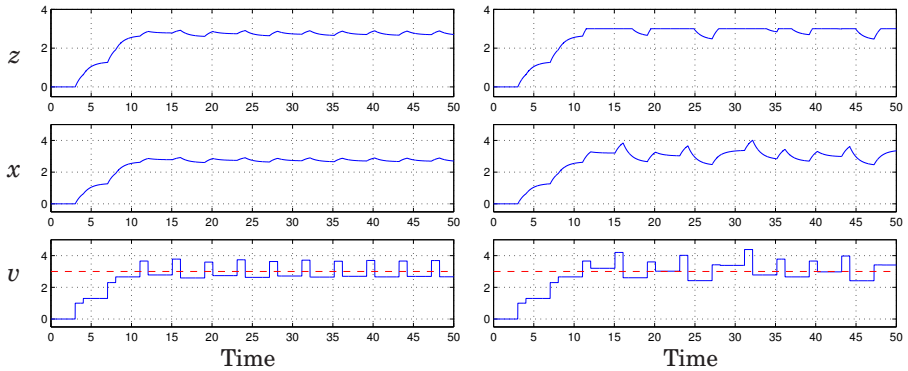

Figure 3.14 Simulations of the probing controller in the case of an input nonlinearity (left) and output nonlinearity (right). A smooth convergence to the saturation can be seen in the input nonlinearity case while sustained oscillations take place around the saturation level in the output nonlinearity case. The following numerical values have been used: T_c=3, T_p=1, K=2.5, y_r=0.2.

In the case of a plant with unit gain, the maximal gain is $K = 2$ that should be compared with $K = \frac{2}{\beta}$ in the case of an output dynamic. The probing controller can no longer compensate for the process dynamic. The small pulse responses fedback by the algorithm when the process is slow will result in a slow convergence speed to the saturation. Below the saturation, the static map $y_\infty(u)$ gives the pulse response $y = \beta u_p^0$ in both cases. The integrating control law leads therefore to a convergence speed V given by

$$V = \frac{K\beta u_p^0}{T_c + T_p}$$

The different constraints on the gain K lead to the upper bounds:

$$\begin{aligned} &\text{Hammerstein case :} && V < \frac{2u_p^0}{T_c + T_p} \\ &\text{Wiener case :} && V < \frac{2\beta u_p^0}{T_c + T_p} \end{aligned} \tag{3.79}$$

From Equation (3.79), the effect of the plant dynamic and the pulse duration on the perfomance are clear. In the Hammerstein system case, arbitrary short pulses could be performed in order to increase the convergence speed to the saturation. In practice, the minimal pulse duration is related to the output noise level. In the Wiener system case, the situation

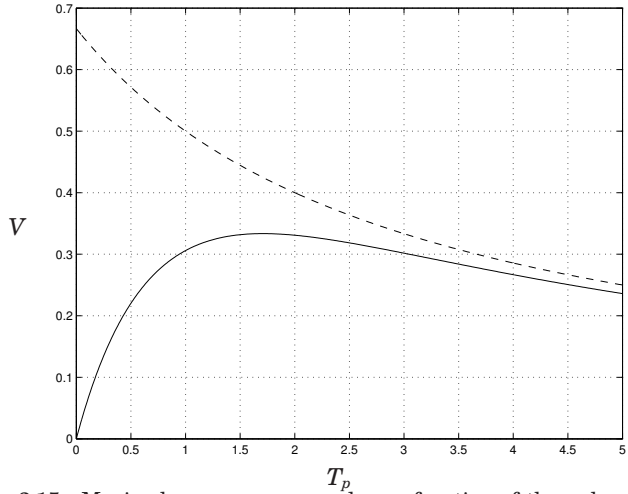

Figure 3.15 Maximal convergence speed as a function of the pulse duration T_p when the saturation is at the input (dashed line) and output (solid line). The numerical values $T_c = 3$, $u_p^0 = 1$ have been used in both cases.

is much different. The influence of the pulse duration is illustrated in Figure 3.15. Small T_p values result in small pulse responses, which in turn are fed back for small input adjustments. Long pulses imply larger pulse periods and reduce the convergence speed, too. There exists an optimal length for the pulses that is a trade-off between frequent updates and long probing.

Another major difference between the two configurations concerns the influence of the output control between the pulses. Since there is no interaction between the output controller and the input dynamic, the waiting time T_c between the pulses cannot be decreased with a fast output control.

3.7 Tuning guidelines for the Wiener-Hammerstein case

Assume now that the process is of Wiener-Hammerstein type, *i.e.* with both input and output dynamics:

$$\begin{aligned} \dot{X}_1 &= A_1 X_1 + B_1 v \\ \dot{X}_2 &= A_2 X_2 + B_2 f(C X_1) \\ y_2 &= C_2 X_2 \end{aligned} \tag{3.80}$$

When f is a piecewise affine function and the probing controller is applied, the interconnected system cannot be described by a piecewise affine

discrete-time system. Preliminary studies indicate that the analysis from the previous sections could still be used to guarantee l_2-stability of the closed-loop. The overall system can be viewed as a perturbed system, the perturbation resulting from the fastest dynamic. Estimation of the l_2-gain of the nominal system and application of the small gain theorem provide some stability guarantees.

Tuning guidelines

Based on the analysis from the last two sections, we can present guidelines for tuning the probing controller. Denote by T_i and T_o the overall time constants for the input and output dynamics, respectively. Denote further by $\sigma_i(t)$, $\sigma_o(t)$ and $\sigma(t)$ the unit step responses of respectively the input, output and overall dynamics.

- Pulse height u_0^p: For a fast convergence speed, it should be taken as large as possible. Constraints on the input and output impose an upper limit for the pulse size.
- Pulse duration T_p: The choice of pulse length is mainly determined by the input dynamic: $T_p \approx 1.5T_i$. When T_i is small, the noise level imposes a lower bound on T_p.
- Setpoint y_r: The desired response size influences the stationary distance to the saturation point and the convergence speed. For a symmetric behavior above and below the saturation, it should be taken as $y_r = \frac{\sigma(T_p)}{2} u_p^0$.
- Waiting time T_c: The input and output dynamics impose a lower limit on T_c. A reasonable choice is $T_c = 2\max\{T_i, T_o\}$.
- Probing gain K: For good performance around the optimal operating point, the gain should not be larger than $K = \frac{1}{\sigma_o(T_p)}$.

When output control takes place between the pulses, the Wiener description (output nonlinearity) is a better description and the performance are mainly limited by the input dynamic. Measurement noise is also a limiting factor. The size of the pulse response is a simple input-output correlation measure that is very sensitive to noise. To reduce the noise sensitivity, the integral of the pulse response could be used for feedback.

3.8 Smooth nonlinearities

The most common extremum seeking problem treated in the literature consists in locating the optimum of a smooth nonlinear function. The stability analysis derived in [Krstic and Wang, 1997] provides a theoretical

foundation for the standard extremum seeking scheme. Based on singular perturbation and averaging analysis, the convergence proof does however not provide any description of the domain of attraction. In [Krstic, 2000], the authors perform a similar analysis on a Wiener-Hammerstein system like (3.80), f being a quadratic function. It will now be shown that the description of the closed-loop system derived in Section 3.2 allows closed-loop stability analysis in the case of a concave nonlinearity. Estimates of the region of attraction can also be computed.

Concave nonlinearity and output dynamics

We now assume that f is strictly concave with a maximum at $u = u^*$. As it was shown in Section 3.3, the closed-loop system has a unique equilibrium point (x_∞, ξ_∞) if $\beta \neq 0$. Denote by $\tilde{X}$ the system state after the origin shift

$$\tilde{X} = \begin{bmatrix} \tilde{x} \\ \tilde{\xi} \end{bmatrix} = \begin{bmatrix} x - x_\infty \\ \xi - \xi_\infty \end{bmatrix} \tag{3.81}$$

Taking an integrator with gain K as controller, the closed-loop system equations corresponding to (3.19) can be written as

$$\begin{aligned} \tilde{X}_{k+1} &= \begin{bmatrix} A_{tot} & 0 \\ KC_{tot} & 1 \end{bmatrix} \tilde{X}_k + \begin{bmatrix} B_{tot}T^{-1} \\ KD_{tot}T^{-1} \end{bmatrix} \begin{bmatrix} f_1(\tilde{u}_k) \\ f_2(\tilde{u}_k) \end{bmatrix} \\ \tilde{u}_k &= \begin{bmatrix} 0 & 1 \end{bmatrix} \tilde{X}_k \end{aligned} \tag{3.82}$$

where

$$\begin{bmatrix} f_1(u) \\ f_2(u) \end{bmatrix} = \begin{bmatrix} f(u + u_\infty) - f(u_\infty) \\ f(u + u_p^0 + u_\infty) - f(u + u_\infty) - f(u_p^0 + u_\infty) + f(u_\infty) \end{bmatrix}$$
$$\begin{bmatrix} f_1(0) \\ f_2(0) \end{bmatrix} = \begin{bmatrix} 0 \\ 0 \end{bmatrix}$$

As f is strictly concave, f_2 is strictly decreasing and there exist $\alpha_1, \alpha_2 \in R$ such that $\alpha_1 < \alpha_2 \leq 0$ and

$$\alpha_1 u^2 < u f_2(u) < \alpha_2 u^2 \tag{3.83}$$

Furthermore, f was assumed to be bounded. Therefore there exists $\alpha_3 > 0$ such that

$$-\alpha_3 u^2 < u f_1(u) < \alpha_3 u^2 \tag{3.84}$$

The closed-loop system is a Lur'e system with two scalar nonlinearities that are cone bounded. The sector conditions characterize well the nonlinearities and absolute stability can thus be investigated using Tsypkin criterion for multivariable systems. A review of the different versions of the Tsypkin criterion can be found in [Larsen and Kokotovic, 2001]. Quadratic stability can be for instance checked by applying the following result:

THEOREM 3.3—[HITZ AND ANDERSON, 1969]
Consider the multivariable system

$$\begin{aligned} x(i+1) &= Ax(i) + B\Phi(y), \quad x \in R^n \\ y(i) &= Cx(i), \quad y \in R^m \\ \Phi(y) &= [\,\phi_1(y_1) \quad \phi_2(y_2), \quad \ldots, \quad \phi_m(y_m)\,] \end{aligned} \tag{3.85}$$

If there exists $K = \mathrm{diag}(k_1, \ldots, k_m) > 0$ such that $K^{-1} + C(zI - A)^{-1}B$ is discrete positive real, then (3.85) is absolutely stable for $\phi_j \in [0, k_j]$.
Remark: The proof is established with the Lyapunov function $V = x^T Px$, where the symmetric matrix $P > 0$ satisfies

$$\begin{bmatrix} P - A^T PA & B^T PA - C^T \\ A^T PB - C & K^{-T} + K^{-1} - B^T PB \end{bmatrix} \geq 0$$

□

Less conservative results can be obtained if the monotonicity of f_2 is taken into account in the analysis as in [Kapila and Haddad, 1996; Park and Kim, 1998]. More general sector conditions can be considered using the S-procedure as in [Boyd *et al.*, 1994], Section 8.1.1.

Example Consider the uncertain process

$$\dot{x} = -x - av^2, \quad a \in [0.5, 1.5] \tag{3.86}$$

When the pulse train is described by $T_p = 1$, $T_c = 2$ and $u_p^0 = 1$, the response to the pulse number k is the output of (3.82) with

$$A_{tot} = 0.094 \qquad B_{tot} = [\,0.3181 \quad 0.6321\,] \tag{3.87}$$

$$C_{tot} = -0.0855 \qquad D_{tot} = [\,-0.5466 \quad 0.6321\,] \tag{3.88}$$

As $\beta = 0.5752 \neq 0$ there is a unique equilibrium (x_∞, u_∞) and it satisfies

$$(u_\infty + 1)^2 - u_\infty^2 = 0 \tag{3.89}$$

$$x_\infty = (1 - A_{tot})^{-1} B_{tot} \begin{bmatrix} -au_\infty^2 \\ -a(u_\infty^2 + 1) \end{bmatrix} \tag{3.90}$$

that is

$$u_\infty = -0.5 \tag{3.91}$$

$$x_\infty = -0.25a \tag{3.92}$$

The functions f_1 can be computed to be

$$f_1(u) = a\{-(u-0.5)^2 + 0.5^2\} \tag{3.93}$$
$$= au(-u+1) \tag{3.94}$$

and f_2 is given by

$$f_2(u) = -2au \tag{3.95}$$

Since $a \in [0.5, 1.5]$, it can be easily shown that

$$f_2 \in \text{sector } [-3, -1] \tag{3.96}$$
$$f_1 \in \text{sector } [-\alpha_3, \alpha_3], \text{ for } -1 - \frac{\alpha_3}{1.5} < u < -1 + \frac{\alpha_3}{1.5} \tag{3.97}$$

Using an integrating feedback law with gain $K = 0.2$, absolute quadratic stability for $\alpha_3 = 30$ could be proven with the Lyapunov function $V = X^T P X$ where P is given by

$$P = \begin{bmatrix} 0.0067 & -0.1209 \\ -0.1209 & 6.8974 \end{bmatrix} \tag{3.98}$$

The analysis is valid only for $u \in [-21, 19]$ and a region of attraction can be estimated using the Lyapunov function. An estimate Ω of the stability domain can be obtained by maximizing $\gamma > 0$ such that

$$\Omega = \{X \in R^2, V(X) < \gamma^2\} \subset \{X = (x,u) \in R^2, -21 < u < 19\} \tag{3.99}$$

Maximization of γ led to the $\gamma = 29.4$. A simulation of the probing controller interconnected with (3.86) and $a = 1.5$ is shown in Figure 3.16. The trajectory is also shown in the plane $(\tilde{x}, \tilde{u})$ together with the guaranteed domain of attraction. Note that, due to the non-stationary state in x at $t = 0$, the probing controller decreases v after the first pulse eventhough v is far below its optimal value.

Wiener-Hammerstein system with quadratic nonlinearity

It is interesting to notice that, when applying the probing technique to this system, it is possible to explicitely integrate the closed-loop equations. The discrete-time representation of the interconnected system becomes quadratic in the state. Stability analysis with guarantees on the domain of attraction can be performed using the sum of squares (SOS) approach, see [Parrilo, 2000] and [Prajna *et al.*, 2004]. This approach offers the possibility to search for polynomial Lyapunov functions by solving a semidefinite program.

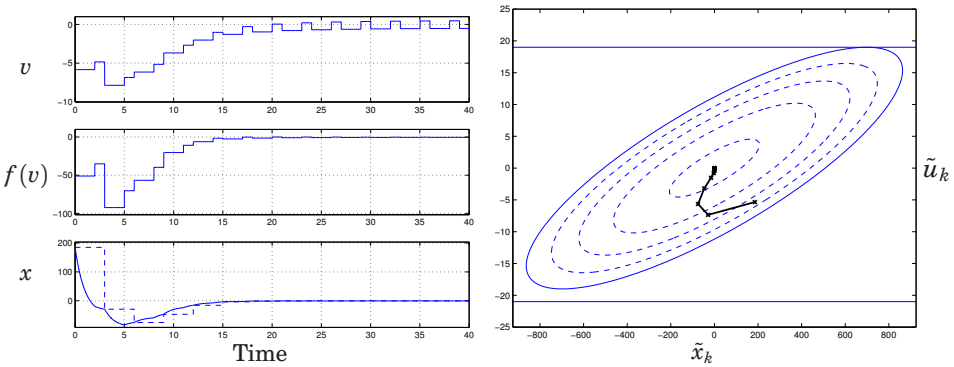

Figure 3.16 Simulation of the probing controller in the case of quadratic input nonlinearity $f(u) = -1.5u^2$. Time trajectory (left) and trajectory in the phase plane $(\tilde{x}, \tilde{u})$ with Lyapunov level curves and a guaranteed domain of attraction (ellipse, solid line).

3.9 Summary

The convergence properties of the probing control strategy has been analysed for plants modeled by a static nonlinearity in series with linear dynamics. It has been shown how a discrete-time representation can be used to analyse stability and performance of the closed-loop system. When the nonlinearity is modeled by a piecewise affine function, as in the bioreactor example, convergence of the probing scheme can be investigated by solving a set of linear matrix inequalities. The analysis methods have been applied to some simple examples where it is desirable to control the process to a saturation. The ability of the probing controller to track a time-varying saturation could also be proved and quantified. Based on those results, tuning guidelines for the probing controller have been derived. Finally, an example where it is desirable to locate an extremum has been studied.

4

Substrate and Temperature Limited Fed-Batch Techniques

4.1 Introduction

The probing feeding strategy described in Chapter 2 is optimal in the sense that it tends to maximize the feed rate with respect to the constraints from the cells and the reactor. High cell density can therefore be achieved in short time, without accumulation of the inhibitive by-product acetate. As far as the recombinant product is concerned, the probing technique leads generally to a good productivity. For an optimized product synthesis, the technique could however be further developped.

When the cell density is high, the maximum oxygen transfer capacity of the reactor may be reached. To prevent a fall of the dissolved oxygen to zero, the feed rate should not be further increased. A safety net in the probing strategy does not allow feed increments when the stirrer speed is close to its maximum. If the oxygen consumption increases further or the oxygen transfer deteriorates, the oxygen level is maintained constant by decreasing the glucose supply rate. The resulting low feed rate may have negative consequences on the protein production. Release of undesirable products into the media, degradation of the recombinant protein (proteolysis) and foaming are examples of complications due to cell stress, see [Rozkov, 2001] and [Han, 2002]. An efficient cultivation technique should therefore avoid the severe glucose limitation that often happens in the late fed-batch phase.

An alternative way to lower the oxygen demand consists in decreas-

ing the temperature of the culture, see [Bauer and White, 1976]. When compared to substrate limited fed-batch, the temperature limited fed-batch (TLFB) technique seems to minimize the release of endotoxins [Silfversparre *et al.*, 2002], as well as the proteolysis rate [Rozkov, 2001]. The main obstacle with the temperature limited fed-batch technique is to achieve a non-growth limiting glucose concentration in the reactor without accumulating acetic acid [Han, 2002]. An on-line glucose sensor is usually not available.

A novel fermentation technique that combines the advantages of the probing strategy and the TLFB technique is proposed in this chapter. The principles of the technique are first explained and illustrated using a bioreactor model. A simple analysis of the oxygen and glucose control loops is also performed. The strategy is finally evaluated experimentally in fed-bacth cultivations with *E. coli*. Glucose, acetate and product data are used for the evaluation and the comparison with the standard SLFB technique.

4.2 Process description

Temperature dependence

The cell metabolism is described by the glucose uptake rate q_g, the oxygen uptake rate q_o, the acetate production rate q_a and the growth rate μ. The metabolic expressions are similar to the one presented in [Åkesson *et al.*, 2001c], and they are given in appendix B.1. The temperature dependence of the growth rate is incorporated into the model using Arrhenius law. A decrease in the medium temperature from 37^{o}C to 25^{o}C has been reported to lower the growth rate by half, see [Pirt, 1985] and [Esener *et al.*, 1983]. When the growth rate is proportional to the glucose uptake rate q_g, one can write $q_g^{max}(T)$ as

$$\begin{aligned} q_g^{max}(T) &= q_{g,37}^{max} e^{-50(\frac{1}{T}-\frac{1}{37})} \\ q_g^{max}(25) &\approx 0.5 q_{g,37}^{max} \end{aligned} \tag{4.1}$$

The uptake rates q_a and q_o are changed in a similar fashion and also the maintenance coefficient q_{mc} [Esener *et al.*, 1983]. It should be noticed that the temperature dependence is almost linear in the range 37^{o}C to 25^{o}C.

Mass balance

The mass balance equations for the media volume V, the glucose concentration G, the acetic acid concentration A, the cell mass X and the oxygen

concentration C_o are:

$$\begin{aligned}
\frac{dV}{dt} &= F \\
\frac{d(VG)}{dt} &= FG_{in} - q_g(G,T)VX \\
\frac{d(VA)}{dt} &= q_a(G,A,T)VX \\
\frac{d(VX)}{dt} &= \mu(G,A,T)VX \\
\frac{d(VC_o)}{dt} &= K_L a(N)V(C_o^* - C_o) - q_o(G,A,T)VX
\end{aligned} \tag{4.2}$$

We strive for a model that is as simple as possible, so the influence of the temperature on $K_L a$ and the solubility of oxygen is neglected. The resulting effect on the oxygen transfer is anyway small in the range 20 ^{o}C to 40^{o}C [Enfors and Häggström, 1994].

Most sensors measure the dissolved oxygen tension O instead of the dissolved oxygen concentration C_o. They are related by Henry's law

$$O = HC_o \tag{4.3}$$

The dynamics in the oxygen probe should also be taken into account and it is modeled by a first order system:

$$T_p \frac{dO_p}{dt} + O_p = O \tag{4.4}$$

The temperature control introduces extra dynamics, also approximated by a first order system

$$T_t \frac{dT}{dt} + T = T_{ref} \tag{4.5}$$

Linearized model

Oxygen dynamic. A linearized model will be used for designing the dissolved oxygen controllers. During short periods of time, the volume V and the biomass X are approximately constant. Assuming that glucose is present in excess ($q_o = q_o^{max}$), the dissolved oxygen dynamics is decoupled from the others and it can be approximated by

$$T_o \frac{d\Delta O}{dt} + \Delta O = K_T \Delta T + K_N \Delta N + d \tag{4.6}$$

where

$$K_T = \frac{\partial q_o}{\partial T} H X (K_L a)^{-1} \qquad T_o = (K L_a)^{-1}$$
$$K_N = \frac{\partial K_L a}{\partial N} (O^* - O)(K_L a)^{-1} \tag{4.7}$$

The signal d models all disturbances acting on the oxygen concentration. When d represents cell growth, it can be written as:

$$d = K_x X \qquad K_x = q_o H (K_L a)^{-1} \tag{4.8}$$

Acetate dynamic. In section 4.5, the impact of acetate concentration on the probing strategy will be examined. A simple model describing the acetate concentration will be needed for the analysis.

Acetate is produced when the glucose uptake rate exceeds a critical value q_g^{crit}, corresponding to the maximal respiratory capacity of the cells $q_o^{max} = Y_{og} q_g^{crit}$. The rate of acetate production is proportional to the glucose excess:

$$q_a^p = Y_{ag}(q_g - q_g^{crit}), \quad q_g > q_g^{crit} \tag{4.9}$$

If acetate is present in the media, it may also be consumed. The consumption requires oxygen and it is therefore limited by the available oxidative capacity of the cells:

$$q_o = \min(q_o^{max}, Y_{og} q_g + Y_{oa} q_a^c) \tag{4.10}$$

where the consumption rate q_a^c follows a Monod-type law:

$$q_a^c = q_a^{c,max} \frac{A}{k_a + A} \tag{4.11}$$

For low acetate concentrations we can make the linear approximation

$$q_a^c \approx \frac{A}{\tau}, \quad \text{with } \tau = \frac{k_a}{q_a^{c,max}} \tag{4.12}$$

The different regimes for the acetate dynamic can finally be approximated by

$$\frac{dA}{dt} = \begin{cases} -\dfrac{A}{\tau} X, & \text{if } Y_{oa}\dfrac{A}{\tau} + Y_{og} q_g < q_o^{max} \\ -\dfrac{1}{Y_{oa}}(q_o^{max} - Y_{og} q_g) X, & \text{if } Y_{oa}\dfrac{A}{\tau} + Y_{og} q_g > q_o^{max} \text{ and } Y_{og} q_g < q_o^{max} \\ Y_{ag}(q_g - q_g^{crit}) X, & \text{if } Y_{og} q_g > q_o^{max} \end{cases} \tag{4.13}$$

4.3 Problem formulation

Balance between oxygen supply and uptake

To prevent from anaerobic conditions, the dissolved oxygen concentration can be maintained at a constant level. This requires a balance between the oxygen uptake rate (OUR) and the oxygen transfer rate (OTR). According to the mass balance equation for oxygen in (4.2), one should have

$$0 = \underbrace{K_L a(N)(O^* - O_{sp})}_{OTR} - \underbrace{q_o(G, A, T)HX}_{OUR} \tag{4.14}$$

Feedback control can be used to achieve this balance throughout the cultivation. The probing approach solves the problem by periodically manipulating OTR and OUR. The basic control sequence can be summarized as follows:

- Increase the feed rate F, *i.e.* G and OUR, if the respiratory capacity of the cells is not exceeded ($q_o < q_o^{max}$). Otherwise decrease F.
- Retrieve the balance between oxygen uptake and supply by acting on OTR.

The probing technique does not only achieve the oxygen balance, but it also maximizes the oxygen uptake rate while avoiding overflow metabolism. The flexibility in the pulse technique makes it possible to use diverse actuators for dissolved oxygen control between the pulses: stirrer speed, air pressure, air flow rate, etc... The volumetric oxygen transfer coefficient $K_L a$ is mainly affected by agitation speed while the oxygen solubility related to O^* is influenced by the aeration rate and the total air pressure. Note that the oxygen transfer can be improved by operating at low oxygen levels O_{sp}.

The oxygen "conductivity" $K_L a$ can also be altered by uncontrolled parameters like broth viscosity, which is affected by antifoam addition or cell lysis.

Operation at the maximum oxygen transfer

When the cell density is high, the oxygen transfer capacity of the reactor OTR^{max} may be reached and the feed rate can no longer be increased. If the oxygen consumption increases due to growth, or if the oxygen transfer deteriorates, the oxygen uptake rate should be lowered to guarantee aerobic conditions. In the probing approach, the sequence of control actions is completed as follows

- No feed increment is allowed if $N > N_{high}$
- Decrease F as long as $N > N_{high2} > N_{high}$

In [Åkesson *et al.*, 2001c] it is proposed to lower the feed supply at a constant rate γ

$$\frac{dF}{dt} = -\gamma F \tag{4.15}$$

For better control performance in presence of quick disturbances, feedback from dissolved oxygen can be used between the pulses, see [Velut, 1999]. The feeding strategy that manipulates the feed rate to control dissolved oxygen concentration is often referred as DO-stat, see [Konstantinov *et al.*, 1990].

Figure 4.1 shows an experiment performed in a 3 l reactor where the probing feeding strategy is used. Here the maximum stirrer speed is reached 2 hours after feed start. Thereafter, the feed is gradually lowered during 6 hours, leading to a decrease by a third. The low feed rate can lead to starvation, which is detrimental for product synthesis.

The model previously presented can be used to illustrate and quantify the starvation level of the cells. Denote by q_g^{res} the residual glucose uptake rate, *i.e.* the amount of glucose per cell and per unit of time, that is not used for maintenance purposes:

$$q_g^{res} = q_g - q_m \tag{4.16}$$

When controlling the dissolved oxygen concentration by changing the feed rate, we get (see appendix B.2)

$$q_g^{res,\ SLFB} = \frac{OTR^{max}}{HY_{og}} \frac{1}{X} - q_m \frac{Y_{og}^m}{Y_{og}} \tag{4.17}$$

When the cell density is high compared to the reactor capacity OTR^{max}, the residual glucose uptake is small and can cause cell stress. Manipulation of the culture temperature may be a less stressful way to lower the oxygen demand when the oxygen transfer capacity of the reactor has been reached. The mass balance equations can again be exploited to give some insight into the TLFB technique. Assuming glucose excess, *i.e.* $q_o(T) = q_o^{max} f(T)$, without acetate accumulation, we have

$$q_g^{res,\ TLFB} = \frac{OTR^{max}}{HY_{og}} \frac{1}{X} (1 - \frac{Y_{og}^m q_m}{q_o^{max}})$$

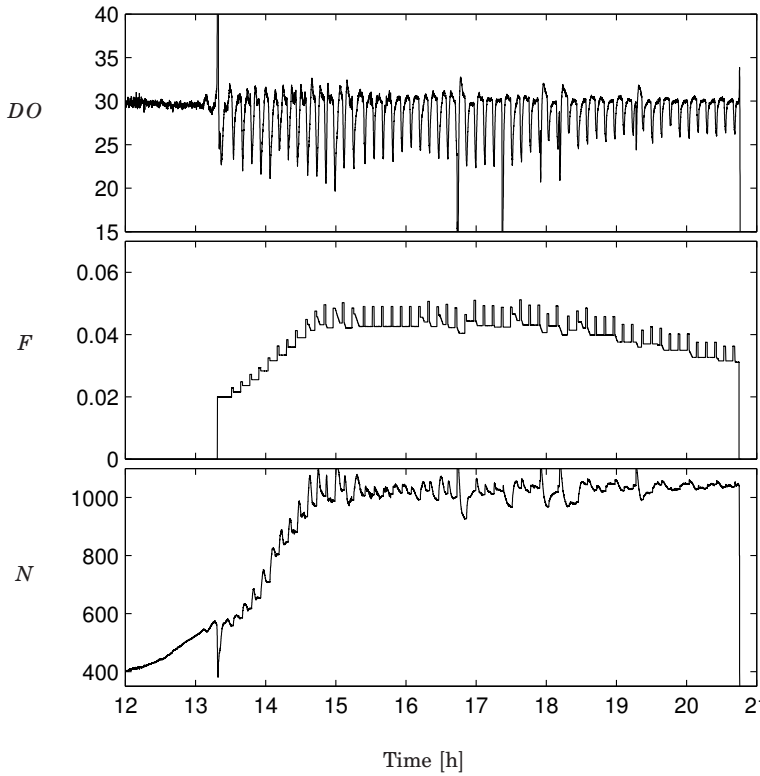

Figure 4.1 A cultivation where the original probing feeding strategy is used. The fed-batch part of the cultivation is shown. From top: dissolved oxygen DO ([%]), Feed F ([l/h]) and the stirrer speed N ([rpm]). At t = 16.7 h and t = 17.5 h antifoam is added which has a large impact on the dissolved oxygen.

It is easy to see that when the maximum oxygen transfer capacity is reached, *i.e.* $q_o^{max} HX > OTR^{max}$, we always have

$$q_g^{res,\ TLFB} > q_g^{res,\ SLFB} \tag{4.18}$$

At high cell density, the difference between the two rates can be significant. When no product is synthetised and all residual glucose is directed to growth ($q_g^{res} = q_{gg}$), our model predicts a linear increase in the biomass in the TLFB case. If the feed rate instead of temperature is used to control DO, the cell density tends exponentially towards a constant value.

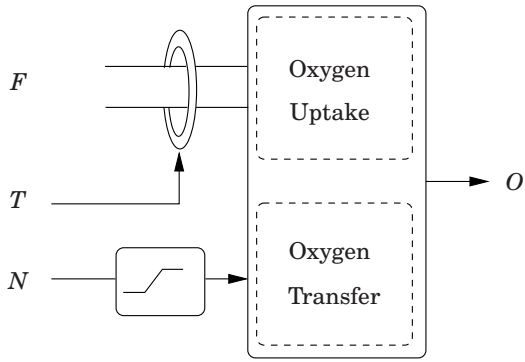

Figure 4.2 Schematic view of the control problem. To achieve a balance between oxygen uptake and transfer three control variables are available: the feed rate F, the stirrer speed N and the temperature T. The feed rate passes through the oxygen consumption bottleneck of temperature dependent size. The stirrer speed operates close to saturation.

Control Problem

Figure 4.2 is an illustration of the control configuration at high oxygen transfer rates. To achieve the dissolved oxygen balance, three control variables are available: the feed rate F, the stirrer speed N and the temperature T. The feed rate passes through the oxygen consumption bottleneck, which has a temperature dependent size. The stirrer speed is close to saturation. The cultivation conditions to be fullfilled for an efficient application of the TLFB technique are: temperature limitation and slight glucose excess.

Glucose excess. Achieving glucose excess implies a significant risk for acetate accumulation to inhibitive levels. The main obstacle with the TLFB technique is to achieve a non growth-limiting substrate concentration without acetate accumulation. Figure 4.3 shows the phase portrait describing the acetate dynamic from (4.13) depending on the input q_g. The objective is to operate in the region Ω_3 where glucose is in excess. In that region, acetate is produced at a rate that is proportional to the distance to q_g^{crit}. If only an approximative value for q_g^{crit} is available and a constant feed rate is applied, acetate could be quickly formed. Feedback appears to be necessary, but the difficulty is that no online measurement of neither glucose or acetate is generally available. Another complication is the temperature dependency of q_o^{max} and thus of q_g^{crit}.

Temperature-based DO control. Temperature should be used to reduce the oxygen uptake and thereby maintain a constant oxygen level.

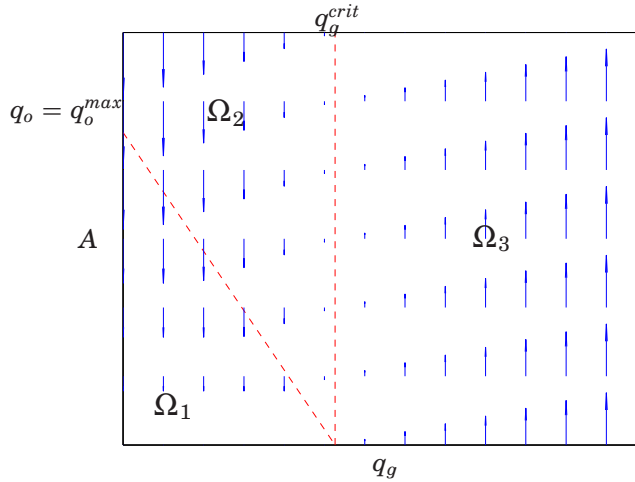

Figure 4.3 Acetate dynamic in the plane (q_g, A). Neglecting the glucose dynamic, the specific glucose uptake rate q_g can be seen as the input: $F \approx K_g q_g$. In the region Ω_3, acetate is produced by overflow metabolism while it is consumed in Ω_1 and Ω_2. Between the two dashed lines, the rate of acetate consumption is limited by the respiratory capacity of the cells $(q_o = q_o^{max})$.

Manipulation of the temperature for feedback control of the oxygen concentration is however not a simple task. There are limitations on the achievable performance of the loop. Compared to the agitation system the cooling process is much slower. Furthermore, there often exist constraints on the rate of change, strongly related to the temperature of the incoming cooling flow.

Efficient utilization of the reactor. Glucose excess and temperature limitation can be achieved at various temperature values. Operation at very low temperature would imply low stirrer speeds and feed rates, and results in a poor utilization of the reactor. The objective will be to exploit the full capacity of the reactor. This implies that feed rate and stirrer speed should be maximized with respect to the constraints, whereas temperature should be as close to 37°C as possible.

4.4 A combined feeding strategy

We will now describe a feeding strategy that combines the advantages of the TLFB technique and probing control. The probing approach can be used to achieve a controlled excess of glucose without acetate accumulation. An efficient control strategy for the regulation of dissolved oxygen will also be proposed.

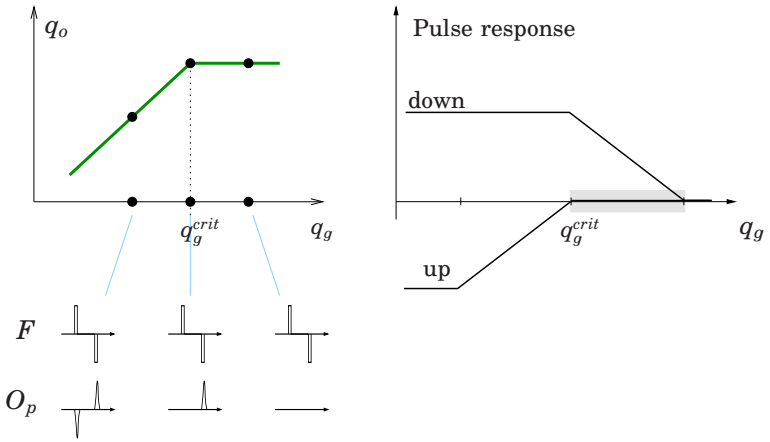

Figure 4.4 The amplitude of the pulse responses in dissolved oxygen as a function of q_g, in the absence of acetate. The shaded area indicates the region where the detection method registers responses to down pulses but not to up pulses.

Feed control

The probing feeding strategy has proven to be an efficient tool for maximizing the feed rate while minimizing acetate production. To achieve a slight glucose excess, down-pulses instead of up-pulses could be performed. When a down-pulse is made the dissolved oxygen signal will increase if the cultivation is glucose limited. The feed rate is adjusted as before depending on the size of the response in the dissolved oxygen. With down pulses a slight glucose excess in the reactor can be achieved. At a given feed rate a down-pulse may indeed lead to a response in the dissolved oxygen when an up-pulse would not, see Figure 4.4.

Contrary to the original probing feeding technique, increments in the feed rate at this stage of the cultivation are allowed for a good control around q_g^{crit}.

Dissolved oxygen control

A good dissolved oxygen control is required for frequent probing and to avoid long periods with a feed rate largely exceeding the respiratory capacity of the cells. There are however fundamental limitations on the achievable performance when controlling dissolved oxygen with temperature. Apart from the possibly slow cooling system, the uncertainty in the temperature influence on the cells represent a strong limitation. As the dynamic is not accurately known, it is not recommended to design a DO controller with a large bandwidth. Dissolved oxygen control based on

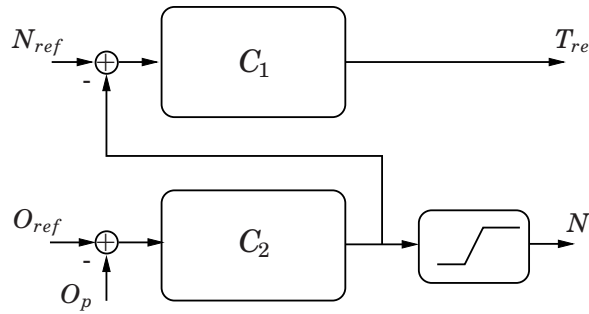

Figure 4.5 Block-diagram over the mid-ranging control scheme. C_1 is a controller manipulating N to take care of the fast disturbances on the output. C_2 manipulates T to maintain N around N_{ref}, away from the saturation.

the sole manipulation of temperature would not be sufficient for a proper application of the probing strategy. On the other hand, the stirrer speed is close to saturation and cannot be solely used. Temperature and stirrer speed should therefore be employed simultaneously to achieve satisfactory performance. Dissolved oxygen control can be viewed as a control allocation problem. To allocate the control signals taking into consideration the static and dynamic constraints, the so-called mid-ranging controller can be used, see [Allison and Isaksson, 1998]. In this configuration, shown in Figure 4.5, two SISO controllers are connected in cascade. The first controller C_1 manipulates the stirrer speed N and it is tuned to handle the fast disturbances. The objective of C_2 with input $N - N^{ref}$ is to keep the control signal N in its operating range. It should take care of slow disturbances such as cell growth. The advantage of this structure is its simplicity. Moreover, the first controller C_1 can be used alone until the control signal N reaches the saturation. The second loop is activated once N enters the saturation region.

Proposed cultivation technique

The early fed-batch phase is run under glucose limited conditions, using the original probing strategy described in [Åkesson *et al.*, 2001b]. When the maximum oxygen transfer capacity is approached, that is when the stirrer speed N reaches N_{ref} close to the maximum value N_{max}, the temperature limitation mode is activated:

- the up-pulses superimposed to the feed are shifted to down pulses and increments are still allowed.
- the temperature loop is activated to keep the stirrer speed close to N_{ref}

The fed-batch technique should result in a maximal utilization of the reactor. Cells are fed at their maximal capacity and the stirrer speed is kept close to its maximum. The feed rate is not used to control DO unless the maximum cooling capacity of the reactor is reached.

4.5 Analysis and tuning

The proposed cultivation technique is based on two separate control loops. The objective of the first loop, involving the feed flow rate, is to achieve a slight glucose excess. The second loop aims at maintaining a constant dissolved oxygen level by manipulation of temperature and stirrer speed. If the temperature controller is appropriately tuned, the coupling between the two loops is weak. The cultivation technique will be analysed in two steps by examining the control loops separately. The dissolved oxygen controller should be tuned in such a way that the loops are weakly coupled.

Feed control

The original probing feeding strategy leads to a stationary specific uptake rate q_g that is below q_g^{crit}. At steady state, some acetate is produced during the probing pulse, but it is rapidly consumed during the following oxygen control phase. According to Figure 4.4, it seems possible to achieve a stationary state above q_g^{crit} by making down-pulses. Since acetate is continuously produced when $q_g > q_g^{crit}$, it is not obvious that such a steady state can be achieved. The model equations from section 4.2 can be used to show the feasibility of the approach and provide some help for the design.

We will investigate whether the probing controller can drive the process to a stationary state in the region Ω_3 of the (q_g, A) plane. By stationary state it is meant that the feed rate computed by the probing controller is, at steady state, a constant corresponding to a q_g value above q_g^{crit}. Since the controller periodically performs probing pulses in the feed rate, a stationary state should be interpreted as a closed trajectory in the plane (q_g, A), see Figure 4.6:

- The acetate accumulated during the control phase should be totally consumed during the probing phase
- The small pulse response should not lead to any feed adjustment

For a pulse response to be visible, the specific oxygen uptake rate should not be saturated during the entire pulse. We should therefore have $X_4 \in \Omega_1$.

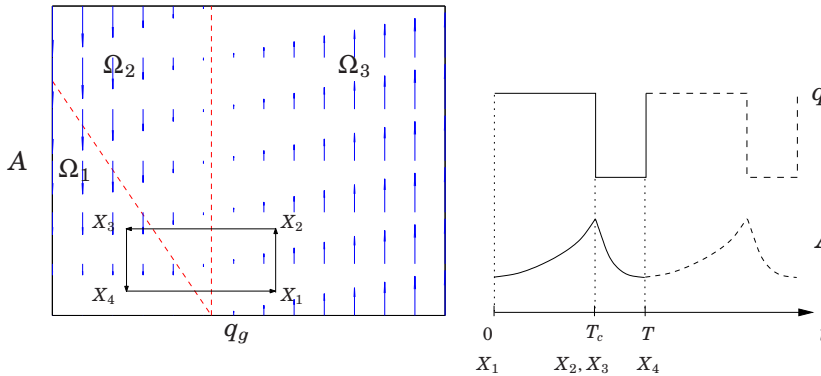

Figure 4.6 Stationary trajectory (q_g, A) in the phaseplane (left) and as a function of time (right). The control phase with length T_c starts at $X_1 \in \Omega_3$: the feed rate is constant and acetate is continuously produced. The probing pulse, performed downwards, results in a jump from X_2 to $X_3 \in \Omega_1$, where acetate is consumed. At the end of the pulse, the feed rate recovers its initial level if the change in the oxygen uptake rate from X_2 to X_3 gives a pulse response $\Delta O = y_r$.

We will restrict the search for steady state solutions $X(t)$ satisfying

$$X(t) \in \begin{cases} \Omega_3 & \text{for } t \in [0, T_c) \\ \Omega_1 & \text{for } t \in [T_c, T) \end{cases} \tag{4.19}$$

According to equation (4.13), the acetate dynamic becomes

$$\frac{dA}{dt} = \begin{cases} Y_{ag}(q_g - q_g^{crit})X & \text{for } t \in [0, T_c) \\ -\dfrac{A}{\tau}X & \text{for } t \in [T_c, T) \end{cases} \tag{4.20}$$

The specific glucose uptake rate is given by

$$q_g(t) = \begin{cases} q_g & \text{for } t \in [0, T_c) \\ q_g - q_g^p & \text{for } t \in [T_c, T) \\ q_g = q_g + \kappa K_g(\Delta O - y_r) & \text{for } t = T \end{cases} \tag{4.21}$$

Neglecting the oxygen dynamic, the size ΔO of a pulse is proportional to the change Δq_o in the specific oxygen uptake rate after a pulse:

$$\Delta O = K_o \left(q_o(T) - q_o(T_c)\right) \tag{4.22}$$

where the specific oxygen uptake rate is a function of q_g and A, see (4.10) and (4.12). By integrating the acetate dynamic along the probing cycle, we get the following condition for (q_g, A) to be a stationary solution

$$A_e \begin{bmatrix} q_g \\ A \end{bmatrix} + a_e = \begin{bmatrix} q_g \\ A \end{bmatrix} \tag{4.23}$$

where A_e and a_e are given in appendix B.3. If the probing gain κ and the control phase duration T_c satisfy

$$0 < T_c < \frac{\tau(1 + e^{T_p X/\tau})}{Y_{oa} Y_{ag} X}\left(\frac{2}{\kappa K Y_{og}} - 1\right) \tag{4.24}$$

$$0 < \kappa \frac{K Y_{og}}{2} < 1 \tag{4.25}$$

then we have a stable stationary point (q_g, A) in the region Ω_3. Condition (4.25) is similar to (3.57) and limits the probing gain. Inequality (4.24) limits the length of the control phase during which acetate accumulates and it shows the importance of a good dissolved oxygen controller. Short probing pulses and a slow acetate consumption impose short control phases. It is also remarkable that a large probing gain imposes a short control phase, which is the opposite of (3.60). Instabilities in the feed rate can be caused by the oxygen dynamic if T_c is too small (see Chapter 3) and by the acetate dynamic when T_c is too large. Choosing $\kappa^{-1} = K_o K_g Y_{og}$ (deadbeat control) and the numerical values listed in appendix, the constraint (4.24) becomes $0 < Tc < 13$ min.

Dissolved oxygen control using mid-ranging

Design procedure. Mid-ranging is a simple control structure that solves the allocation problem. A benefit of having two SISO controllers concerns the design procedure: the controllers can be tuned one at a time just like in conventional cascade control. Mid-ranging and conventional cascade control are actually closely related. The mid-ranging control problem

$$\begin{aligned} y &= P_1 \begin{bmatrix} 1 & P_2 \end{bmatrix} u \\ u &= \begin{bmatrix} 1 & C_2 \end{bmatrix}^T C_1 y \end{aligned}$$

is the formal dual problem of the cascade control problem

$$\begin{aligned} y &= \begin{bmatrix} 1 & P_2 \end{bmatrix}^T P_1 u \\ u &= C_1 \begin{bmatrix} 1 & C_2 \end{bmatrix} y \end{aligned}$$

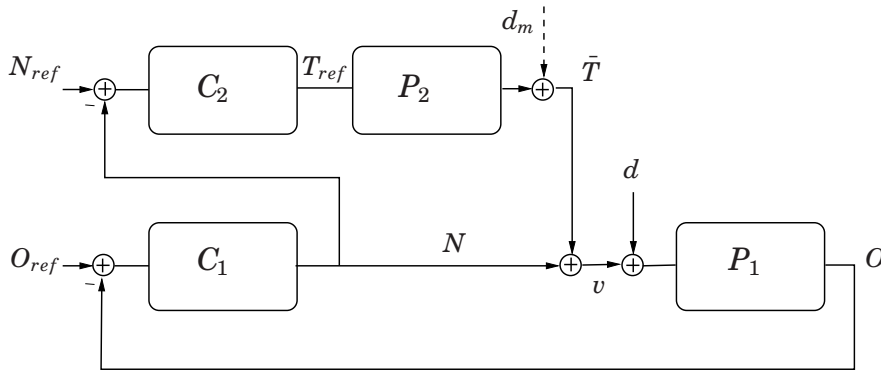

Figure 4.7 Oxygen control using a mid-ranging configuration. Disturbances like feed changes or cell growth are modeled by the signal d. The virtual input d_m represents unmodeled temperature dynamics.

A dual relationship can also be demonstrated using the method presented in [Bernhardsson and Sternad, 1993]. The close correspondence between mid-ranging control and cascade control strengthens the design procedure in two steps. The fast controller can be designed separately to get satisfactory performance before the activation of the second loop. The second controller should be tuned in such a way that it does not interfere with the initial control loop at high frequencies. We assume that both controllers are PI controllers and that C_1 has already been designed. We will now present some guidelines for the design of the second controller.

The closed-loop system for dissolved oxygen control is represented in Figure 4.7. Disturbances on the dissolved oxygen representing growth or feed changes are modeling by the signal d. The input d_m represents unmodeled dynamics in the temperature model.

The role of C_2 is to compensate for the saturation in u_1 by increasing the control authority in the low frequency range. An integrator in C_2 is thus necessary to get $N = N_{ref}$ at stationarity in spite of constant disturbances d.

In order to understand how the control allocation is influenced by C_2, one can write the total control effort v as ($N_{ref} = 0$):

$$v = \bar{T} + N = (1 - P_2C_2)N$$

At those frequencies where P_2C_2 is small compared to 1, the temperature controller is not active. Both controllers work equally at frequencies ω such that $|P_2C_2(i\omega)| \approx 1$. To guarantee that temperature does not work

at high frequencies, C_2 can be chosen to be an integrator

$$C_2 = \frac{k_i}{s} \tag{4.26}$$

The choice of the integrator gain k_i is a compromise between robustness and performance.

Robustness. To guarantee some stability robustness in presence of uncertainty in the temperature dynamic, a constraint of the following type could be satisfied:

$$M_s = ||S||_\infty < \alpha \tag{4.27}$$

where the sensitivity function can be computed to be

$$S = G_{\bar{T},d_m} = \frac{1}{1 + G_{N,\bar{T}} P_2 C_2} \tag{4.28}$$

Similarly to cascade control, the inner loop transfer function $G_{N,\bar{T}} = \frac{P_1 C_1}{1+P_1 C_1}$ can be approximated by the constant 1 when the bandwidth of the inner loop is greater than that of $P_2 C_2$. A low value for $||S||_\infty$ will ensure a well-damped behavior, which is of primary importance to avoid overreaction of the temperature.

Performance. The disturbance d includes a ramp function modeling the cell growth. This leads to a stationary error $N_\infty - N_{ref}$ depending on the integrator gain:

$$N_\infty - N_{ref} = \frac{1}{k_i P_2(0)} \Delta d \tag{4.29}$$

The ramp disturbance reduces the operating range of the stirrer speed for a good rejection of fast disturbances. The integrator gain should therefore be chosen large enough for a sufficient margin to the saturation:

$$N_\infty - N_{ref} < \beta (N_{max} - N_\infty) \tag{4.30}$$

The integrator gain should be chosen in such a way that a typical short term perturbation does not saturate the stirrer speed. To satisfy both constraints (4.27) and (4.30), it might be necessary to decrease the reference value N_{ref}, at the expense of a lower utilization of the reactor.

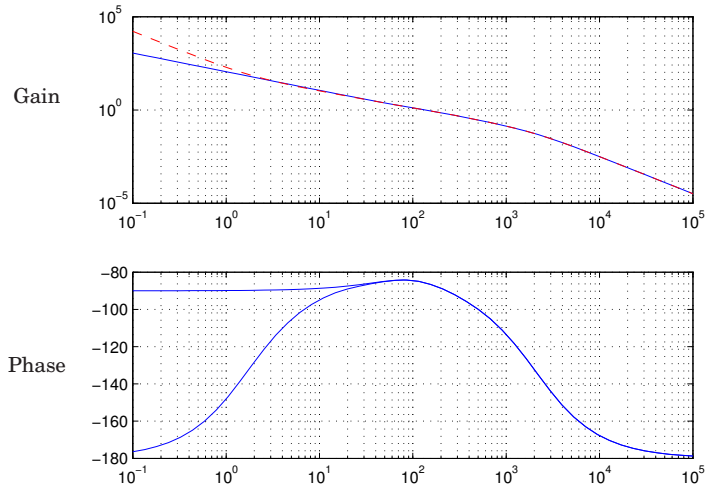

Figure 4.8 Bode plots for the open-loop system P_1C_1 without the temperature controller (dashed) and $P_1C_1(1 + P_2C_2)$ with the temperature controller (solid).

Numerical example. We can now apply the design procedure on the bioreactor example, using numerical values corresponding to a laboratory-scale reactor, see Appendix B.4. The oxygen dynamic, described by P_1 and P_2 is obtained after linearization of the reactor model, see Section 4.2.

$$\begin{aligned} P_1 &= \frac{K_N}{(T_o s + 1)(T_p s + 1)} \\ P_2 &= \frac{\frac{K_{ot}}{K_N}}{T_t s + 1} \end{aligned} \tag{4.31}$$

The controller manipulating the stirrer speed is a PID with gain $K = 18$ and integral time $T_i = 40\ s$. This gives good performance when operating at $N \approx 1000\ rpm$, see [Åkesson and Hagander, 1999]. The maximal stirrer speed is $N_{max} = 1100\ rpm$. A growth of 6 $g/l/h^{-1}$ is modeled by the disturbance $d = 40/s$. To guarantee $M_s < 1.5$ and a static error less than 50 rpm in presence of the load disturbance d, we should choose k_i in the range $0.17 - 0.5$. We take $k_i = 0.3$, which leads to a M_s value of 1.3.

Figure 4.8 shows a bode diagram for the loop gain with and without the extra loop involving the temperature. The controller C_2 contributes to a larger gain in the low frequency region and prevents the stirrer speed from saturating. Its influence around the cross-over frequency is negligible. A

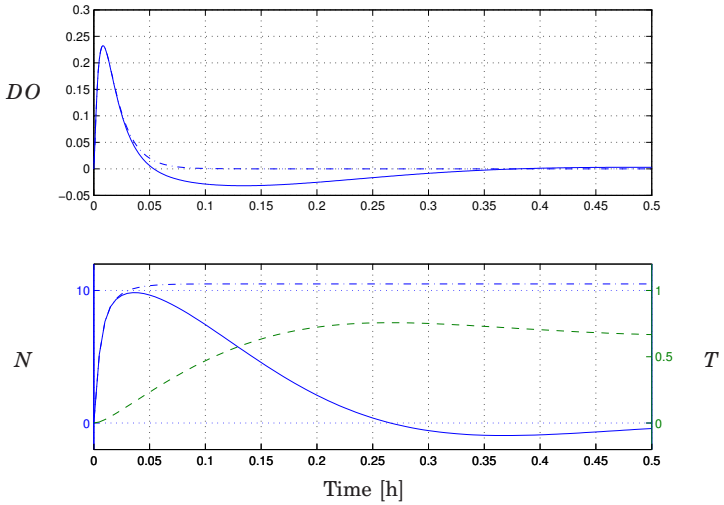

Figure 4.9 Step disturbance simulation of the dissolved oxygen control loop. Top: dissolved oxygen DO ([%]). Bottom: stirrer speed N ([rpm]) in solid and temperature T ([^{o}C]) in dashed. The simulation result shown in dashdot is without the temperature control loop.

step response simulation is shown in Figure 4.9. The amplitude of the step corresponds to a feed change as large as a pulse. The disturbance results in a peak in the agitation of 10 rpm, which is small compared with the available margin to the saturation (100 rpm). Note that the disturbance rejection at the output is almost unchanged when using the additional loop.

Nonlinear considerations. The design procedure was based on linear analysis. When large disturbances like antifoam addition perturb the process, the agitation speed will inevitably saturate. To avoid wind-up phenomena, an anti-windup scheme is often implemented to keep the control signal close to saturation $N \approx N_{max}$. If the reference value N_{ref} is chosen close to N_{max}, the input to the temperature controller C_2 will be constant and small during saturation of N. The temperature loop will then be broken and ineffective. For reasonable performance during saturation, the agitation speed should not be quickly reset by the anti-windup controller. An alternative would be to use the anti-windup controller input $sat(N) - N$, as an extra input to the temperature controller. It would increase the control authority of the temperature controller when the agitation saturates.

4.6 Evaluation of the control strategy

The fermentation technique previously described will now be evaluated using simulations and experiment.

Simulation

The full nonlinear model given in section 4.2 is used together with the numerical values listed in the appendix to simulate a bioreactor running in fed-batch mode. Figure 4.10 shows the result of a simulation.

When the stirrer speed has reached $N_{ref} = 1000rpm$ at $t \approx 1\ h$, the second controller is activated and the temperature starts to decrease. The acetate accumulation after activation of the temperature controller is rapidly consumed. At $t \approx 2.5\ h$ a stationary state is achieved as predicted by the simple analysis from Section 4.5. The pulse responses are of desired size and no feed adjustment is done. The acetate pattern is as it was expected: short accumulation phases are followed by consumption phases. The acetate accumulation is controlled. Temperature decreases slowly to compensate for the increasing oxygen demand from the growing biomass. At $t \approx 3h$, a disturbance modeling a degradation of the oxygen transfer is introduced. The agitation reacts rapidly to control the oxygen level and the next pulse is not delayed.

When the control phase is long ($T_c = 15\ min$), no stationary state is achieved and acetate follows another pattern with large accumulations (Figure 4.10, dotted line). This could also be predicted by (4.24).

Experiment

The new fermentation technique was implemented and tested on a 3 l bioreactor. Figure 4.12 shows the fed-batch part of an experiment with *E. coli*. Temperature control was performed using pulse-width modulation of the cold and hot water flows. At $t \approx 15\ h$ the initial glucose amount from the batch phase is totally consumed and the glucose starts to be fed into the reactor. After 1.5 h of feeding the stirrer speed reaches $N_{ref} = 1000\ rpm$ and the temperature starts to decrease. The pulses in the feed are performed downwards to achieve a slight glucose excess. The initial decrease in the temperature does not seem to affect the dissolved oxygen concentration. This can be explained by the model which predicts a lack of authority when the glucose is not in excess, see Appendix B.1. It may also due to the weaker influence of the temperature around 37 ^{o}C. Induction of the recombinant protein occurs at $t = 16\ h$. At $t = 17\ h$ no pulse response is visible in the oxygen signal, which indicates that glucose is in excess. The feed is consequently decreased to avoid large acetate accumulations. As far as the dissolved oxygen control is concerned, good performance

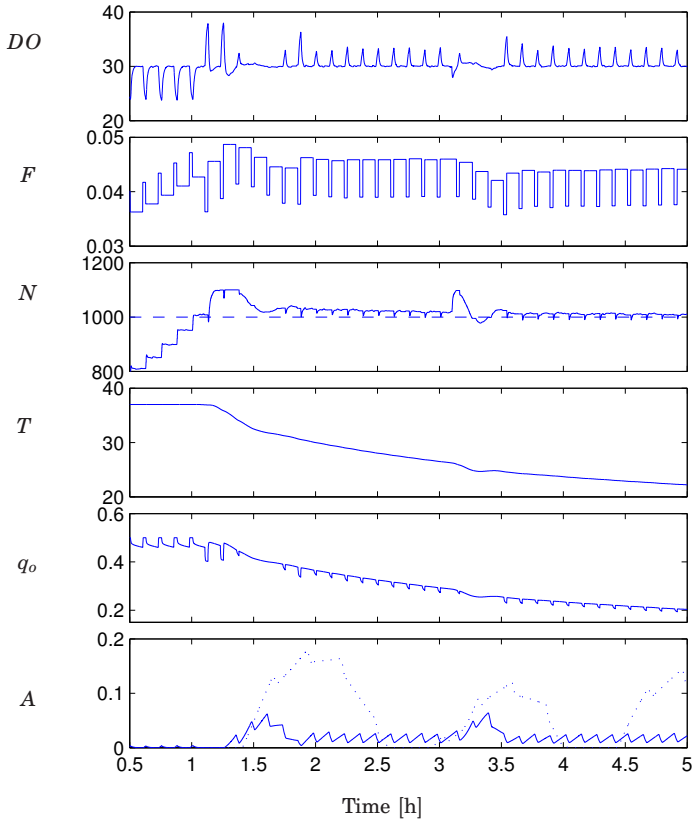

Figure 4.10 Simulation of the nonlinear model using the modified probing strategy. From top: dissolved oxygen DO([%]), feed rate F([l/h]), stirrer speed N([rpm]), temperature T([^{o}C]), specific oxygen uptake rate q_o([1/h]), acetate A([g/l]). At $t \approx 1\ h$ up-pulses are shifted to down-pulses and the temperature starts to decrease. At $t \approx 3\ h$ a decrease in K_La modeling a degradation of the oxygen transfer is introduced. The acetate in dotted line is the result of a control phase with length $T_c = 15\ min$.

is achieved. Dissolved oxygen is rapidly brought back to the setpoint after every pulse. Fast disturbances are taken care by the agitation speed, which operates around N_{ref}. Temperature decreases slowly from 37 ^{o}C to 25 ^{o}C to compensate for the increasing oxygen demand due to protein production and growth.

Unlike the substrate-limiting technique, over-feeding can easily occur after the maximum stirrer speed is reached. Indications of glucose excess

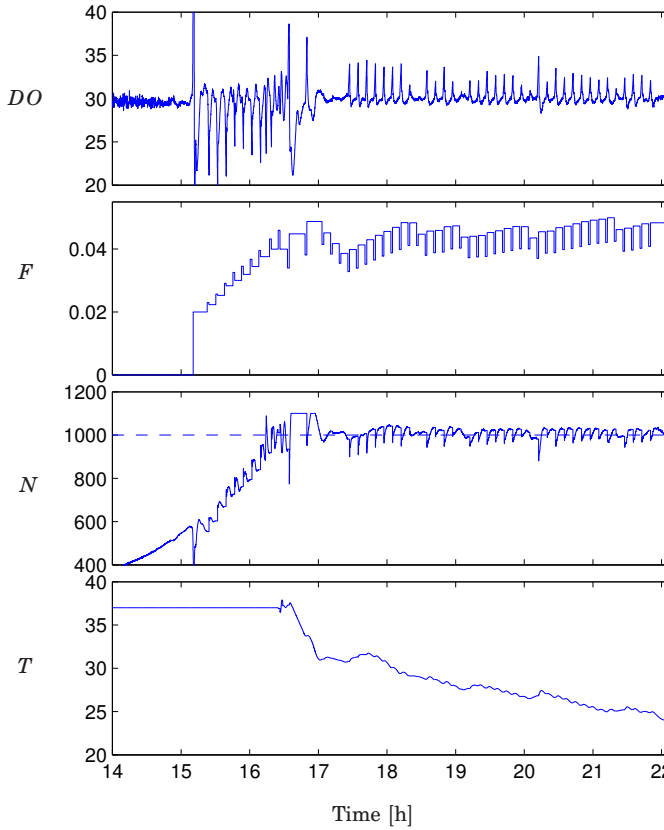

Figure 4.11 Fed-batch part of an experiment using the novel fermentation technique. From top: DO ([%]) dissolved oxygen, F ([l/h]) feed, N ([rpm]) stirrer speed, T ([^{o}C]) temperature. N_{ref} is dashed.

from the probing pulses led to a decrease in the feed at four occasions. This shows the importance of the glucose feeding in temperature limited fed-batch cultivations. It is interesting to compare the feed profiles from figures 4.1 and 4.12. In the first experiment, a 30% decrease in the feed was necessary to keep the reactor working in aerobic conditions. In the second experiment, the temperature was instead lowered and it was never necessary to decrease the feed to control the dissolved oxygen. This should be a less stressful way to limit the oxygen demand of the bacteria. The efficiency of the novel technique with respect to protein production will be evaluated in the following section.

4.7 Experimental evaluation

An evaluation of the cultivation technique with respect to glucose, acetate and product data will now be presented. Two different *E. coli* strains were cultivated, *E. coli* BL21(DE3) and *E. coli* W3110, in two different sets of reactors.

Material and methods

E. coli BL21(DE3) *E. coli* BL21(DE3) was cultivated in defined media producing xylanase cloned in pET22b [Norberg Karlsson *et al.*, 1998]. The enzyme production was induced by adding IPTG 1 - 1.5 hours after feed-start. Inoculum (1 ml) from frozen stocks were incubated at 30°C over night in 100 ml medium, containing (per liter) 10 g glucose, 2 g $(NH_4)_2SO_4$, 14.6 g K_2HPO_4, 3.6 g $NaH_2PO_4 \cdot (H_2O)$, 0.5 g $(NH_4)_2$-K-citrat, 2 ml 1 M $MgSO_4 \cdot 7(H_2O)$, 0.1 g ampicillin and 2 ml trace elements solution [Holme *et al.*, 1970]. The cultivation was performed in a 3 l bioreactor, (Belach bioteknik AB, Stockholm, Sweden) with a final volume of 2 l. The pH was kept at 7 by titration with 6.7 M aqueous ammonia. The temperature was 37°C unless otherwise stated and the aeration was 2 liters/min. The feed was started when the dissolved oxygen tension increased abruptly, and it consisted of (per liter) 500 g glucose, 50 ml 1 M $MgSO_4$ and 10 ml trace element solution. The dissolved oxygen sensor used was a polarographic electrode and its temperature dependence was low. Data logging, dissolved oxygen control and the feeding strategy were implemented on a standard PC using the industrial control system SattLine (ABB Automation, Malmö, Sweden) or Industrial IT (ABB Automation, Malmö, Sweden).

Samples were withdrawn through a sampling port at the bottom of the reactor, using 25 ml pre-sterilised metal-capped glass tubes.

- Optical density (OD) was determined at 620 nm. Samples were appropriately diluted with 0.9 % (w/v) NaCl at OD values exceeding 0.5.
- Cell dry weight (CDW) was determined after centrifuging (1400 g, 15 min, at room temperature) triplicate samples (4 ml) in preweighed glass tubes. After centrifugation, cell-pellets were dried over night (105 °C) and subsequently weighed to determine CDW.
- Samples for glucose and acetic acid determinations were collected in tubes half filled with 0.132 M perchloric acid (ice cold) and centrifuged (1400 g, 10 min, at room temperature). The supernatant

was dispensed (1 ml portions) into eppendorf tubes and neutralized with 3.6 M K_2CO_3 and kept frozen (-20 ^{o}C). The samples were then analyzed with a high performance liquid chromatography (HPLC) system (Agilent 1100 series). An organic acid and alcohol analysis ion-exclusion column (Micro-Guard precolumn cation H-cartridge (30 x 4.6 mm) followed by an Aminex HPX-87-H (300 x 7.8 mm), BioRad, Hercules, USA) was used at 50 ^{o}C with 80 mM H_2SO_4 as mobile phase at flow rate of 0.6 mL/min followed by refractive index detection.

- Xylanase activity was determined using the DNS (3,5-dinitrosalicylic acid) method [Bailey *et al.*, 1992]. The activity was determined under the conditions described in [Norberg Karlsson *et al.*, 1998] using xylose as standard (2-10 mM). Enzyme blanks were prepared for each sample by incubating the substrate, 1% (w/v) birch xylan (Birch 7500, Roth, Karlsruhe, Germany), at 65 ^{o}C for 5 min, then adding the DNS-reagent and immediately thereafter the enzyme. The xylanase activity was expressed in units (U) defined as the amount catalyzing the transformation of 1 μmol of the substrate per minute under standard conditions.

E. coli W3110 *E. coli* W3110 was cultivated in defined media producing the protein ZZT2 which was cloned in pRIT44T2. The protein production was induced by adding indole-3-acrylic acid 3.5 hours after the feed-start. Colonies from an agar plate were used to inoculate shake-flasks with defined media containing (per liter) 10 g glucose, 0.1 g tryptophan, 0.1 g thiamin, 2.64 g $(NH_4)_2SO_4$, 2 g Na_2SO_4, 14.6 g K_2HPO_4, 3.6 g $NaH_2PO_4{\cdot}(H_2O)$, 1 g $(NH_4)_2$-H-citrat, 2 ml 1 M $MgSO_4{\cdot}7(H_2O)$, 0.1 g ampicillin and 3 ml trace elements solution [Holme *et al.*, 1970]. When the OD has reached 5 the 100 liters stainless steel bioreactor containing 50 liters of the media mentioned above was inoculated. pH was regulated at 7.0 by addition of 25 % ammonia solution. The temperature was 35^{o}C - 31 ^{o}C and the airflow was 1.5 vvm. The feed was started when the dissolved oxygen increased abruptly and it contained (per liter) 500 g glucose, 0.1 g tryptophan, 0.1 g thiamin, 5.36 g $(NH_4)_2SO_4$, 4 g Na_2SO_4, 29.2 g K_2HPO_4, 7.2 g $NaH_2PO_4{\cdot}(H_2O)$, 2 g $(NH_4)_2$-H-citrat, 2 ml 1 M $MgSO_4{\cdot}7(H_2O)$, 0.1 g ampicillin and 3 ml trace elements solution. The dissolved oxygen sensor used was a polarographic electrode. A combination of two control systems was used to control the cultivation, BioPhantom (Belach bioteknik AB, Stockholm, Sweden) and SattLine (ABB Automation, Malmö, Sweden).

Samples were withdrawn through a sampling port at the bottom of the reactor. Cell dry weight (CDW) was determined after centrifuging

(5000 rpm, 10 min, at room temperature) triplicate samples (5 ml) in pre-weighed glass tubes. After centrifugation, cell-pellets were dried for 24 hours (105 ^{o}C) and subsequently weighed to determine CDW.
The optical density (OD) was determined at 550 nm. Samples were appropriately diluted with phosphate, PBS at OD values exceeding 0.3.

Dissolved oxygen control The dissolved oxygen is controlled between the pulses using the stirrer speed. A gain-scheduled PID with respect to the stirrer speed is used and a set-point value of 30 % is chosen. During a feed pulse the stirrer speed is frozen.

Temperature Control A well tuned temperature controller is important when the temperature is to be changed. Here the temperature control is performed by a proportional pulse-width modulation of the cold and hot water flows.

Results

Three cultivations with *E. coli* BL21(DE3) and one using *E. coli* W3110 are presented. These results were obtained at a first attempt.

E. coli BL21(DE3) The reference cultivation where the original probing feeding strategy is used is shown in figure 4.1. During the later part of the cultivation the controller lowers the feed to keep the reactor working in aerobic conditions.

In figure 4.12 the other two cultivations are shown where the modified feeding strategy is used. During the later part of the cultivation the temperature is here decreasing to a final value of 22 ^{o}C.

Figure 4.13 shows the cell mass, acetic acid, glucose and product activity. The cell mass obtained in the reference cultivation is 34 g/l. With the modified feeding strategy the cell mass produced is a bit larger, around 41 g/l. In the reference cultivation the final glucose and acetic acid concentrations in the reactor are 0.1 g/l. With the modified feeding strategy the final glucose concentration is 1.2 g/l and the final acetic acid concentration is 0.3 g/l. The specific enzyme activity starts to decrease 3.5 h-4.5 h after feed start in all three cultivations. With the modified feeding strategy, the apparent decrease in specific activity could be explained by a ceased production of active enzyme (and unchanged activity in U/l during the last hour of the production phase). In the reference cultivation, both the activity (U/l) and specific activity decreased (the latter from 7200 U/g CDW to 2600 U/g CDW). In addition a significant increase in activity in the cell broth was monitored in the reference cultivation (indicating cell-lysis) (figure 4.13), and despite combining cell broth and intracellular activity the total activity was reduced at the end of the cultivation.

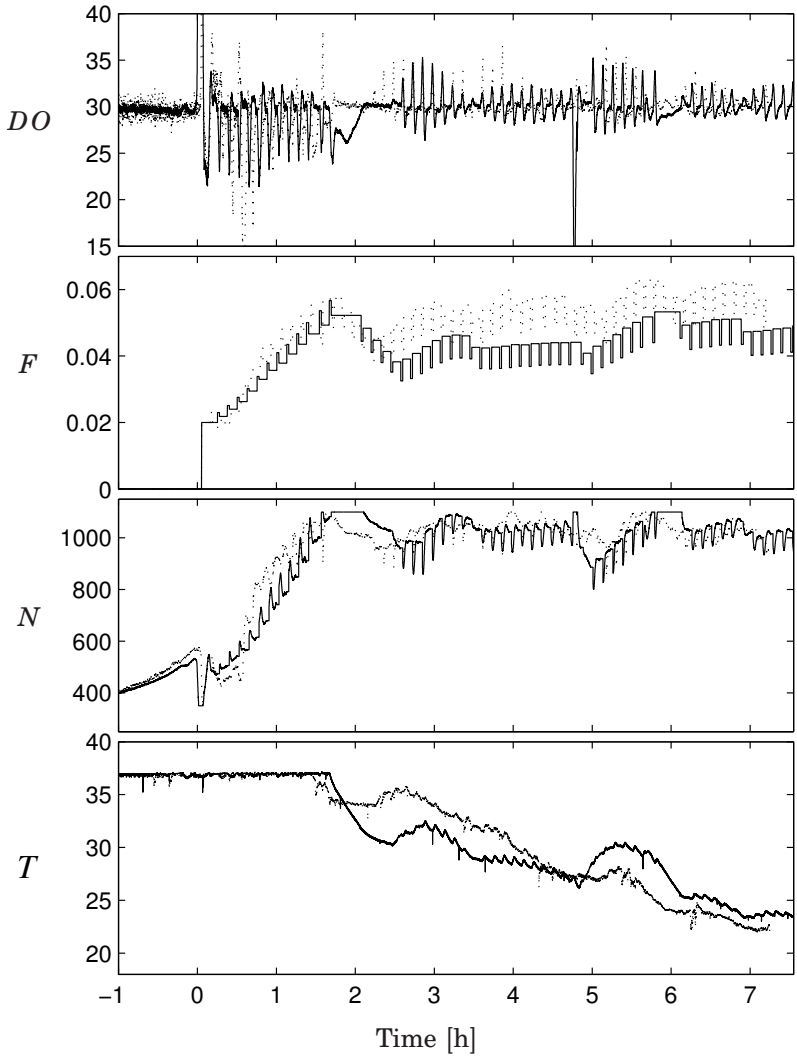

Figure 4.12 Experiments with *E. coli* BL21(DE3) using the modified probing feeding strategy. The fed-batch part of the cultivation is shown. From top: DO dissolved oxygen, F feed, N stirrer speed, T temperature. At t = 18.2 h a filter in the outlet gas is replaced (solid). N_{ref} = 1000 RPM

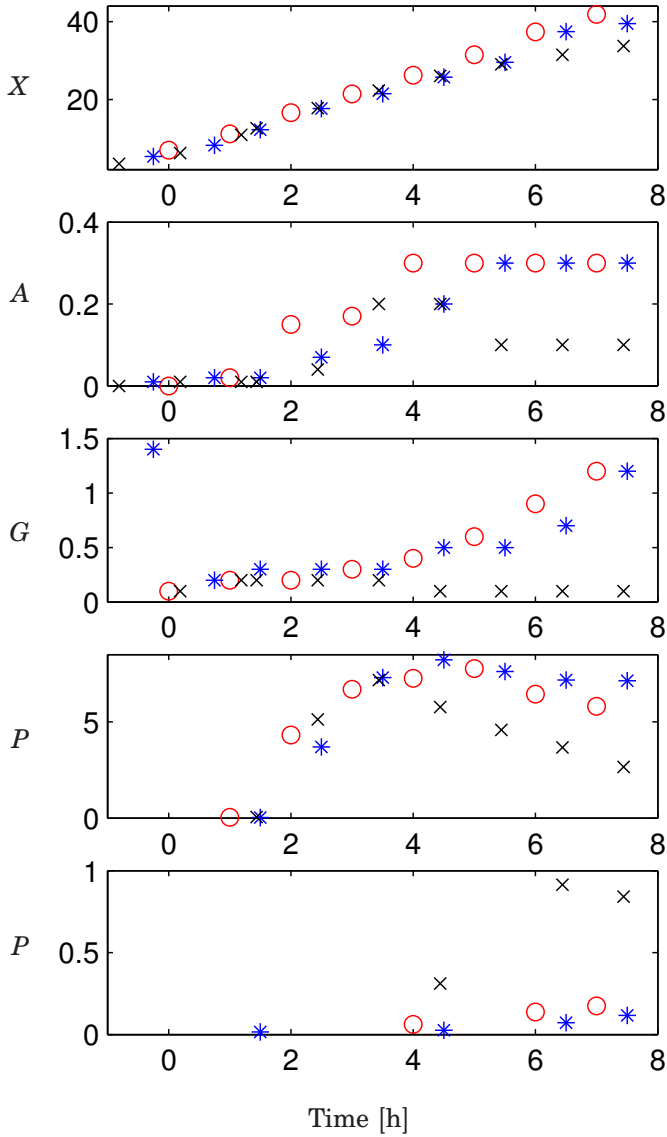

Figure 4.13 From top: X ([g/l]) cell mass, A ([g/l]) acetic acid, G ([g/l]) glucose concentration, P ([U/mg CDW]) specific product activity in the cells and P ([U/mg CDW]) specific product activity in the broth for the three experiments with *E. coli* BL21(DE3). The reference cultivation (x), the other two where the modified feeding strategy is used denoted o (dashed in figure 4.12) and * (solid in figure 4.12). Time after feedstart.

E. coli W3110 A cultivation where the modified feeding strategy is used is shown in figure 4.14. The temperature is first decreasing to 32 ^{o}C and then increasing again to 35 ^{o}C in order to keep the stirrer working at its maximum. The final cell mass achieved is around 27 g/l.

Discussion

The goal is to utilize the reactor as effectively as possible with respect to the production of the recombinant protein. When producing xylanase using the original probing feeding strategy, a decrease in enzyme activity was observed approximately 2 h after induction (figure 4.13 (x), [Ramchuran *et al.*, 2002]). This may be due to the low glucose concentration in the reactor which could lead to stress for the bacteria. The low glucose concentration is the result of the limitation in the oxygen transfer capacity of the reactor. To keep the reactor working under aerobic conditions when the maximum stirrer speed is reached the feed-rate is decreased as described previously.

Another way to handle the limitation in the oxygen transfer is to lower the temperature, which is done in the modified feeding strategy. As seen in figure 4.12 and figure 4.13 the strategy leads to reproducible results. A higher glucose concentration is achieved, around 1 g/l, without significant acetic acid accumulation (figure 4.13 (o and x)). Avoiding accumulation of acetic acid is important since high levels inhibit growth and production.

A lower temperature and a higher glucose concentration seem to be less stressful for the bacteria and the decrease in xylanase activity (U/l) during the late production phase can be avoided (figure 4.13 (o and *)). One reason for the higher xylanase activity is that the proteolysis of the produced enzyme occurs to lesser extent when using the temperature limited fed-batch technique in comparison to the substrate limited limited fed-batch [Rozkov, 2001]. In an attempt to verify if the cells are less stressed the amount of endotoxins was analyzed, but the results were inconclusive. Thus the result from [Silfversparre *et al.*, 2002] that the amount of endotoxins released is smaller for the temperature limited fed-batch technique could not be confirmed when compared to our substrate limited fed-batch technique. During the reference cultivation more foaming was observed during the last hours, indicating cell-lysis. The larger amount of active xylanase in the broth (figure 4.13(x)) further supports this idea. Thus in this case, with *E. coli* BL21(DE3) producing xylanase, the modified feeding strategy is the preferred technique.

The usefulness of the modified feeding strategy is further demonstrated on another *E. coli* strain cultivated in a larger bioreactor, see figure 4.14. The temperature is not decreasing as much as in the cultivations shown in figure 4.12. The reason is that the cell mass after induction is increasing less. During the 8 hours of production the cell mass

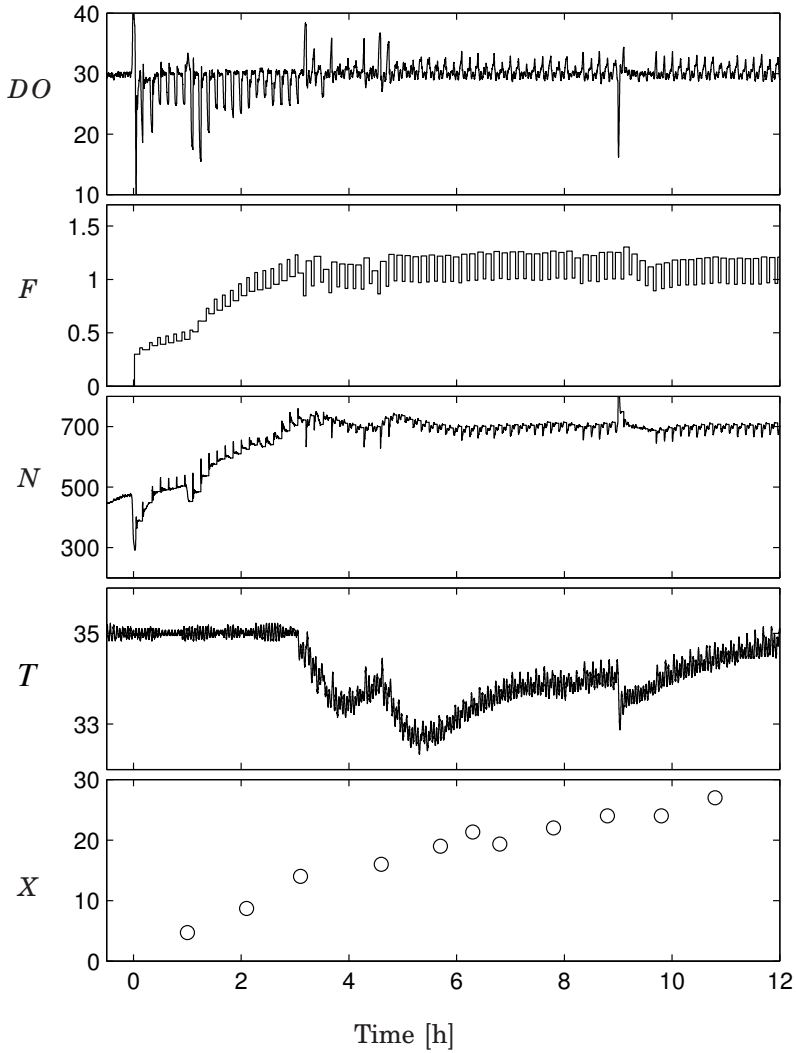

Figure 4.14 Experiment with *E. coli* W3110 using the modified probing feeding strategy. The fed-batch part of the cultivation is shown. From top: DO dissolved oxygen, F feed, N stirrer speed, T temperature, P reactor pressure, X cell mass. At t = 9 h antifoam is added. N_{ref} = 700 RPM

increases from 20 g/l to 27 g/l. The cell mass for *E. coli* BL21(DE3) is increasing from 12 g/l to 40 g/l during the 6 hours of production-phase. Thus the need for a temperature decrease to lower the oxygen demand is smaller for *E. coli* W3110 than for the *E. coli* BL21(DE3) construct. The small temperature change indicates that the difference between the probing feeding strategy and the modified feeding strategy is small when using this *E. coli* strain.

The modified feeding strategy is the preferred cultivation technique when the oxygen demand of the cultivation is increasing during the production phase. The temperature in the reactor is the highest possible considering the oxygen limitation and the stirrer speed is kept close to its maximum (figure 4.12, figure 4.14). When the total oxygen consumption does not increase significantly after induction the proposed technique behaves as the original probing feeding strategy.

4.8 Summary

A novel cultivation technique combining the advantages of probing control and temperature limited fed-batch technique has been presented. By performing down-pulses in the feed rate, a controlled excess in glucose can be achieved. For a frequent probing, an efficient dissolved oxygen controller manipulating temperature and agitation in a mid-ranging configuration has been proposed. The feasibility of the technique was demonstrated by simulations and experiments. Tuning guidelines based on simple analyses were also presented. The proposed technique has been implemented on different platforms. It was evaluated in cultivations with *E. coli* BL21(DE3) producing xylanase. A 20 % larger cell mass was obtained and the degradation of the enzyme activity was much smaller when comparing the new technique to the probing feeding strategy. The modified strategy was also tested in a cultivation with *E. coli* W3110. It is the preferred cultivation technique when the oxygen transfer limitation of the reactor is reached and one wants to continue to produce the recombinant protein.

5

Large Scale and Complex Medium

5.1 Introduction

The efficiency of the probing technique has been demonstrated by many experimental results. The feeding strategy was principally employed for fed-batch fermentations of *Escherichia coli* in laboratory scale reactors, using defined medium, see [Åkesson, 1999]. It has also been tested with success on other microorganisms presenting similar types of overflow metabolism phenomenon, see for instance [de Maré *et al.*, 2003] or [Fredriksson, 2001]. A natural continuation in the technique development would be its transfer to industrial applications.

A major concern in process development is to derive simple methods that achieve sustained performance throughout the different stages of the process. An important part of the development is concerned with scale-up. The change of reactor scale is known to have negative effects on the process productivity, see for instance [Enfors *et al.*, 2001], [Bylund *et al.*, 2000] and [Bylund *et al.*, 1998]. The transfer of the probing technique to a large scale bioreactor is not a trivial task. In a production-scale bioreactor, concentration gradients can be expected due to imperfect mixing. When a highly concentrated feed is added at a limiting rate substrate gradients are normally observed. Gradients are highly dependent on the reactor design and they are more pronounced at high consumptions rates. In presence of spatial heterogeneities the interpretation of a pulse response is naturally more difficult. It raises the question whether a local pulse response is good enough to represent the global state of the reactor. Furthermore, dissolved oxygen control, crucial in the probing technique, may not be satisfactory enough. Maintaining a constant oxygen level through-

out a fermentation involves various variables such as agitation speed, headspace pressure and aeration rate with their specific constraints and dynamics. The first objective of this chapter is to show the feasibility of the probing approach in large scale systems. Based on experimental results on industrial fermentors, scale-related effects will be discussed.

In order to enhance the productivity of a process, complex or semi-complex media can be used in place of defined media. The metabolic shifts occuring in connection with the depletion of preferred substrates can lead to quick variations in the glucose or oxygen demand. Moreover, large disturbances on the dissolved oxygen signal, that are not related to glucose consumption are potentially susceptible to perturb the probing strategy. An automated feeding strategy working in such an eventful environment would be of great help for production or process development. The second objective of the chapter is to study the impact of a complex feed on the probing feeding strategy.

The performance and limitations of the probing strategy will be evaluated in large scale systems and in systems with complex medium. Two series of experiments are used for the evaluation. The first set of fermentations was carried out with a defined medium in a 12 m^3 tank. In the second group of experiments, performed in a 7.5 m^3 tank, the medium contained complex compounds. The evaluation includes a performance assessement from a control perspective and, when available, an analysis based on offline data such as glucose, acetate and product concentrations.

5.2 Cultivation procedure and material

To facilitate future references to the different setups and experiments, we will refer to the following cases

- Process A: the process performed in the 12 m^3 reactor using defined medium.
- Process B: the process performed in the 7.5 m^3 reactor using complex medium.

The cultivations from each process will also be numbered. The first fermentation in Process A will for instance be denoted by A1. A schematic view of the two processes is shown in Figure 5.1.

Process A

Two fed-batch cultivations using a recombinant *Escherichia coli* strain were performed in a 12 m^3 stirred tank reactor. The volume after inoculation was 3500 l, with a glucose concentration of 15 g/l. The glucose

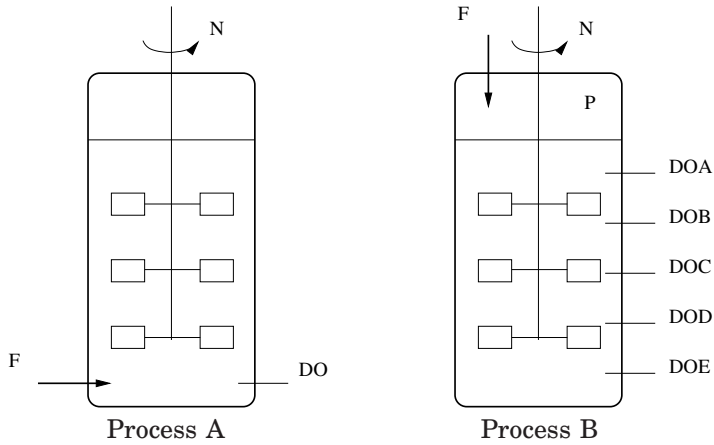

Figure 5.1 Two large-scale reactor setups with feeding points (F), dissolved oxygen (DO) probe location and dissolved oxygen control variables. N and P respectively denote agitation speed and pressure.

feed ($600\ g/l$) was injected into the reactor through a port located in the wall at the bottom part of the tank. The feed flow to the fermenter was regulated by a flow control valve. The pH was kept at 7.0 by addition of ammonia. The temperature, regulated at 30^oC was increased before induction to 37^oC within a few minutes. The air flow rate was $260m^3/h$ and the pressure was stepwise increased to reach 1.1 bar overpressure before induction. The dissolved oxygen concentration was monitored by a polarographic oxygen electrode at the bottom part of the tank and controlled by varying the stirrer speed in the range 50-130 rpm. The exhaust gas was analysed using a gasanalyser with a paramagnetic cell for oxygen measurement and infrared for carbondioxid measurement. Conventional reactor control and data logging was made by SattCon31-90 together with SattGraph1200 control systems. The probing-control algorithm was also implemented in the SattCon system.

Process B

Organism. The recombinant bacterial culture used in this study has been described previously [Bylund *et al.*, 2000; Castan and Enfors, 2002; Castan *et al.*, 2002a; Castan *et al.*, 2002b]. It is the wild-type *Escherichia coli* K12 strain W3110, with a pBR322-derived plasmid coding for recombinant human growth hormone (rhGH).

Medium. As described in [Castan and Enfors, 2002; Castan *et al.*, 2002a; Castan *et al.*, 2002b; Forsberg *et al.*, 1997] the cultivation medium is a glucose mineral salt medium, which has minor modifications in salts concentration and the inclusion of a complex nitrogen source.

Bioreactor. The total capacity of the reactor was 7.5 m^3. The height to diameter ratio was 3.5. The post-sterilization volume was adjusted to 3120 L, and inoculated with 480L of secondary seed. The bioreactor was equipped with 5 dissolved oxygen probes, spaced evenly from the bottom to top of the reactor. The agitation system consisted of three impellers (28 inch diameter) positioned approximately at heights equivalent to a volume of 800, 2700 and 4700 l. Consequently, the fermentation started with the highest impeller out of solution. To maintain adequate dissolved oxygen, pressure and stirrer speed could be varied in the range of $80 - 200$ rpm and $3 - 20$ psig, respectively. The pH was controlled around 7.0, and temperature at 34^oC. A sterile 60% glucose feed was supplied via a top port in the head plate of the bioreactor. The hydrostatic headpressure of the feed tank was maintained above 20 psig. Feed flow control was achieved through a Micromotion meter and the Wonderware Control system. The probing feeding strategy was also implemented in the Wonderware system.

Analytical methods. Glucose and acetate concentrations were measured by an online analyser. The limit of detection was 0.2 g/l for glucose and 2.0 $mmol/l$ for acetate. Optical density was continuously monitored by an on-line Optek ASD25-BT-N Near Infrared Sensor. Samples for product analyses were treated by osmotic shock as described in [Castan *et al.*, 2002b]. Determination of product purity and quantity can also be found in [Castan *et al.*, 2002b]. Purity and quantity of rhGH were determined by isocratic reverse-phase high performance liquid chromatography (RP-HPLC). Three peaks (A to C) were identified and characterized with RP-HPLC: peak A contained (Met(O)125)-rhGH and (des-Phe1, des-Pro2)-rhGH; peak B contained (Met(O)14)- rhGH, (des-Phe1)-rhGH (LMW), (clipped 142/143)-rhGH (clip-2), and deamidated rhGH; and peak C contained rhGH and (trisulfide Cys182-Cys189)-rhGH.

5.3 Control strategy

Feeding strategy

The feedback algorithm regulating the feed rate is given in appendix. A proportional controller is used to adjust the feed rate after every pulse.

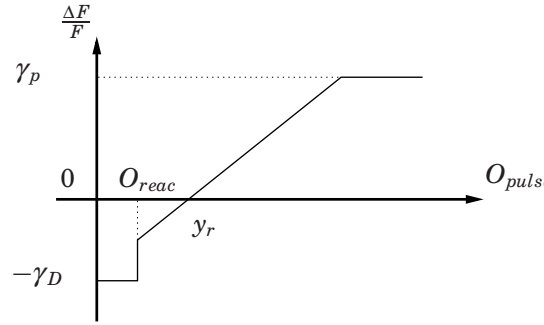

Figure 5.2 Relative feed rate adjustment as a function of the pulse response. When the pulse response O_{pulse} exceeds the reaction level O_{reac}, the feed adjustment is proportional to $O_{pulse} - y_r$. If O_{pulse} is below O_{reac}, overfeeding is assumed and the feed rate is decreased with a fixed proportion. A maximal feed increment equal to the pulse size can be implemented.

Due to the measurement noise in the oxygen signal, a moving average is used for the computation of the pulse response. Figure 5.2 shows the controller gain as a function of the pulse response. The desired size for the pulse response is y_r. The discontinuity in the gain at low pulse responses is meant for a faster feed rate decrease in case of overfeeding. The parameter values used in the different experiments are listed in Appendix C.2. In all experiments, the feed flow rate is manually decreased in connection with induction, to a level in agreement with the standard protocol.

Process A. The feed rate is started after depletion of the initial batch amount, detected by a peak in the dissolved oxygen. No feed increment larger than the size of a pulse is allowed.

Process B. The feed is started after depletion of the initial glucose, monitored by the glucose analyser. No saturation of the probing gain is implemented. After feed start, the profile from the control cultivations is first applied. Pulses are superimposed on the top of the profile and when clear responses become visible in the dissolved oxygen signal, the feeding strategy is fully activated. The bottom probe signal is used to compute the response to a pulse in the feed. The pulse experiments differ from the reference cultivations only in the growth phase, preceding the product synthesis.

Auxiliary control loops

As it is shown in Chapter 3, the performance of the probing strategy is highly sensitive to the auxiliary loops for feed flow control and dissolved

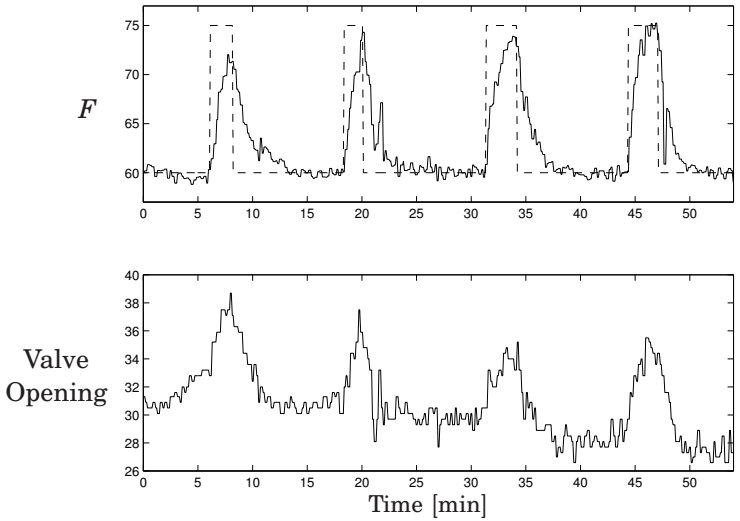

Figure 5.3 Process A. Tuning of the feed flow controller manipulating the valve opening. Top: Feed rate F [l/h]. Bottom: Valve opening [%]. The parameters of feed flow controller have been changed from $K = 1$, $T_i = 50\ s$ to $K = 2$, $T_i = 50\ s$ at $t = 12\ min$ and finally to $K = 1.5$, $Ti = 35\ s$ at $t = 42\ min$. The two first pulses have length 2 min and 1.6 min whereas the last two pulses are 3 minutes long.

oxygen control. Compared to the case of a predetermined feed profile, extra effort should be devoted to the design of these control loops.

Feed flow control system The probing feeding strategy requires a good control of the glucose flow entering the bioreactor. Exact dosing and fast setpoint following are essential conditions in order to perform small and short pulses in the feed rate. For this purpose a controller using on-line measurements of the feed flow was used. Figure 5.3 shows the tuning phase of the PI-controller that manipulates the valve opening in Process A. The achievable settling time of this loop gives a lower bound on the pulse duration. After tuning for fast response to set-point changes, the pulse length was fixed at 3 minutes.

Similar response times could be achieved in Process B, using a peristaltic pump (data not shown).

Dissolved oxygen control The settling time of the dissolved oxygen control loop imposes a lower bound on the time interval between two successive pulses. For regular feed rate updates, it is essential that dissolved oxygen recovers quickly to the setpoint after every pulse. The controller should also compensate for an exponentially growing oxygen demand.

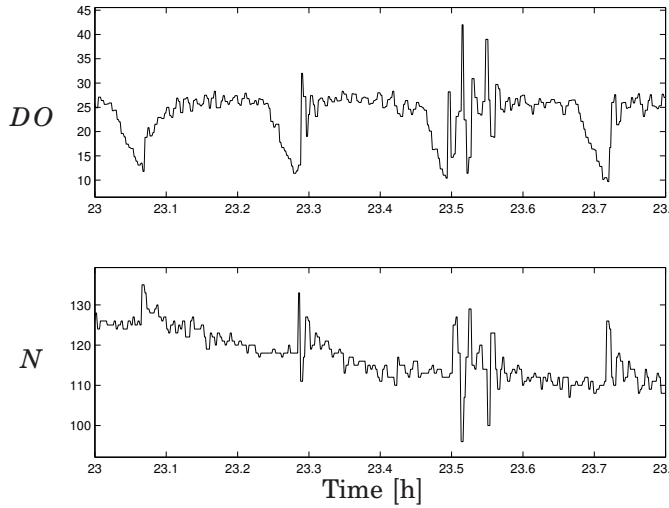

Figure 5.4 Dissolved oxygen control in Cultivation A1. Top: dissolved oxygen tension DO [l/h]. Bottom: Agitation speed N [rpm]. The integral time T_i has been changed from 100 s to 130 s at time $t = 23.65h$.

Process A A SattCon PI controller is used to maintain the dissolved oxygen tension at the desired level by manipulating the agitation speed. To get good performance throughout the cultivation, one needs to manually adjust the parameters of the controller. The integral time is typically increased to reduce the oscillations occuring at low stirrer speeds, see Figure 5.4. The manual adjustments correspond in fact to a gain scheduling from the stirrer speed.

Process B Dissolved oxygen tension is measured at five different locations in the reactor. A PID controller manipulating either agitation speed or back-pressure in the headspace is used to maintain a constant dissolved oxygen level at the bottom of the reactor (DOE). Based on the upper probe reading (DOB), the setpoint for the dissolved oxygen signal is changed to avoid oxygen limitations. The switch between agitation and pressure control is done manually, based on the available margin of each control signal. The aeration rate is manually increased to achieve an air flow rate between 1 and 1.5 vvm, and avoid large oxygen gradients.

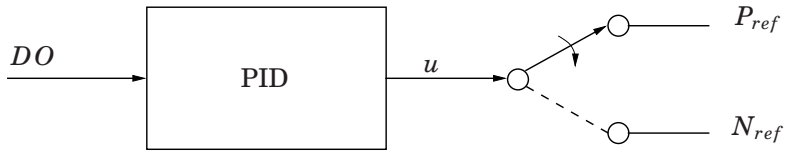

Figure 5.5 Process B. Schematic view of the dissolved oxygen controller. The output u to the PID controller determines the setpoint for either back-pressure or stirrer speed. The connection switch is performed maunally by the operator.

5.4 Results

The feeding strategy was implemented and tested on two different platforms. A total of five large scale fed-batch cultivations were carried with the probing technique. Two experiments were run in the 12 m^3 reactor where the effect of the scale could be investigated. Three other cultivations were performed in the 7.5 m^3 tank to study the combined effect of the scale and the complex medium.

Process A

The experiment results are shown in Figure 5.6, Figure 5.7 as well as in the appendix. Apart from the final product quantity, no offline data is available. For evaluation of the probing technique, the relative size of the pulse responses has been computed and plotted.

The first experiment was mainly used for tuning the probing controller and the auxiliary loops. A predetermined feed profile was applied until a good dissolved oxygen controller became available. After activation of the pulse programme the feed rate increased from 55 l/h to 75 l/h until the maximum stirrer speed was reached. In the later part of the cultivation the safety net in the controller lowered the feed rate to avoid anaerobic conditions. Production of the recombinant protein was induced at time $t \approx 11.4\ h$. The first experiment made it possible to test the performance of the feed profile and demonstrate the feasibility of probing control in large scale. No signs of overfeeding could be observed in the dissolved oxygen signal: the relative size of the pulse responses is approximately constant throughout the fermentation. The reactor capacity could be fully exploited after activation of the feeding strategy.

In the second cultivation, the probing strategy was active all the time except between $t = 10.4\ h$ and 12 h where it was turned off for induction of the product synthesis. After feed start, the feed rate remained approximately constant. Thereafter, the feedback algorithm increased ex-

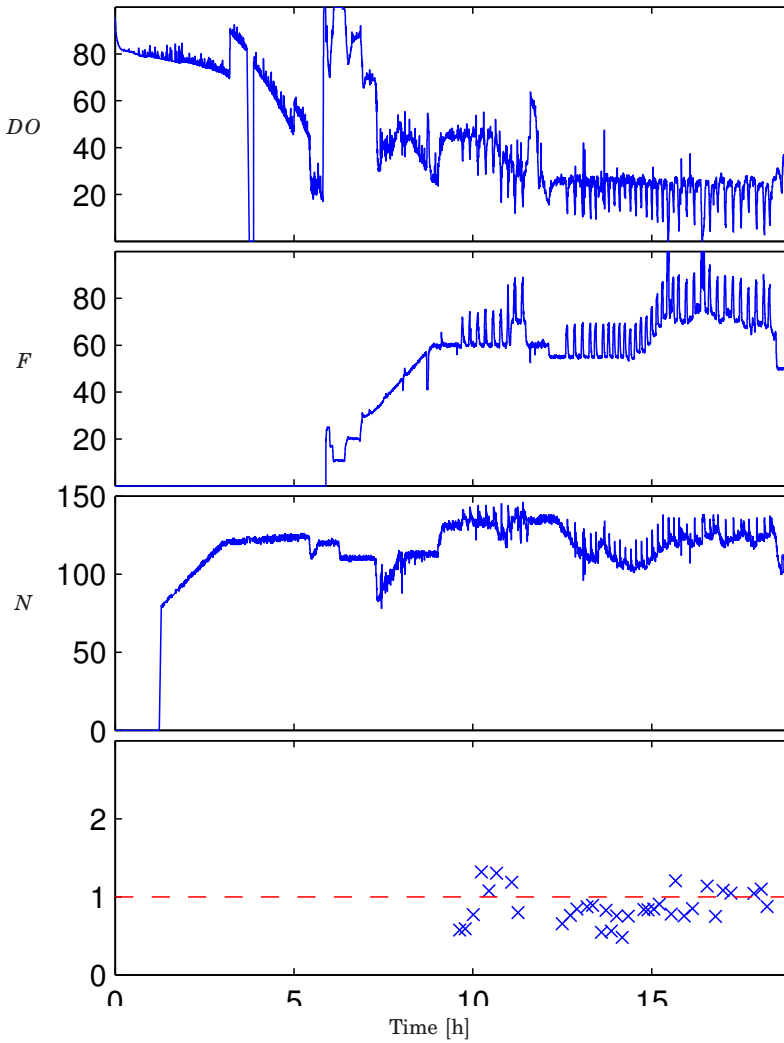

Figure 5.6 Fermentation A1. From top to bottom: dissolved oxygen tension at the bottom probe (DO, %), feed flow rate (F, l/h), agitation speed (N, rpm), normalized pulse response.

ponentially the feed rate until the maximum stirrer speed was reached. Induction of the recombinant protein occured at time $t = 11.4\ h$. The pulse programme, reactivated at $t = 12\ h$ without feed increment, decreased the feed rate when no pulse response was observed. After $t = 14\ h$, the feed rate increased again until the maximum stirrer was attained.

The main limitation was the oxygen transfer capacity of the reactor.

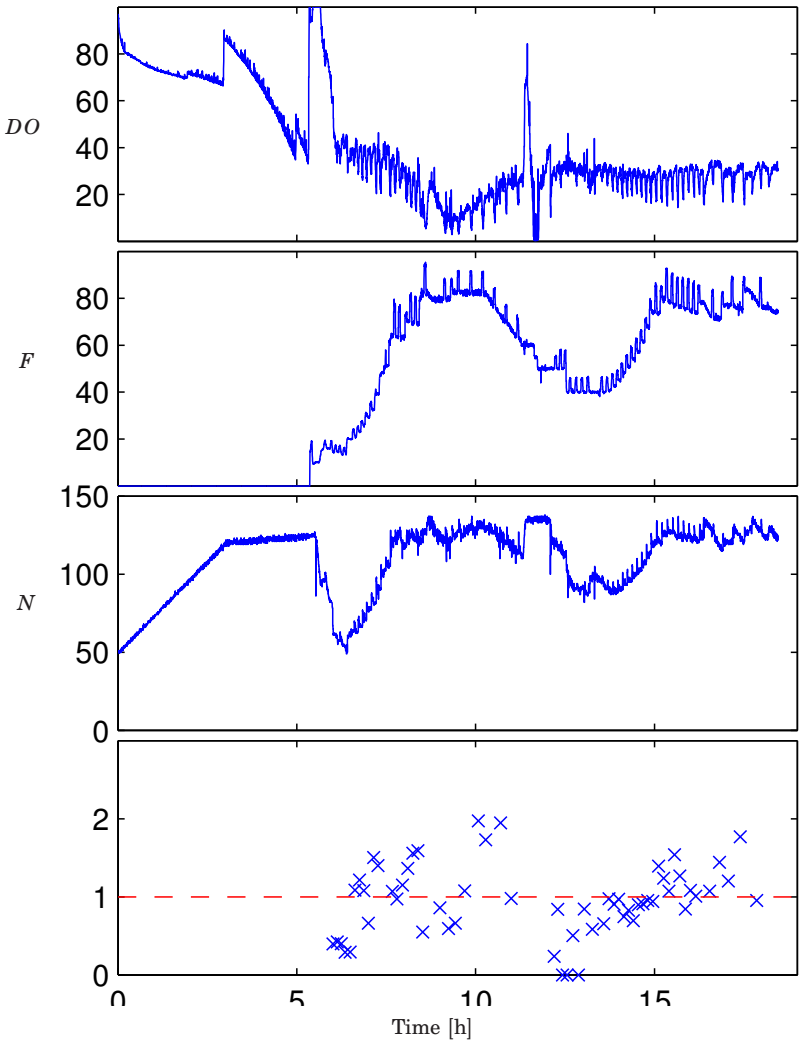

Figure 5.7 Fermentation A2. From top to bottom: dissolved oxygen tension at the bottom probe (DO, %), feed flow rate (F, l/h), agitation speed (N, rpm), normalized pulse response.

Although the pressure was increased a few times to get a higher oxygen transfer, the agitation speed remained close to its maximum value most of the time. Figure 5.8 shows the performance of the feed flow safety net. The antifoam addition at $t = 26.97\ h$ provoked a fast decrease in the oxygen level and as a consequence the saturation of the stirrer speed. In order to get the oxygen level back to the setpoint of 30%, the feed rate

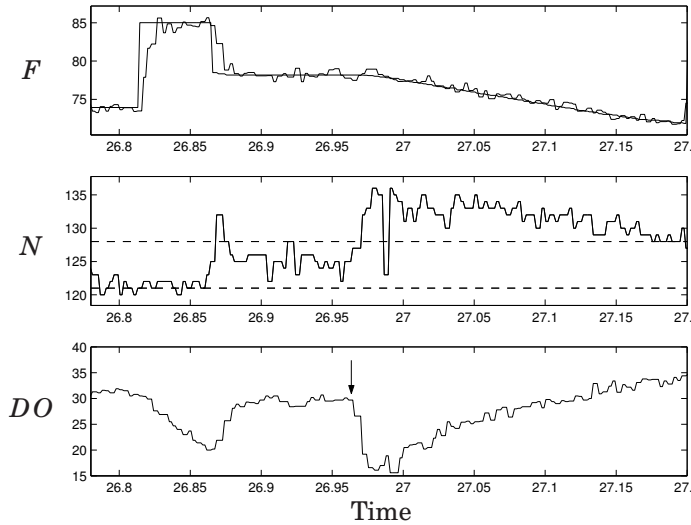

Figure 5.8 Operation close to maximum stirrer speed in Fermentation A2. From top: feed rate (F, [l/h]), agitation speed (N, rpm) and dissolved oxygen (DO, %). Antifoam is added at time 26.97 h. As long as the agitation speed exceeds 128 rpm the feed rate is decreased. When it is above 121 rpm no feed increment is allowed.

was decreased at a constant rate until the agitation speed came below $N = 128\ rpm$. The safety net avoids anaerobic conditions and leaves a margin to the saturation for the stirrer speed.

Limitations from the metabolism could be observed in the pulse responses after induction in A2. The relative size of the pulse response is clearly lower than 1 at two stages: at the activation of the pulse programme and during the post-induction phase. The small oxygen responses observed at $t \approx 6\ h$ are actually related to the unsteady character of that cultivation stage: the oxygen level was not stabilized at the setpoint 40 % and furthermore, the feed flow controller was not well-tuned. The absence of well-tuned controllers rather than the glucose level was the origin of the small oxygen responses during this period. In the early post-induction phase of the second cultivation overfeeding may have caused the small pulse responses. It has been reported that the critical glucose concentration, above which the oxygen uptake saturates, decreases after induction, see for instance [Åkesson *et al.*, 1999]. This saturation has probably been approached when no pulse response could be seen in the dissolved oxygen signal. The manual decrease in the feed rate before induction did apparently not suffice to prevent overfeeding.

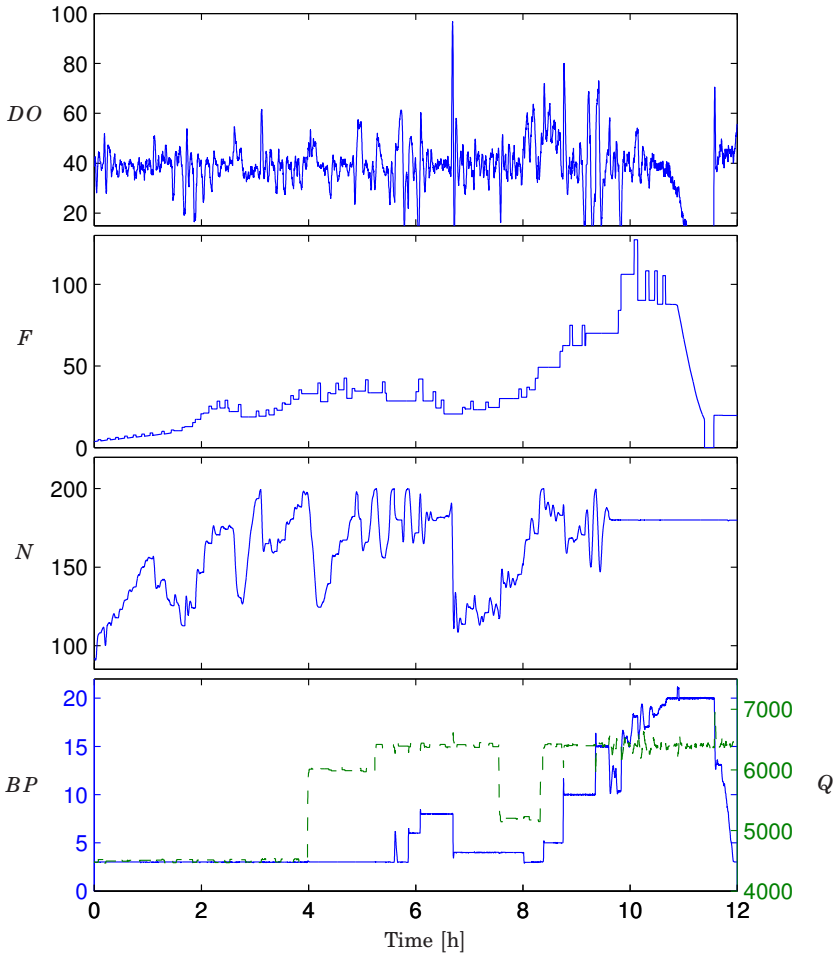

Figure 5.9 Fermentation B1. Part of a probing experiment from feed start to induction. From top to bottom: dissolved oxygen tension at the bottom probe (DO, %), feed flow rate (F, arbitrary unit), agitation speed (N, rpm), back-pressure (BP, psig) and aeration rate (Q, l/min, dashed)

Process B

Results from cultivations B1 and B2 are shown in Figure 5.9, Figure 5.10. The pulse programme was activated two and a half hours after feed start when pulse responses started to be visible in the dissolved oxygen signal.

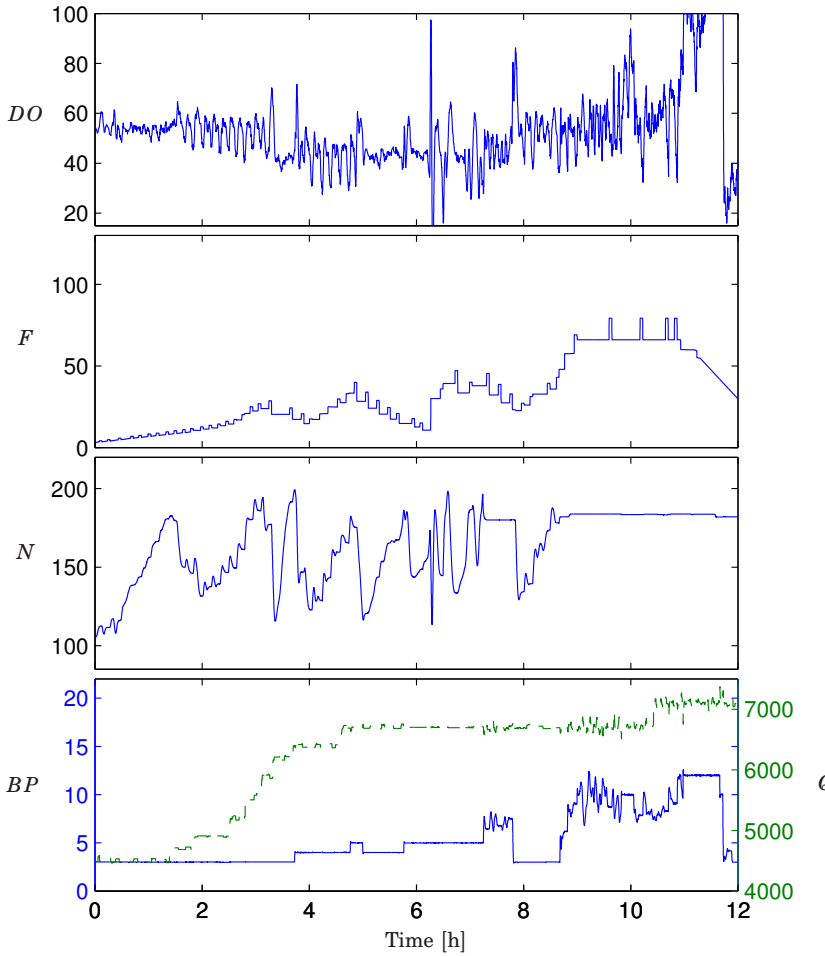

Figure 5.10 Fermentation B2. Part of a probing experiment from feed start to induction. From top: dissolved oxygen tension at the bottom probe (DO, %), feed flow rate (F, arbitrary unit), agitation speed (N, rpm), back-pressure (BP, psig) and aeration rate (Q, l/min, dashed)

Both cultivations can be divided into two phases. In the first phase, which lasts about eight hours, the feed rate is limited by the cell metabolism. Indeed, the feedback algorithm decreased or stopped increasing the glucose flow rate at many occasions. The second phase is characterized by the limitation in the oxygen transfer. After eight hours of feeding the feed

rate is rapidly increased until maximal stirrer speed and pressure are attained.

The probing technique was able to limit glucose accumulation in the reactor, using feedback from the dissolved oxygen signal. Figure 5.12, a close-up of experiment B1 between $t = 0.75\ h$ and $t = 3.75\ h$ illustrates the performance of the probing technique when the glucose demand is not monotonically increasing. The feedback algorithm gradually slowed down the pace of the feed rate increase to finally lower the feed rate twice, and thereby end the starting glucose accumulation.

In fermentation B2 the glucose concentration attained a maximum of $2\ g/l$, which is 40 % lower than the best of five reference cultivations. The result from the first pulse experiment is similar to the worst case obtained with the fixed feed profile. The acetate concentration could be kept below $11\ mM$ in the first phase of both cultivations, compared to $9.5 \pm 2.5 mM$ in the reference runs. The acetate accumulation ($26\ mM$) in the late part of B1 is to be compared with $19\ mM$ in one of the reference run. Oxygen limitation rather than glucose excess caused the acetate accumulation before induction in B1. The major part of the acetate was indeed produced after glucose achieved its maximum concentration.

The OD measurements in Figure 5.11 show a similar growth pattern in the control and experimental cultivations. A higher growth rate can however be noticed in the pulse experiments in the late part of the second phase. This is due to the higher feed rate that was delivered by the probing programme to fully exploit the reactor capacity.

As far as the product amount is concerned, the probing technique led to good results. The product synthesis is similar to the reference cultivations. The lower product amount in B1 can be explained by the acetate accumulation at the beginning of the production phase.

The product quality obtained with the probing strategy is slightly lower than in the reference cultivations, but better than in [Bylund *et al.*, 2000]. The probing pulses do not seem to be harmful for product synthesis. The loss in productivity is mainly due to the presence of the product-related impurity Peak B, which mainly contains clipped product variants. The expression of Peak B may be correlated with the prolonged elevated backpressure, which did occur in the probing experiments, relative to the reference cultivations.

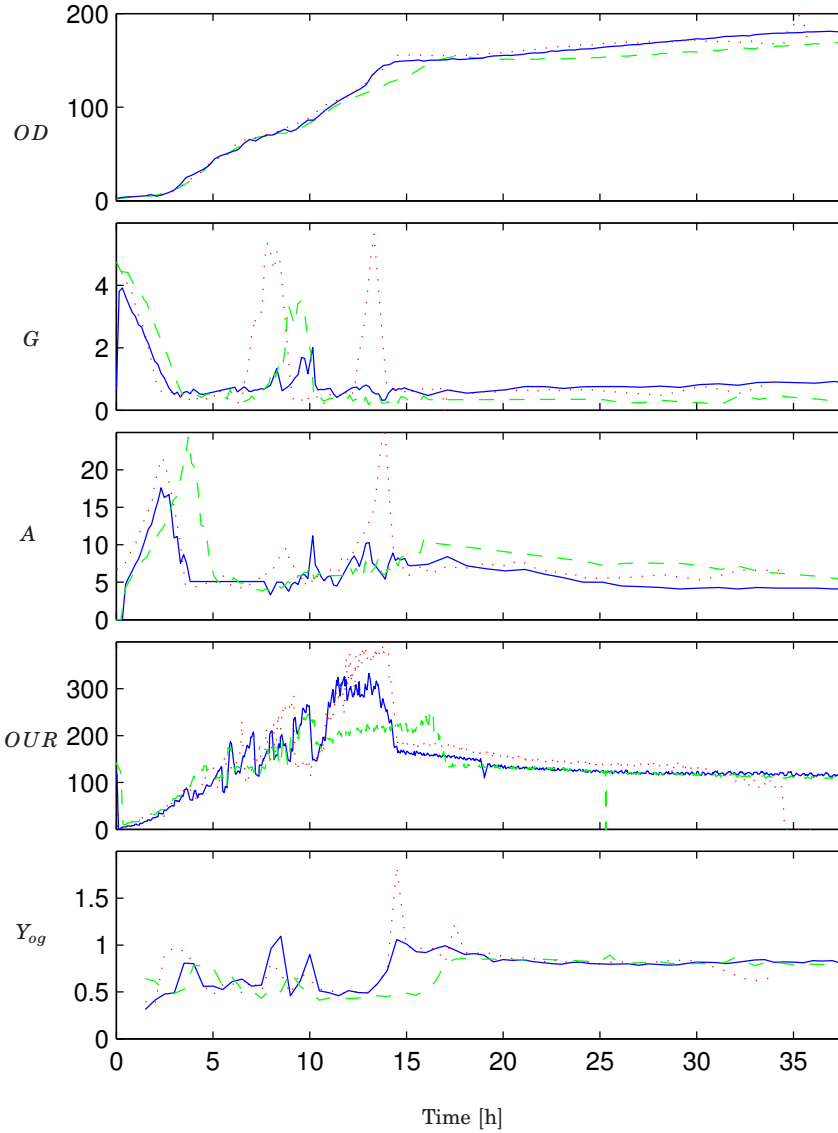

Figure 5.11 Results from fermentation B2 (solid), B1 (dotted) and reference (dashed). From top: optical density (OD), glucose concentration (G, g/l), acetate concentration (A, mM), oxygen uptake rate (OUR, mM/lh), yield coefficient of oxygen per glucose consumed (Y_{og} g/g)

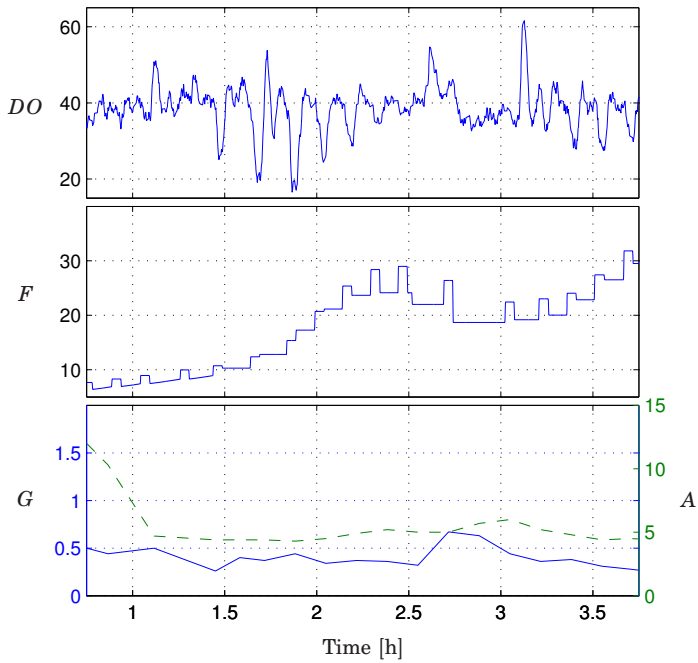

Figure 5.12 Part of fed-batch experiment B2, illustrating the behavior of the probing strategy in presence of complex compounds. From top: dissolved oxygen (DO, %), feed rate (F, arbitrary unit), glucose (G, g/l, solid) and acetate (A, mM, dashed). The manual decrease at t=2.5h would have been made automatically if the controller was fully activated.

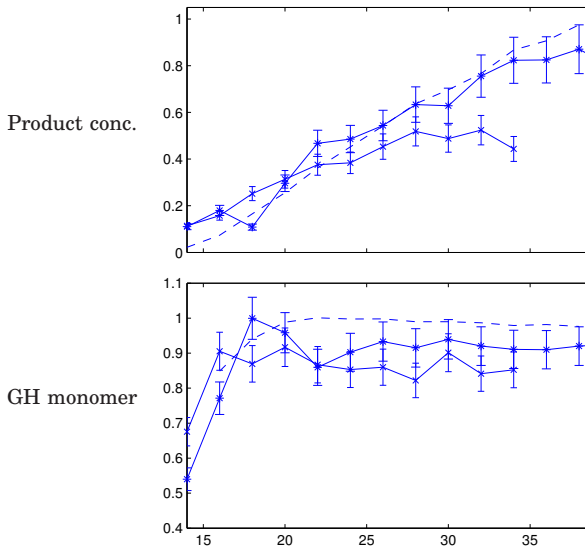

Figure 5.13 Process B. Product synthesis in the pulse experiments compared to the reference cultivations. From top: product concentration (arbitrary unit), GH monomer (arbitrary unit). Average of five reference cultivations (dashed), B1 ('x') and B2 ('*'). Values are shown with their standard deviation.

5.5 Discussion

Satisfactory results have been obtained with the probing feeding strategy after few trials. Some effects related to the scale and the complex medium could be identified.

Influence of the scale

The transfer of the probing control strategy from small scale to large scale was not performed without any difficulties. The probing controller was designed taking into consideration the large scale characteristics. Compared to small scale, longer pulses were for instance made to compensate for the slower dynamics of the mixing and the feed flow control system.

Heterogeneities. Gradients of oxygen and glucose were observed in the experimental cultivations.

Glucose gradients were visible and could be detected in the pulse responses at several occasions. Smaller responses were often observed at the top probe, indicating a higher glucose concentration close to the feedpoint. Due to the limited size of the feeding zone, no global glucose accumulation were generally seen. At large uptake rates the gradient effects are accentuated and there might be a risk of overfeeding when evaluating the pulse response only at the bottom probe. Figure 5.14 shows a part of the fed-batch B1. The pulse in the feed at $t \approx 9.75\ h$ resulted in large responses in the lower part of the reactor while no response was visible at the top. The large response, fedback by the probing algorithm, led to a considerable increase in the feed and also glucose accumulation. This runaway tendency in the later part of the growth phase was avoided in B2 by setting a limit for the maximal feed rate. An alternative could be to compute the pulse response as an average of the responses at all probes. Analysis of the outgas can also be helpful in the interpretation of the pulse responses. In Process A, the oxygen concentration in the outgas is clearly affected by the variations in the feed rate, see Figure 5.15. The outgas measurement provides average information about the reactor state and it is not sensitive to local fluctuations.

Even in absence of global glucose accumulation, the high glucose concentration combined with the lower oxygen supply at the top of the reactor may lead to problematic oxygen limitations. In [Swartz, 1996], the authors points out the risk for a rapid propagation of oxygen limited zones to the entire reactor. Indeed, at low oxygen concentrations, *E. coli* switches to an inefficient respiratory pathway, requiring more oxygen per glucose. The resulting increased oxygen consumption will expand the region of low oxygen levels. To avoid oxygen limitation at the top of the reactor, the dissolved oxygen setpoint was increased each time the top probe reading

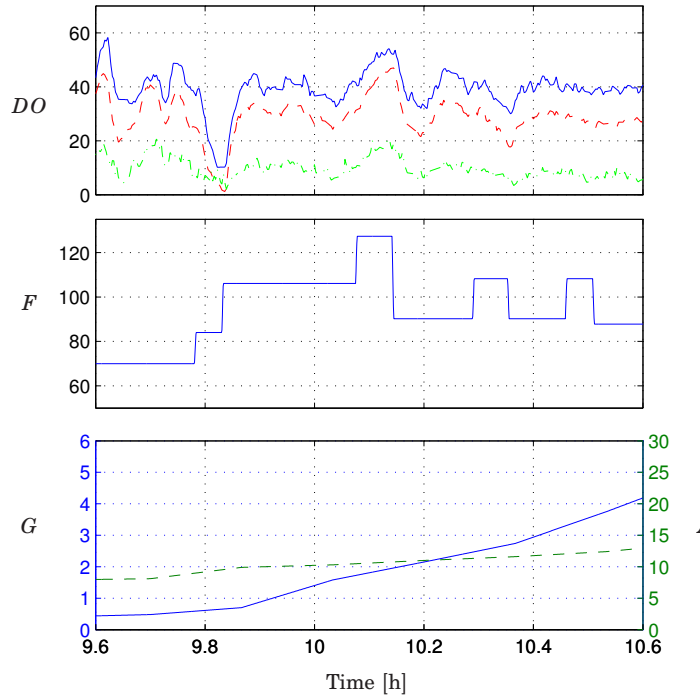

Figure 5.14 Part of fed-batch experiment B1. From top: Dissolved oxygen (DOE, DOD, DOC %), feed rate (F, arbitrary unit), glucose (G, g/l, solid) and acetate (A, mM, dashed).

(DOB) showed low values. It should finally be pointed out that the reactor configuration affects the mixing dynamics and the gradient pattern. Larger gradients are present in a tall and top-fed bioreactor like Process B. A bottom-fed reactor presents a better homogeneity, see [Bylund *et al.*, 1998; Swartz, 1996]. No runaway tendency was reported in Process A.

Wide operating range. Compared to the batch and continuous modes, the fed-batch regime leads to much larger process variations. A fed-batch fermentation is often divided into different phases: batch, growth and production. The process variations are more pronounced in a fermenter with large capacity. In Process B, the maximal feed rate was 20 times higher than the start value. For sustained performance throughout the cultivation, particular attention should be paid to the control design, *i.e.* controller structure and tuning.

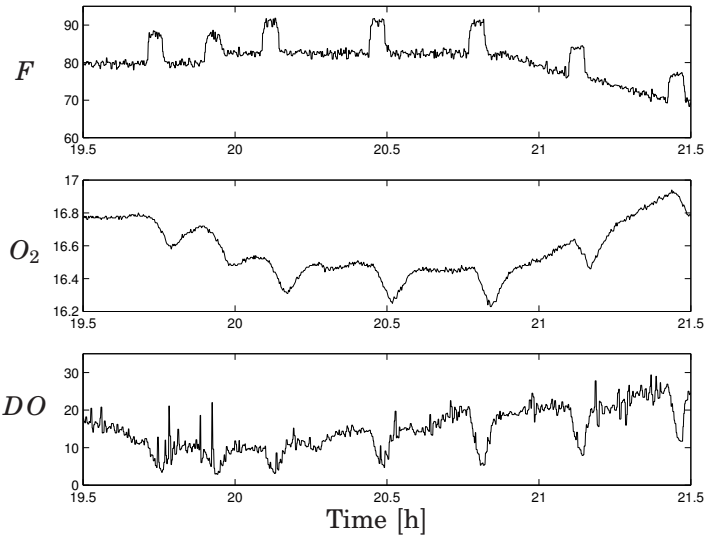

Figure 5.15 Fermentation A2. Pulse responses in the outgas and the dissolved oxygen signal. Note that the DO-setpoint was decreased to 20% from $t = 19.5\ h$ to $t = 20.2\ h$. From top: feed rate (F, l/h), oxygen concentration (O_2, %), dissolved oxygen (DO,%).

The runaway tendency previously mentioned could also be an indication that different settings for the probing controller are necessary. The change in the process gain requires a lower probing gain at high oxygen transfer rates.

A major concern was the dissolved oxygen control. The performance of this loop affects the frequency of the probing pulses and as a consequence the overall performance of the strategy. Some difficulties to stabilize the oxygen level were experienced a couple of hours before induction in B1 and B2. The probing pulses were delayed because of oscillations in the oxygen signal. The oscillations may have been sustained by the spatial inhomogeneities as described in [Swartz, 1996].

To improve the oxygen supply rate in Process B, multiple actuators were used: agitation, air flow or pressure. It is however not a trivial task to design an effective control scheme that takes into account the actuator dynamics, the signals operating range and the user's preferences. A common approach is to manipulate one control signal at a time and switch from one to another when saturation occurs. Manual switching between pressure and agitation control was performed in B1 and B2. Operation close to the saturation of the stirrer speed, with many switches, turned out to be delicate. For better control performance without manual inter-

vention, a configuration using selectors and similar to mid-ranging could be applied, see Chapter 4.

Operation close to the maximum oxygen transfer capacity proved to be highly sensitive to disturbances. In fermentation B1, a sudden increase in the oxygen demand in connection with induction occured when the pressure and the agitation speed were saturated. The dissolved oxygen concentration fell to zero and led to acetate formation. A sufficient buffer in the oxygen transfer capacity turns out to be necessary to cope with this rapid and large regime change. This problem is accentuated by the fact that induction time in Process B is not exactly predictible. When oxygen concentration is controlled by means of multiple variables, it is more convenient to express the buffer size by means of a global variable such as the oxygen uptake rate.

Influence of the complex medium

Results from previous studies of the rhGH process on complex medium show that many free amino acids deplete during the linear feeding phase. The resulting metabolic shifts imply quickly changing demands in oxygen and glucose.

Time-varying glucose demand. As it was expected glucose tended to accumulate in the early fed-batch phase but the probing controller reacted by decreasing the feed rate. The same decreasing feed pattern around t=3 h and t=5 h could be observed in the probing fermentations.

The actual capacity of the cells to consume glucose can be computed a posteriori using glucose measurements. A dynamic mass balance equation for glucose can be written as

$$\frac{d(VG)}{dt} = F_{in}G_{in} - q_g VX$$

The actual glucose uptake rate can be expressed as

$$GUR = q_g VX = F_{in}G_{in} - \frac{d(VG)}{dt}$$

Figure 5.16 shows the actual feed flow rate together with the feed rate "$F_{limiting}$"$= \frac{GUR}{G_{in}}$ that would be in agreement with the actual cell capacity.

The feed profile in the control cultivation tended to be non glucose-limiting in three time intervals. The feed rate should have been lowered three times to avoid glucose accumulation, and increased after 8 hours to exploit the full reactor capacity. It is remarkable that the probing technique reproduced this "ideal" profile using only the information from the

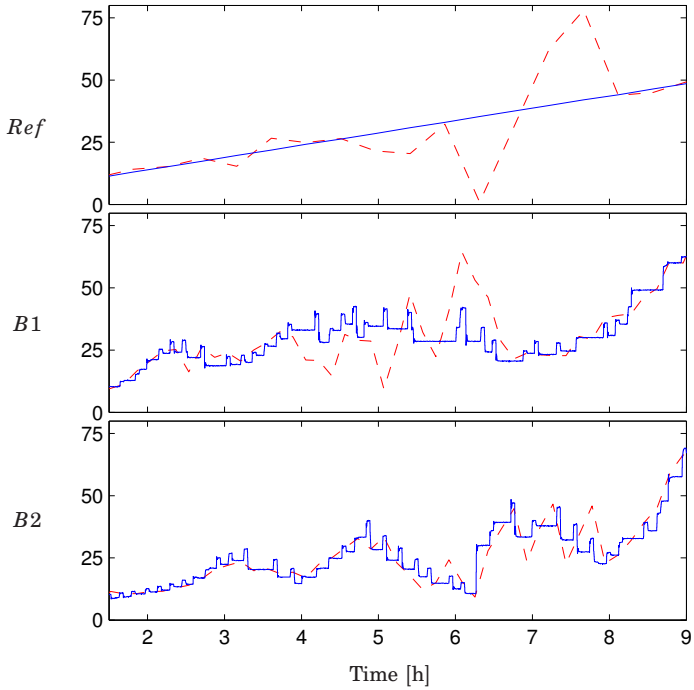

Figure 5.16 Process B. Feed flow rate (arbitrary unit, solid) and feed rate corresponding to the cell capacity (arbitrary unit, dashed).

dissolved oxygen signal. The performance of the probing controller is better in the last run because of an improved tuning. The main parameter changes were an increase in both, the desired pulse response y_r and the decrement factor γ_d.

The rapid changes in the glucose need can drive the probing controller to states where it is no longer efficient. When the feed rate is so low that it barely suffices for maintenance purposes, the pulse responses are unexpectedly small. In this extreme situation, the probing controller will not increase the feed rate as it should. Such situations were encountered after the temporary glucose accumulations in B1 and B2. Based on the abnormally low oxygen uptake rates at this stage of the cultivation, the feed rate was manually increased.

A safety net similar to the one for high oxygen transfer rates can be implemented for an automatic increase in the feed at low oxygen supply rates.

Disturbances on the oxygen signal. The resulting metabolic shifts cause perturbations in the dissolved oxygen signal that are not related to the glucose consumption. Such disturbances occuring during a probing pulse may result in unappropriate feed adjustments and glucose accumulation. Such a perturbation, with no apparent correlation with the probing pulse, occured in the B1 fermentation at $t \approx 5\ h$ and was partially responsible for the first glucose accumulation. Those disturbances, specific to complex medium, are more likely to interfere with the pulse responses in a large scale reactor because of the longer pulses. To reduce the sensitivity of the probing controller to disturbances in the oxygen tension, small gains should be used, which would result in a degradation of the controller tracking ability.

In order to probe frequently and quickly correct the feed rate after a possibly erroneous interpretation of a pulse response, a good dissolved oxygen controller is crucial. The requirements on the oxygen controller is however very high, it should compensate for very fast and large disturbances. At time $t \approx 8\ h$ in cultivation B2, a sudden decrease in the oxygen uptake rate from 270 mM/lh to 170 mM/lh results in a fall in the agitation speed and pressure respectively from 180 rpm and 8 $psig$ to 120 rpm and 3 $psig$.

5.6 Summary

In spite of all difficulties previously mentioned, the probing technique showed good performance in large-scale fermenters, using either defined or complex media. The feeding strategy has succeeded in the sense that good results have been obtained after few trials. No sign of glucose accumulation was visible in Process A and lower glucose levels were observed in Process B. As far as product data is concerned, the productivity is similar to the reference cultivations using an optimized profile.

The transfer of the probing technique to large scale reactors was overall successful. Compared to other feeding strategies, a lot of effort should be devoted to the dissolved oxygen control design. The sensitivity to substrate gradients appeared to be rather limited. However, in a top-fed reactor running at high consumption rates, feedback from several oxygen sensors could be implemented for an increased safety.

The use of complex medium means inevitable disturbances for the probing feeding strategy. It also places greater expectations on the dissolved oxygen control for an unchanged probing frequency. The performance of the strategy was however surprisingly good. A safety net involving the oxygen uptake rate can also be implemented to help the probing controller to leave the low feed rates region.

Even if cultivation B2 performed better than any control cultivation regarding glucose accumulation, it did not improve the product synthesis. Because of the particular feeding phase in the probing experiments, the culture state prior to induction might be different from the control cultivations. The fixed conditions during the production phase that was applied in all cultivations were adapted to the reference cultivations. An adjustment to new conditions for the pulse experiments may give a better productivity.

The probing technique can be of great help in process development. Considerable time can be gained at every stage to derive a feed profile that exploits the full capacity of the reactor while minimizing acetate production. Since the pulses do not seem to be harmful for the productivity, they could be superimposed to an optimized profile for monitoring purposes.

6

Concluding Remarks

6.1 Summary

This thesis has examined a control strategy that is able, with limited process knowledge, to drive a plant to its maximum capacity. Stability and performance analysis was performed for a class of systems inspired by a bioreactor model. A new feeding strategy utilizing variations in temperature has also been proposed and evaluated experimentally. Finally, the industrial relevance of the probing technique has been discussed and shown based on experimental results in large scale reactors. The influence of the reactor scale and the medium composition on the feed strategy was in particular studied.

Analysis of the probing technique

The probing control strategy has been analysed for systems consisting of a linear, time-invariant system in series with a static nonlinearity. A discrete-time representation of the closed-loop system has been derived to facilitate the analysis. The particular problem of driving a process to a saturation has been studied in details. Tuning guidelines based on local and global analysis have been derived for this specific problem. The ability of the probing technique to locate an extremum has also been illustrated and shown on a particular example.

Design of a feeding strategy

A new feeding strategy for reactors with limited oxygen transfer capacity was proposed. It combines the advantages of probing control and temperature limited fed-batch. A controlled excess of glucose is achieved by means of the probing approach. Dissolved oxygen is controlled by manipulation of agitation and temperature in a mid-ranging configuration. Experimen-

tal results showed the efficiency of the proposed technique, which results in a higher biomass and a minor degradation of the recombinant protein.

Evaluation on industrial plants

The probing feeding strategy has been tested for large scale fermentations on defined and complex media. Good performance could be achieved from the first attempts. The control strategy showed a good flexibility with respect to the reactor design, in particular the feed supply system and dissolved oxygen control. The effect of the scale appeared to be rather limited, but in case of a top-fed reactor running at high consumption rates, extra information could be used to increase the robustness of the technique. This is the combined effect of complex medium and large scale that is limiting the achievable performance. The application of the probing strategy can represent a considerable gain of time in process development. Compared to other feeding strategies special effort must however be devoted to the design of the dissolved oxygen controller.

6.2 Suggestions for future work

A major advantage with the probing technique is the low demand for process-specific knowledge. This is an indication for good robustness properties of the control strategy with respect to model uncertainty. It would be of interest to derive some guarantees for robust stability when applying the probing scheme to an uncertain process. A related issue concerns the impact of measurement noise on the overall performance. How does noise affect the transient and stationary behaviors of the probing controller? There are obviously less noise-sensitive ways to estimate the local process gain than computing the pulse response size. A true correlation measure like in the standard extremum seeking scheme would be an alternative.

In the large scale experiments, dissolved oxygen can be controlled by manipulating many variables. The need for a systematic way to allocate a control effort among redundant actuators is obvious. The method should account for the static constraints and the dynamics of the actuators.

In spite of the good results obtained in the large-scale cultivations, the probing strategy appeared to be more sensitive to disturbances. Feedback from a single oxygen probe is indeed sensitive to local variations and disturbances. To improve the robustness of the strategy, information from various measurements could be combined in the algorithm. When available, the signal from several probes or the oxygen concentration in the outgas could be integrated into the feedback law.

7

References

Åkesson, M. (1999): *Probing Control of Glucose Feeding in Escherichia coli Cultivations*. PhD thesis ISRN LUTFD2/TFRT--1057--SE, Department of Automatic Control, Lund Institute of Technology, Sweden.

Åkesson, M. and P. Hagander (1999): "A gain-scheduling approach for control of dissolved oxygen in stirred bioreactors." In Chen *et al.*, Eds., *Preprints 14th World Congress of IFAC*, vol. O, pp. 505–510. Beijing, P.R. China.

Åkesson, M. and P. Hagander (2000): "A simplified probing controller for glucose feeding in *Escherichia coli* cultivations." In *The 39th IEEE Conference on Decision and Control*, vol. 1, pp. 4520–4525.

Åkesson, M., P. Hagander, and J. P. Axelsson (2001a): "Avoiding acetate accumulation in *Escherichia coli* cultures using feedback control of glucose feeding." *Biotechnology and Bioengineering*, **73:3**, pp. 223–230.

Åkesson, M., P. Hagander, and J. P. Axelsson (2001b): "An improved probing controller for substrate feeding in fed-batch culteres of *E. coli*: simulations and experiments." In Dochain and Perrier, Eds., *Proceedings of the 8th International Conference on Computer Applications in Biotechnology June 24–27, 2001, Quebec City, Canada*, pp. 219–224. CAB8, Montreal, June 2001.

Åkesson, M., P. Hagander, and J. P. Axelsson (2001c): "Probing control of fed-batch cultures: Analysis and tuning." *Control Engineering Practice*, **9:7**, pp. 709–723.

Åkesson, M., E. Nordberg Karlsson, P. Hagander, J. P. Axelsson, and A. Tocaj (1999): "On-line detection of acetate formation in *escherichia coli* cultures using dissolved oxygen responses to feed transients." *Biotechnology and Bioengineering*, **64:5**, pp. 590–598.

Allison, B. J. and A. J. Isaksson (1998): "Design and performance of midranging controllers." *Journal of Process Control*, **8:5**, pp. 469–474.

Åström, K. J. and B. Wittenmark (1995): *Adaptive Control*. Addison-Wesley, Reading, Massachusetts.

Bailey, M., P. Biely, and K. Poutanen (1992): "Interlaboratory testing of methods for assay of xylanase activity." *Journal of Biotechnology*, **23**, pp. 257–270.

Bauer, K., A. Ben-Bassat, M. Dawson, V. de la Puente, and J. Neway (1990): "Improved expression of human interleukin-2 in high-cell-density fermentor cultures of *Escherichia coli* K-12 by a phosphotransacetylase mutant." *Appl. Environ. Microbiol.*, **56**, pp. 1296–1302.

Bauer, S. and M. D. White (1976): "Pilot scale exponential growth of *Escherichia coli* W to high cell concentration with temperature variation." *Biotechnology and Bioengineering*, **18**, pp. 839–846.

Bech Jensen, E. and S. Carlsen (1990): "Production of recombinant human growth hormone in *Escherichia coli:* expression of different precursors and physiological effects of glucose, acetate and salts." *Biotechnol. Bioeng.*, **36**, pp. 1–11.

Bernhardsson, B. and M. Sternad (1993): "Feedforward control is dual to deconvolution." *International Journal of Control*, **57:2**, pp. 393–405.

Boyd, S., L. E. Ghaoui, E. Feron, and V. Bslkrishnan (1994): *Linear Matrix Inequalities in system and Control Theory*. SIAM.

Bylund, F., A. Castan, R. Mikkola, A. Veide, and G. Larsson (2000): "Influence of scale-up on the quality of recombinant human growth hormone." *Biotechnology and Bioengineering*, **69:2**, pp. 119–128.

Bylund, F., E. Collet, S.-O. Enfors, and G. Larsson (1998): "Substrate gradient formation in the large-scale bioreactor lowers cell yield and increases by-product formation." *Bioprocess and Biosystems Engineering*, **18:3**, pp. 171–180.

Castan, A. and S.-O. Enfors (2002): "Formate accumulation due to dna release in aerobic cultivations of *Escherichia coli*." *Biotechnology and Bioengineering*, **77:3**, pp. 324–328.

Castan, A., H. J., and S.-O. Enfors (2002a): "The use of flow cytometry to detect nucleic acids attached to the surface of *Escherichia coli* in high cell density fed-batch processes." *Biotechnology Letters*, **24:3**, pp. 219–224.

Castan, A., A. Nasman, and S.-O. Enfors (2002b): "Oxygen enriched air supply in *Escherichia coli* processes: production of biomass and recombinant human growth hormone." *Enzyme and Microbial Technology*, **30:7**, pp. 847–854.

de Maré, L., L. Andersson, and P. Hagander (2003): "Probing control of glucose feeding in *Vibrio cholerae* cultivations." *Bioprocess and Biosystems Engineering*, **25**, January, pp. 221–228.

de Maré, L., S. Velut, P. Hagander, and M. Åkesson (2001): "Feedback control of flow rate from a peristaltic pump using balance measurements." In *European Control Conference*.

Doran, P. (1998): *Bioprocess Engineering*. Academic Press.

Dumont, G. A. and K. J. Åström (1988): "Wood chip refiner control." *IEEE Control Systems Magazine*, April, pp. 38–43.

Enfors, S.-O. and L. Häggström (1994): *Bioprocess technology: Fundamentals and Applications*. Department of Biotechnology, Royal Institute of Technology, Stockholm, Sweden.

Enfors, S. O., M. Jahic, M. Xu, B.and Hecker, B. Jurgen, B. Jurgen, E. Kruger, T. Schweder, G. Hamer, and D. O'Beirne (2001): "Physiological responses to mixing in large scale bioreactors." *Journal of Biotechnology*, **85:2**, pp. 175–185.

Esener, A. A., J. A. Roels, and N. W. F. Kossen (1983): "Theory and applications of unstructured growth models: kinetics and energetic aspects." *Biotechnology and Bioengineering*, **25**, pp. 2803–2841.

Ferrari-Trecate, G., F. A. Cuzzola, D. Mignone, and M. Morari (2001): "Analysis and control with performance of piecewise affine and hybrid systems." In *Proceedings of the American Control Conference*.

Forsberg, G., M. Forsgren, M. Jaki, M. Norin, C. Sterky, Å. Enhörning, K. Larsson, M. Ericsson, and P. Björk (1997): "Identification of framework residues in a secreted recombinant antibody fragment that control production level and localization in *Escherichia coli*." *J. Biol. Chem.*, **272**, pp. 12430–12436.

Fredriksson, J. (2001): "Probing control of glucose feeding in cultivation of *Saccharomyces cerevisiae*." Master's thesis ISRN LUTFD2/TFRT--5660--SE. Department of Automatic Control, Lund Institute of Technology, Sweden.

Gäfvert, M., K.-E. Årzén, L. M. Pedersen, and B. Bernhardsson (2004): "Control of GDI engines using torque feedback exemplified by simulations." *Control Engineering Practice*, **12:2**, pp. 165–180.

Guay, M. and T. Zhang (2003): "Adaptive extremum seeking control of nonlinear dynamic systems with parametric uncertainties." *Automatica*, **39**, pp. 1283–1293.

Han, L. (2002): *Physiology of Escherichia coli in Batch and fed-batch cultures with special emphasis on amino acids and glucose metabolism*. PhD thesis, Department of Biotechnology, Royal Institute of Technology, Stockholm, Sweden. ISBN 91-7283-276-2.

Hitz, L. and B. Anderson (1969): "Discrete positive-real functinos and their applications to system stability." In *Proceedings of the Institution of Electrical Engineers*, vol. 116, pp. 153–155.

Holme, T., S. Arvidsson, B. Lindholm, and B. Pavlu (1970): "Enzymes-laboratory-scale production." *Process Biochem*, **5**, pp. 62–66.

Johansson, M. (1999): *Piecewise Linear Control Systems*. PhD thesis ISRN LUTFD2/TFRT--1052--SE, Department of Automatic Control, Lund Institute of Technology, Sweden.

Johansson, M. and A. Rantzer (1998): "Computation of piecewise quadratic Lyapunov functions for hybrid systems." *IEEE Transactions on Automatic Control*, **43:4**, pp. 555 –559.

Jönsson, U., C.-Y. Kao, A. Megretski, and R. A. (2004): "Iqcbeta: A matlab toolbox for robust stability and performance analysis." Technical Report. Massachusetts Institue of Technology, University of Melbourne, Royal Institue of Technology, Lund Institute of Technology, http://www.ee.mu.oz.au/staff/cykao/.

Kapila, V. and W. Haddad (1996): "A multivariable extension of the tsypkin criterion using a lyapunov-function approach." *IEEE Transactions on Automatic Control*, **41:1**.

Konstantinov, K., M. Kishimoto, T. Seki, and T. Yoshida (1990): "A balanced DO-stat and its application to the control of acetic acid excretion by recombinant *Escherichia coli*." *Biotechnology and Bioengineering*, **36**, pp. 750–758.

Krstic, M. (2000): "Performance improvement and limitations in extremum seeking control." *Systems & Control Letters*, **39**, pp. 313–326.

Krstic, M. and H.-H. Wang (1997): "Design and stability analysis of extremum seeking feedback for general nonlinear systems." In *Proceedings of the Conference on Decision & Control*, vol. 36.

Larsen, M. and P. Kokotovic (2001): "A brief look at the tsypkin criterion:from analysis to design." *International Journal of Adaptive Control and Signal Processing*, **15**, pp. 121–128.

Lee, S. Y. (1996): "High cell-density culture of *Escherichia coli*." *TIBTECH*, **14**, pp. 98–105.

Lin, H., B. Mathiszik, B. Xu, S. Enfors, and P. Neubauer (2001): "Determination of the maximum specific uptake capacities for glucose and oxygen in glucose-limited fed-batch cultivations of escherichia coli." *Biotechnology and Bioengineering*, **73:5**, pp. 347–357.

Liu, J., G. Olsson, and B. Mattiasson (2004): "Monitoring and control of an anaerobic upflow fixed-bed reactor for high-loading-rate operation and rejection of disturbances." *Biotechnology and Bioengineering*, **87:1**, pp. 43–53.

Luli, G. W. and W. R. Strohl (1990): "Comparison of growth, acetate production, and acetate inhibition of *Escherichia coli* strains in batch and fed-batch fermentations." *Appl. Environ. Microbiol.*, **56**, pp. 1004–1011.

Marcos, N., M. Guay, D. Dochain, and T. Zhang (2004): "Adaptive extremum-seeking control of a continuous stirred tank bioreactor with haldane's kinetics." *Journal of Process Control*, **14**, pp. 317–328.

Norberg Karlsson, E., E. Bartonek-Roxå, and O. Holst (1998): "Evidence for substrate binding of a recombinant thermostable xylanase originating from *Rhodothermus marinus*." *FEMS Microbiology Letters*, **168**, pp. 1–7.

O'Beirne, D. and G. Hamer "The utilisation of glucose/acetate mixtures by escherischia coli w3110 under aerobic conditions."

Park, P. and S. Kim (1998): "A revisited tsypkin criterion for discrete-time nonlinear lur'e systems with monotonic sector-restrictions." *Automatica*, **34:11**, pp. 1417–1420.

Parrilo, P. A. (2000): *Structured Semidefinite Programs and Semialgebraic Geometry Methods in Robustness and Optimization*. PhD thesis, California Institute of Technology.

Pirt, S. J. (1985): *Principles of microbe and cell cultivation*. Blackwell Scientific Publications.

Popovic, D., M. Jankovic, S. Magner, and A. Teel (2003): "Extremum seeking methods for optimization of variable cam timing engine operation." In IEEE, Ed., *American Control Conference, 2003. Proceedings of the 2003*, vol. 4, pp. 3136–3141.

Prajna, S., A. Papachristodoulou, P. Seiler, and P. A. Parrilo (2004): *SOSTOOLS: Sum of squares optimization toolbox for MATLAB*.

Prieto, M. A., B. Galán, B. Torres, A. Ferrández, C. Fernández, B. Miñambres, J. García, and E. Díaz (2004): "Aromatic metabolism versus carbon availability: the regulatory network that controls catabolism of

less-preferred carbon sources in escherichia col." *FEMS Microbiology Reviews*, **28:4**.

Qiu, J., J. R. Swartz, and G. Georgiou (1998): "Expression of active human tissue-type plasminogen activator in *Escherichia coli*." *Applied and Environmental Microbiology*, **64**, pp. 4891–4896.

Ramchuran, S., E. Nordberg Karlsson, S. Velut, L. de Maré, P. Hagander, and O. Holst (2002): "Production of heterologous thermostable glycoside hydrolases and the presence of host-cell proteases in substrate limited fed-batch cultures of *Escherichia coli* bl21(de3)." *Applied Microbiology and Biotechnology*, **60:4**, pp. 408–416.

Rozkov, A. (2001): *Control of proteolysis of recombinant proteins in Escherichia coli*. PhD thesis, Department of Biotechnology, Royal Institute of Technology, Stockholm, Sweden. ISBN 91-7283-160-X.

Silfversparre, G., S.-O. Enfors, L. Han, L. Häggstöm, and H. Skogman (2002): "Method for growth of bacteria, minimising the release of endotoxins from the bacteria into the surrounding media." Patent: International publication number WO 02/36746.

Solyom, S. and A. Rantzer (2002): "The servo problem for piecewise linear systems." In *Proceedings of the Fifteenth International Symposium on Mathematical Theory of Networks and Systems*. Notre Dame, IN.

Sternby, J. (1980): "Extremum control systems—An area for adaptive control?" In *Preprints Joint American Control Conference (JACC)*. San Francisco.

Swartz, J. R. (1996): *Method of determining propensity of dissolved oxygen instability*. Number 5487980. United States Patent.

Taherzadeh, M., C. Niklasson, and G. Lidén (2000): "On-line control of fed-batch fermentation of dilute-acid hydrolyzates." *Biotechnology and Bioengineering*, **69:3**.

Teel, A. and D. Popovic (2001): "Solving smooth and nonsmooth multivariable extremum seeking problems by the methods of nonlinear programming." In *Proceedings of the American Control Conference*, vol. 3, pp. 2394–2399.

Velut, S. (1999): "Control of substrate feeding in escherichia coli cultures." Master's thesis ISRN LUTFD2/TFRT--5626--SE. Department of Automatic Control, Lund Institute of Technology, Sweden.

Wang, H.-H., Y. S., and K. M. (2000): "Experimental application of extremum seeking on an axial-flow compressor." *Control Systems Technology, IEEE Transactions on*, **8:2**, pp. 300–309.

Xu, B., M. Jahic, and S.-O. Enfors (1999): "Modeling of overflow metabolism in batch and fed-batch cultures of *Escherichia coli*." *Biotechnology Progress*, **15:1**, pp. 81–90.

Yee, L. and H. W. Blanch (1992): "Recombinant protein expression in high cell density fed-batch cultures of *Escherichia coli*." *Bio/ Technology*, **10**, pp. 1550–1556.

Yongaçoglu, S., I. Dunn, and J. R. Bourne (1982): "Experiments with an adaptive-questing computer control strategy for the biological oxidation of inhibitory substrates." In Halme, Ed., *First IFAC Workshop on Modelling and Control of Biotechnical Processes*, pp. 291–297. Helsinki, Finland.

Zabriskie, D., D. Wareheim, and M. Polansky (1987): "Effects of fermentation feeding strategies prior to induction on expression of a recombinant malaria antigen in *Escherichia coli*." *Journal of Industrial Microbiology*, **2**, pp. 87–95.

A

Further Details for Chapter 3

A.1 Further details for Section 3.2

Output control between the pulses

The process model has an additional input w used for output control between the pulses:

$$\dot{x} = Ax + B_1 f(v) + B_2 w \tag{A.1}$$

During the regulation phase, the process input v is kept constant while the second input w regulates the output z:

$$t \in [kT,\ kT + T_c) \begin{cases} \dot{x} = Ax + B_1 f(u_k) + B_2 w \\ \dot{x_c} = A_c x_c + B_c z \\ w = C_c x_c + D_c z \end{cases} \tag{A.2}$$

where $x_c \in R^m$ is the controller state of the output control loop. After integration between kT and $kT + T_c$, we get

$$\begin{bmatrix} x(kT + T_c) \\ x_c(kT + T_c) \end{bmatrix} = A_{d1} \begin{bmatrix} x(kT) \\ x_c(kT) \end{bmatrix} + (A_{d1} - I) d_1 f(u_k) \tag{A.3}$$

where A_{d1} and d_1 are given by

$$\begin{aligned} A_{d1} &= e^{A_{c1} T_c} & d_1 &= A_{c1}^{-1} \begin{bmatrix} B_1 \\ 0 \end{bmatrix} \\ A_{c1} &= \begin{bmatrix} A + B_2 D_c C & B_2 C_c \\ B_c C & A_c \end{bmatrix} \end{aligned} \tag{A.4}$$

assuming invertibility of A_{c1}. During the probing phase the control signal w is kept constant and a pulse is performed:

$$t \in [kT + T_c,\ kT + T) \begin{cases} \dot{x} = Ax + B_1 f(u_k + u_p^0) + B_2 w(kT + T_c) \\ \dot{x_c} = 0 \end{cases} \tag{A.5}$$

After integration between $kT + T_c$ and $kT + T$, we get

$$\begin{bmatrix} x(kT+T) \\ x_c(kT+T) \end{bmatrix} = A_{d2} \begin{bmatrix} x(kT+T_c) \\ x_c(kT+T_c) \end{bmatrix} + (A_{d2} - I) d_2 f(u_k + u_p^0) \tag{A.6}$$

where A_{d2} and d_2 are given by

$$A_{d2} = \begin{bmatrix} e^{AT_p} & 0 \\ 0 & I \end{bmatrix} \qquad d_2 = \begin{bmatrix} A^{-1}B_1 \\ 0 \end{bmatrix} \tag{A.7}$$

The response to a pulse y_k satisfies equation (3.12) where

$$\begin{aligned} A_{tot} &= A_{d2}A_{d1} & B_{tot} &= [\, A_{d2}(A_{d1} - I)d_1 \quad (A_{d2} - I)d_2 \,] \\ C_{tot} &= C(A_{d2} - I)A_{d1} & D_{tot} &= C(A_{d2} - I)\,[\, (A_{d1} - I)d_1 \quad d_2 \,] \end{aligned} \tag{A.8}$$

A transfer function similar to (3.14) can also be derived

$$G_{tot}(z) = C(A_{d2} - I)(zI - A_{d1}A_{d2})^{-1}\,[\, z(A_{d1} - I)d_1 \quad (zI - A_{d1})d_2 \,]$$

Output nonlinearity

In the case of an output nonlinearity f, the response y_k to a pulse is given by

$$\begin{aligned} x_{k+1} &= A_{d2}A_{d1}x_k + (A_{d2}A_{d1} - I)du_k + (A_{d2} - I)du_p^0 \\ y_{1,k} &= C(A_{d2}A_{d1}x_k + (A_{d2}A_{d1} - I)du_k + (A_{d2} - I)du_p^0) \\ y_{2,k} &= C(A_{d1}x_k + (A_{d1} - I)du_k) \\ y_k &= f(y_{1,k}) - f(y_{2,k}) \end{aligned} \tag{A.9}$$

where $A_{d1} = e^{AT_c}$, $A_{d2} = e^{AT_p}$ and $d = A^{-1}B$

A.2 Further details for Section 3.4

Region description

The region $\mathbf{X} = \{X \in R^n,\ EX + e \succeq 0\}$ is unbounded in the direction V if for some $X_0 \in \mathbf{X}$, one or two of the following statement is true

- for all $\lambda > 0$, $X_0 + \lambda V \in \mathbf{X}$
- for all $\lambda < 0$, $X_0 + \lambda V \in \mathbf{X}$

which is equivalent to

- for all $\lambda > 0$, $E(X_0 + \lambda V) + e \succeq 0$
- for all $\lambda < 0$, $E(X_0 + \lambda V) + e \succeq 0$

Letting λ go to $+\infty$ or $-\infty$ implies that EV is either (componentwise) non-positive or non-negative. After the coordinate change $X = TZ$, the region $\mathbf{X}$ can be described as follows

$$\mathbf{X} = \{Z = T^{-1}X,\ ETZ + e \succeq 0\} \tag{A.10}$$

$$= \{Z = \begin{bmatrix} z_s \\ z_u \end{bmatrix},\ ET(\begin{bmatrix} z_s \\ 0 \end{bmatrix} + \begin{bmatrix} 0 \\ 1 \end{bmatrix} z_u) + e \succeq 0\} \tag{A.11}$$

$$= \{Z = \begin{bmatrix} z_s \\ z_u \end{bmatrix}, ET \begin{bmatrix} 0 \\ 1 \end{bmatrix} z_u \succeq -ET \begin{bmatrix} z_s \\ 0 \end{bmatrix} - e\} \tag{A.12}$$

When $\mathbf{X}$ is unbounded in the z_u eigendirection ($V = T \begin{bmatrix} 0 \\ 1 \end{bmatrix}$), we know that $ET \begin{bmatrix} 0 \\ 1 \end{bmatrix}$ is of definite sign (componentwise) and $\mathbf{X}$ can be written as

$$\mathbf{X} = \{Z \mid \alpha_j z_u \leq [\, G_j \quad g_j \,] \begin{bmatrix} z_s \\ 1 \end{bmatrix}\} \tag{A.13}$$

where $\alpha_j \in \{0, 1\}$ or $\alpha_j \in \{0, -1\}$.

Proof of Theorem 3.1

The first inequality in the statement guarantees positivity of V in $\mathbf{X}$. Negativity of ΔV on $\mathbf{X}$ will be proven in two steps:

$$Z_\partial \in \partial\mathbf{X} \ \Rightarrow\ \Delta V(Z_\partial) < 0 \tag{A.14}$$

$$Z \in \mathbf{X} \ \Rightarrow\ \Delta V(Z) < \Delta V(Z_\partial) \text{ for some } Z_\partial \ \in \partial\mathbf{X} \tag{A.15}$$

The set $\partial\mathbf{X}$, on the cell boundary, can be written as

$$\partial\mathbf{X} = \bigcup_{j \in I_1} \partial\mathbf{X}_j \tag{A.16}$$

with

$$\partial\mathbf{X}_j = \{\bar{Z} |\ z_u = G_j z_s + g_j < G_i z_s + g_i \ \ i \in I_1\} \tag{A.17}$$

which can be rewritten as

$$\partial \mathbf{X}_j = \{\bar{Z} = \bar{H}_j \begin{bmatrix} z_s \\ 1 \end{bmatrix} \ | F_j \begin{bmatrix} z_s \\ 1 \end{bmatrix} \succeq 0\} \tag{A.18}$$

We will first show the inequality (A.14). Multiplying both sides of (3.42) by $[\, z_s \quad 1\,]^T$ we get

$$\begin{bmatrix} z_s \\ 1 \end{bmatrix}^T \bar{H}_j \bar{T}^T (\bar{A}^T \bar{P} \bar{A} - \bar{P}) \bar{T} \bar{H}_j \begin{bmatrix} z_s \\ 1 \end{bmatrix} + \begin{bmatrix} z_s \\ 1 \end{bmatrix}^T F_j^T \bar{U}_j F_j \begin{bmatrix} z_s \\ 1 \end{bmatrix} < 0$$

which implies that that $\Delta V(Z) < 0$ for all $Z \in \partial \mathbf{X}_i$. We will now prove that (3.43) implies (A.15). Take $Z \in \mathbf{X}$. From (3.36) we have

$$\Delta V(Z) = \begin{bmatrix} z_s \\ 1 \end{bmatrix}^T \begin{bmatrix} M_{ss} & M_s^T \\ M_s & m \end{bmatrix} \begin{bmatrix} z_s \\ 1 \end{bmatrix} + 2 \begin{bmatrix} z_s \\ 1 \end{bmatrix}^T \begin{bmatrix} M_{su} \\ m_u \end{bmatrix} z_u$$

M_{su} can be easily computed to be of the form:

$$M_{su} = (A_s - I)\bar{Q}_{su}$$

Since $\bar{Q}$ is such that $\bar{Q}_{su} = 0$, the cross-term $z_u z_s$ in ΔV vanishes:

$$\Delta V(Z) = \begin{bmatrix} z_s \\ 1 \end{bmatrix}^T \begin{bmatrix} M_{ss} & M_s \\ M_s^T & m \end{bmatrix} \begin{bmatrix} z_s \\ 1 \end{bmatrix} + 2 m_u z_u$$

Noting that

$$m_u = l^T \begin{bmatrix} 0 & \bar{T}^T (\bar{A}^T \bar{P} \bar{A} - \bar{P}) \bar{T} \\ \bar{T}^T (\bar{A}^T \bar{P} \bar{A} - \bar{P}) \bar{T} & 0 \end{bmatrix} l > 0$$

it follows that for all $j \in I_1$

$$m_u z_u < m_u \, [\, G_j \quad g_j \,] \begin{bmatrix} z_s \\ 1 \end{bmatrix}$$

Take now j_0 such that for all $j \in I_1$

$$[\, G_j \quad g_j \,] \begin{bmatrix} z_s \\ 1 \end{bmatrix} \succeq [\, G_{j_0} \quad g_{j_0} \,] \begin{bmatrix} z_s \\ 1 \end{bmatrix}$$

We have then the following inequality

$$\Delta V(Z) < \Delta V(H_{j_0} \begin{bmatrix} z_s \\ 1 \end{bmatrix}) \text{ and } \ F_{j_0} \begin{bmatrix} z_s \\ 1 \end{bmatrix} \succeq 0$$

implying that

$$\Delta V(Z) < \Delta V(Z_\partial) \ \ Z_\partial = H_{j_0} \begin{bmatrix} z_s \\ 1 \end{bmatrix} \in \partial \mathbf{X}_{j_0}$$

Proof sketch for Theorem 3.2

We first notice that the matrices $\bar{A}_i$ and $\bar{B}_i$ describe the dynamic of the error $X - X_r$:

$$\begin{aligned} X(k+1) - X_r(k+1) &= A_i(X(k) - X_r(k)) + A_i(I - A_{i_0})^{-1}B_{i_0}r(k) + B_i r(k) \\ &\quad + a_i - (I - A_{i_0})^{-1}B_{i_0}r(k+1) \\ &= A_i(X(k) - X_r(k)) - (I - A_{i_0})^{-1}B_{i_0}(r(k+1) - r(k)) \\ &\quad + \underbrace{B_i + (A_i - I)(I - A_{i_0})^{-1}B_{i_0}r(k) + a_i}_{=\,0 \text{ for } i = i_0} \end{aligned}$$

Introducing the input $\Delta r(k) = r(k+1) - r(k)$ we get

$$\begin{bmatrix} X - X_r \\ 1 \\ r \end{bmatrix}_{k+1} = \underbrace{\begin{bmatrix} A_i & a_i & B_i + (A_i - I)(I - A_{i_0})^{-1}B_{i_0} \\ 0 & 1 & 0 \\ 0 & 0 & 1 \end{bmatrix}}_{\bar{A}_i} \begin{bmatrix} X - X_r \\ 1 \\ r \end{bmatrix}_k + \underbrace{\begin{bmatrix} -(I - A_{i_0})^{-1}B_{i_0} \\ 0 \\ 1 \end{bmatrix}}_{\bar{B}_i} \Delta r_k$$

The result follows from the matrix inequalities, similarly to the continuous-time case in [Johansson and Rantzer, 1998].

A.3 Further details for Section 3.5

Closed-loop matrices

The closed-loop system can be represented by a piecewise affine system with input $r(k)$:

$$X(k+1) = A_i X(k) + B_i r(k) + a_i, \quad i = 1, 2, 3$$

The dynamic in each region is described by the matrices

$$A_1 = \begin{bmatrix} e^{AT} & (e^{AT} - I)A^{-1}B \\ KC(e^{AT} - e^{AT_c}) & 1 + KC(e^{AT} - e^{AT_c})A^{-1}B \end{bmatrix}$$
$$a_1 = \begin{bmatrix} 0 \\ -Ky_r \end{bmatrix} + \begin{bmatrix} I \\ KC \end{bmatrix} (e^{AT_p} - I)A^{-1}Bu_p^0$$
$$A_2 = \begin{bmatrix} e^{AT} & (e^{AT} - e^{AT_p})A^{-1}B \\ KC(e^{AT} - e^{AT_c}) & 1 + KC(e^{AT_p} - I)(e^{AT_c} - I)A^{-1}B \end{bmatrix}$$
$$a_2 = \begin{bmatrix} 0 \\ -Ky_r \end{bmatrix}$$
$$A_3 = \begin{bmatrix} e^{AT} & 0 \\ KC(e^{AT} - e^{AT_c}) & 1 \end{bmatrix}, \quad a_3 = \begin{bmatrix} 0 \\ -Ky_r \end{bmatrix}$$

and

$$B_1 = \begin{bmatrix} 0 \\ 0 \end{bmatrix}, \quad B_2 = \begin{bmatrix} (e^{AT_p} - I)A^{-1}B \\ KC(e^{AT_p} - I)A^{-1}B \end{bmatrix}, \quad B_3 = \begin{bmatrix} (e^{AT} - I)A^{-1}B \\ KC(e^{AT} - e^{AT_c})A^{-1}B \end{bmatrix}$$

The matrix A_1 has 1 as eigenvalue, with an associated eigendirection V_1 given by

$$V_1 = \begin{bmatrix} A^{-1}B \\ -1 \end{bmatrix}$$

The matrix A_3 has 1 as eigenvalue, with an associated eigendirection V_3 given by

$$V_3 = \begin{bmatrix} 0 \\ 1 \end{bmatrix}$$

Local analysis

The local analysis in every region of the state space can easily be done using the transfer functions G_1 and G_2. The pulse response y_k is given by

$$y_k = \begin{cases} G_1(z)u_k + G_2(z)u_p^0 & \text{in } \mathbf{X}_1 \\ G_1(z)u_k + G_2(z)(r - u_k) & \text{in } \mathbf{X}_2 \\ G_1(z)r & \text{in } \mathbf{X}_3 \end{cases} \tag{A.19}$$

With the the controller

$$(z - 1)u_k = K(y_k - y_r) \tag{A.20}$$

the closed-loop system becomes

$$u_k = \begin{cases} K\dfrac{G_2(z)u_p^0 - y_r}{z - 1 - KG_1(z)} & \text{in } \mathbf{X}_1 \\ K\dfrac{G_2(z)r - y_r}{z - 1 + K(G_2(z) - G_1(z))} & \text{in } \mathbf{X}_2 \\ K\dfrac{G_1(z)r - y_r}{z - 1} & \text{in } \mathbf{X}_3 \end{cases} \tag{A.21}$$

Root-locus inspection when K varies can be performed to locate the closed-loop poles in every region. We consider the case of a first order process model and derive necessary conditions for global stability, based on local analysis.

Region $\mathbf{X}_1$**.** The closed-loop is described by

$$u_k = K\frac{bca^{-1}(z - e^{-aT_c})(1 - e^{-aT_p})u_p^0 - y_r(z - e^{-aT})}{(z-1)(z - e^{-aT} - Kbca^{-1}e^{-aT_c}(1 - e^{-aT_p}))} \tag{A.22}$$

The second pole is inside the unique disc when

$$e^{aT_c} > e^{-aT_p} + K\frac{bc}{a}(1 - e^{-aT_p}) \tag{A.23}$$

in that case the integrator is driving u_k towards the saturation if

$$bca^{-1}(1 - e^{-aT_c})(1 - e^{-aT_p})u_p^0 - y_r(1 - e^{-aT}) > 0 \tag{A.24}$$

which is equivalent to $y_r < \beta u_p^0$.

Region $\mathbf{X}_2$**.** Since

$$G_2 - G_1 = bca^{-1}(1 - e^{-aT_p})(1 - e^{-aT_c})z(z - e^{-aT})^{-1} \tag{A.25}$$

the closed-loop dynamic becomes

$$u_k = K\frac{bca^{-1}(z - e^{-aT_c})(1 - e^{-aT_p})r - y_r(z - e^{-aT})}{(z-1)(z - e^{-aT}) - K\frac{bc}{a}(1 - e^{-aT_p})(1 - e^{-aT_c})z} \tag{A.26}$$

Jury's stability test for second order systems leads to

$$0 < K\frac{bc}{a}(1 - e^{-aT_c})(1 - e^{-aT_p}) < 2(1 + e^{-aT}) \tag{A.27}$$

or

$$0 < K\beta < 2\frac{1 + e^{-aT}}{1 - e^{-aT}} \tag{A.28}$$

Region $\mathbf{X}_3$**.** For u_k to decrease towards the saturation we should have $G_1(1)r - y_r < 0$ that is $y_r > 0$.

B

Further Details for Chapter 4

B.1 Reactor model with temperature dependency

Metabolic rates

The temperature influence on all maximal specific uptake rates is modelled by a multiplicative factor $f(T)$ defined by

$$f(T) = e^{-50(\frac{1}{T}-\frac{1}{37})} \tag{B.1}$$

The maximal uptake rates $q_a^{c,max}(T)$, $q_g^{max}(T)$, $q_o^{max}(T)$ and the maintenance coefficient $q_{mc}(T)$ can thus be written as

$$q_a^{c,max}(T) = q_{a,37}^{c,max} f(T) \tag{B.2}$$
$$q_g^{max}(T) = q_{g,37}^{max} f(T) \tag{B.3}$$
$$q_o^{max}(T) = q_{o,37}^{max} f(T) \tag{B.4}$$
$$q_{mc}(T) = q_{mc,37} f(T) \tag{B.5}$$

The uptake rates for acetic acid and glucose are modeled by Monod kinetics:

$$q_a^{c,pot}(A,T) = q_a^{c,max}(T)\frac{A}{k_a + A} \tag{B.6}$$
$$q_g(G,T) = q_g^{max}(T)\frac{G}{k_s + G} \tag{B.7}$$

Part of the glucose is used for maintenance:

$$q_m(T) = \min(q_g(G,T), q_{mc}(T)) \tag{B.8}$$

For clarity purposes the argument T is omitted in the following equations. The acetic acid formation q_a and the growth uptake q_{gg} are described by:

$$q_a = q_a^p - q_a^c \tag{B.9}$$

$$q_{gg} = q_g - q_m \tag{B.10}$$

where q_a^p is the production of acetic acid and q_a^c stands for the acetic acid consumption. Splitting into an oxidative flow and a fermentative flow gives:

$$q_{gg}^{ox} = \min((q_o^{max} - q_m Y_{om})/Y_{og}, q_{gg}) \tag{B.11}$$

$$q_{gg}^{fe} = q_{gg} - q_{gg}^{ox} \tag{B.12}$$

The specific acetate production, acetate consumption, growth rate and oxygen uptake rate are given by the following equations:

$$q_a^p = q_{gg}^{fe} Y_{ag} \tag{B.13}$$

$$q_a^c = \min(q_a^{c,pot}, (q_o^{max} - q_{gg}^{ox} Y_{og} - q_m Y_{om})/Y_{oa}) \tag{B.14}$$

$$\mu = q_{gg}^{ox} Y_{xg}^{ox} + q_{gg}^{fe} Y_{xg}^{fe} + q_{ac} Y_{xa} \tag{B.15}$$

$$q_o = q_{gg}^{ox} Y_{og} + q_m Y_{om} + q_{ac} Y_{oa} \tag{B.16}$$

A consequence of the model assumptions is that the saturation in the oxygen uptake rate occurs for the same values of G and A independently of T.

Linearized model

A linearised model of the process which is valid when $q_o < q_o^{max}$ is given by:

$$T_o \frac{d\Delta DO}{dt} + \Delta DO = K_{og}\Delta q_G + K_{ot}\Delta T + K_N \Delta N$$

$$T_g \frac{d\Delta q_G}{dt} + \Delta q_G = K_{gf}\Delta F + K_{gt}\Delta T$$

$$K_{gf} = \frac{G_i}{VX} \qquad K_{gt} = \frac{\partial q_g}{\partial T} X$$

$$T_g = (\frac{\partial q_g}{\partial G} X)^{-1} \qquad K_{og} = -Y_{og} H X (K_L a)^{-1}$$

The static gain from ΔT to ΔDO is given by:

$$\begin{aligned} K_{og}K_{gt} + K_{ot} &= -Y_{og}HX(K_La)^{-1}\frac{\partial q_g}{\partial T} + \frac{\partial q_o}{\partial T}HX(K_La)^{-1} \\ &= HX(K_La)^{-1}(\frac{\partial q_o}{\partial T} - Y_{og}\frac{\partial q_g}{\partial T}) \\ &= 0 \end{aligned}$$

Thus the temperature has a limited stationary effect on the dissolved oxygen concentration when $q_o < q_o^{max}$.

B.2 Temperature- versus feed-based DO control

Feed based DO control

A constant dissolved oxygen concentration requires that

$$0 = OTR^{max} - q_oHX$$

where the specific oxygen uptake rate is given by

$$q_o = (Y_{og}q_g^{res} + Y_{og}^m q_g^m)$$

The residual glucose uptake rate can be solved from the previous equations:

$$q_g^{res,SLFB} = \frac{OTR^{max}}{HXY_{og}} - \frac{Y_{og}^m q_m}{Y_{og}}$$

Temperature-based DO control

The stationary mass balance for oxygen leads to

$$0 = OTR^{max} - q_o^{max}f(T)HX$$

Using temperature to maintain DO at a constant level leads to

$$f(T) = \frac{OTR^{max}}{HXq_o^{max}}$$

Assuming glucose excess without acetate accumulation, we have

$$q_o^{max}f(T) = (Y_{og}q_g^{res} + Y_{og}^m q_g^m)f(T)$$

The glucose that is consumed for non-maintenance purposes is then

$$q_g^{res,TLFB}(T) = \frac{OTR^{max}}{HXY_{og}}(1 - \frac{Y_{og}^m q_m}{q_o^{max}})$$

Comparison

We can notice that

$$q_g^{res,TLFB} > q_g^{res,SLFB} \Leftrightarrow OTR^{max} < HXq_o^{max} \tag{B.17}$$

implying that when the maximum oxygen transfer of the reactor is reached, the temperature-based DO control is preferable. When no product is formed, all residual glucose is directed to growth. Using the first strategy, we get

$$\dot{X} = q_g^{res,SLFB} X = \frac{OTR^{max}}{HY_{og}} - \frac{Y_{og}^m q_m}{Y_{og}} X$$

implying that X converges to a constant

$$X_\infty = \frac{OTR^{max}}{HY_{og}^m q_m} \tag{B.18}$$

whereas in the temperature-based DO control case, the cell density is increasing linearly:

$$\dot{X} = q_g^{res,TLFB} X = \frac{OTR^{max}}{HY_{og}} (1 - \frac{Y_{og}^m q_m}{q_o^{max}})$$

B.3 Steady state with down-pulses

Integration of the acetate dynamic in the two regions leads to

$$A(T_c) = A(0) + Y_{ag}(q_g - q_g^{crit})T_c X \tag{B.19}$$

$$A(T) = A(T_c)e^{-\frac{T_p X}{\tau}} = (A(0) + Y_{ag}(q_g - q_g^{crit})T_c X)e^{-\frac{T_p X}{\tau}} \tag{B.20}$$

The specific oxygen uptake rate at $t = T_c$ and $t = T$ is given by

$$q_o(T_c) = q_o^{max} \tag{B.21}$$

$$q_o(T) = Y_{og}(q_g - q_g^p) + \frac{Y_{oa}}{\tau} A(T) \tag{B.22}$$

The change in the specific glucose uptake rate after the pulse becomes

$$q_g(T) = q_g(0) + \kappa K_g(K_o(q_o(T) - q_o(T_c)) - y_r) \tag{B.23}$$

The condition

$$q_g(T) = q_g(0) \tag{B.24}$$
$$A(T_c) = A(0) \tag{B.25}$$

can be written in matrix form

$$\begin{bmatrix} q_g(T) \\ A(T) \end{bmatrix} = A_e \begin{bmatrix} q_g(0) \\ A(0) \end{bmatrix} + a_e \tag{B.26}$$

where A_e and a_e are given by

$$A_e = \begin{bmatrix} 1 - \kappa K(Y_{og} + Y_{oa}Y_{ag}\frac{T_c X}{\tau}e^{-\frac{XT_p}{\tau}}) & -\frac{\kappa}{\tau}Y_{oa}Ke^{-\frac{XT_p}{\tau}} \\ XT_cY_{ag}e^{-\frac{XT_p}{\tau}} & e^{-\frac{XT_p}{\tau}} \end{bmatrix} \tag{B.27}$$

$$a_e = \begin{bmatrix} \kappa K_g(Y_{og}K_o(q_g^p + q_g^{crit}) - y_r + \frac{Y_{oa}}{\tau}Y_{ag}T_cK_oq_g^{crit}e^{-XT_p/\tau}) \\ -Y_{ag}XT_cq_g^{crit}e^{-XT_p/tau} \end{bmatrix} \tag{B.28}$$

Jury's stability test can be applied to get a necessary and sufficient condition for A_e to be stable:

$$0 < T_c < \frac{\tau(1 + e^{T_pX/\tau})}{Y_{oa}Y_{ag}X}(\frac{2}{\kappa KY_{og}} - 1) \tag{B.29}$$
$$0 < \kappa < \frac{2}{K_oK_gY_{og}} \tag{B.30}$$

When the conditions (B.29) and (B.30) are fullfilled, the equilibrium point $X_1 = (q_{g,\infty}, A_\infty)$ is stable and given by

$$q_{g,\infty} = q_g^{crit} + \frac{e^{XT_p/\tau}}{Y_{ag}XT_c}A_\infty > q_g^{crit} \tag{B.31}$$
$$A_\infty = \frac{Y_{ag}T_cX\tau(-y_r + K_oY_{og}q_g^p)}{K_o(Y_{og}\tau(e^{T_pX/\tau} - 1) + Y_{oa}Y_{ag}T_cX)} \tag{B.32}$$

B.4 Operating point and numerical values

The operating point that is chosen for the analysis is

$$OTR = OTR^{max} = K_La(N_{ref})(O^* - O_{sp}) \tag{B.33}$$
$$q_o = q_o^{max} \tag{B.34}$$

with $K_L a = \alpha(N - N_0)$. The cell density X becomes

$$X = \frac{OTR^{max}}{q_o^{max} H} \tag{B.35}$$

The gains K_o, from q_o to O, and K_g, from F to q_g, are given by

$$K_o = \frac{HX}{K_L a} \approx \frac{O^* - O}{q_o^{max}} \tag{B.36}$$

$$K_g = \frac{G_i}{VX} = \frac{G_i q_o^{max} H}{VOTR^{max}} \tag{B.37}$$

The approximation is based on the stationary equations (4.2). The numerical values used in the simulations and in the analysis are given in Table B.1.

Table B.1 Numerical values corresponding to a laboratory-scale bioreactor with *E. coli*.

Symbol	Value	Description
G_{in}	500 g/l	glucose conc. in feed
H	14000	Henrys const.
k_s	0.01 g/l	sat. const. for gluc. uptake
k_a	0.05 g/l	sat. const. for acet. uptake
α	3 (h rpm)$^{-1}$	oxygen transf. const.
N_0	289 rpm	oxygen transf. const.
$q_{a,37}^{c,max}$	0.2 g/gh	max. spec. acet. uptake
$q_{g,37}^{max}$	1.5 g/gh	max. spec. glucose uptake
$q_{g,37}^{crit}$	1.25 g/gh	crit. glucose uptake
$q_{mc,37}$	0.15 g/gh	maintenance coefficient
$q_{o,37}^{max}$	0.66 g/gh	max. spec. oxygen uptake
Y_{ag}	0.55 g/g	acetate/glucose yield
Y_{oa}	0.55 g/g	oxyg./acet. yield
Y_{og}	0.50 g/g	oxyg./gluc. yield for growth
Y_{om}	1.07 g/g	oxyg./gluc. yield for maint.
Y_{xa}	0.4 g/g	biomass/acet. yield
Y_{xg}^{ox}	0.51 g/g	oxidative biomass/gluc.
Y_{xg}^{fe}	0.15 g/g	fermentative biomass/gluc.
V	2 l	reactor volume
T_p	30 s	oxyg. probe time cst
T_t	4 min	time cst of temp. dyn.
O_{sp}	30 %	setpt for DO

C

Further Details for Chapter 5

C.1 Algorithm

Init

$F_{control} = F_0$
$I = 0$
Reset the timer $(t = 0)$
Go to **Control**

Control

Activate DO control
$DOcontrol = On$

Decrease the feed when max oxygen transfer capacity
IF $N_{sensor} > N_{high2}$
  $F_{control} = F_{control} - \frac{h}{T_{control}} \gamma F_{control}$
END

Wait for steady state in DO before making a pulse
IF $t > T_{control}$
  O_{mean} = mean value of O_p over the last 30 seconds.
  IF $|O_{mean} - O_{sp}| < O_{tol}$
    Reset the timer$(t = 0)$
    Go to **Probing**
  END
END

Probing

Freeze the stirrer speed

$DOcontrol = Off$

Make a pulse
$F_{pulse} = \gamma_p F_{control}$
$F_{sp} = F_{control} + F_{pulse}$

Compute the response in DO and update the feed
IF $t > T_{pulse}$
  O_{mean} = mean value of O_p over the last 30 seconds.
  $O_{pulse} = O_{mean} - O_{sp}$
  IF $O_{pulse} < O_{reac}$ *(detected overfeeding)*
    $\Delta F = -\gamma_D F_{control}$
    $I = 0$
  ELSE
    $e = O_{pulse} - y_r$
    $\Delta F = (ke + k_i I) F_{control}/(100 - O_{sp})$
    $I = I + e$
    IF $N_{sensor} > N_{high}$ AND $\Delta F > 0$
      $\Delta F = 0$ *(no increment when close to max oxygen transfer)*
    END
  END
  $F_{control} = F_{control} + \Delta F$
  $F_{sp} = F_{control}$
  Reset the timer$(t = 0)$
  Go to **Control**
END

C.2 Parameter values

The nominal values used in the experiments are listed in Table C.1 and Table C.2

Table C.1 Nominal values used in Process A.

Symbol	Value	Description
$T_{control}$	6 min	time between pulses
T_{pulse}	3 min	pulse duration
y_r	10 %	setpoint for pulse resp.
O_{sp}	30 %	setpoint for DO level
O_{reac}	3 %	reaction level
N_{high}	121 rpm	limit for feed incr.
N_{high2}	128 rpm	limit before feed decrease
γ_P	0.2	rel. pulse size
γ_D	0.2	rel. dec. if no response
γ	10 %	rel. dec. if $N > N_{high2}$
k	0.95	gain of probing contr.
k_i	0	int. gain of probing contr.

Table C.2 Nominal values used in Process B.

Symbol	Value	Description
$T_{control}$	6 min	time between pulses
T_{pulse}	3 min	pulse duration
O_{tol}	1.5 %	tol. level for new pulse
y_r	5 %	setpoint for pulse resp.
O_{sp}	40-55 %	setpoint for DO level
O_{reac}	2.5%	reaction level
P_{high}	15 psig	limit for feed incr.
P_{high2}	18 psig	limit before feed decrease
γ_P	0.2	rel. pulse size
γ_D	0.2	rel. dec. if no response
γ	10 %	rel. dec. if $P > P_{high2}$
k	1-1.2	gain of probing contr.
k_i	0	int. gain of probing contr.